SYNTHESIS OF ALKALINE-EARTH ZEOLITES

Thesis by

Shervin Khodabandeh

In Partial Fulfillment of the Requirements

for the Degree of

Doctor of Philosophy

California Institute of Technology

Pasadena, California

1997

(Submitted May 29, 1997)

to my parents

Acknowledgements

I am gratefully indebted to Professor Mark Davis for his wisdom, encouragement, and support during the course of this work, and for allowing me to dabble in various areas of material synthesis and characterization not necessarily related to my thesis project. The true value of all I learned from him during my four years at Caltech goes far beyond what is presented here.

I would also like to thank the members of my thesis committee, Professor George Gavalas, Professor Konstantinos Giapis, and Professor George Rossman for their interest in this work.

Help and support from Davis group members (both past and present) is greatly appreciated. In particular, Chris Dartt, John Lewis, John Nagel, Raul Lobo, Michael Tsapatsis, C-Y Chen and Miguel Camblor were instrumental during my initiation into the Davis group and zeolite research. I am also very grateful to Hubert Koller and Larry Beck for all the time they spent teaching me about solid-state NMR.

A great number of people helped make my personal experience at Caltech most enjoyable. Although the mere mention of everyone's name will take up many pages, recognition of a few extraordinary characters is absolutely necessary. It is hard for me to imagine what time at Caltech would have been like without the novel dimensions added to my life by these individuals. Some of the most notable memories will be of: Alex Katz, his musical talents and culinary expertise; Paul Wagner, his spontaneity and ability to transcend time; the Commander, his global perceptions and his decisive mandates; and Frédéric Vaudry, his tenacity and his passion for life. I am also thankful to Cheryl Anderson for numerous stimulating discussions over various high-calorie desserts; Larry and Dara Beck for many enjoyable dinners and conversations; Chris Dartt for keeping his calm while dealing with my aggressive style of asking harmless

questions; Simon and Leon Yeung for many excellent Chinese dinners; and Cecilia Tse for helping me see the simplicity in seemingly complex things. But most importantly, I am thankful to these individuals for their friendship and support. Additionally, Mehrdad Mahmoudi-Zarandi, Jean-Yves Bouget, Neil Fernandez, Rudy Danner, Peter Seidel, Mike Gordon, Stephen Glade, Mike Vicic, and Clemens Freyhardt have left lasting impressions and will be greatly missed.

Over the past several years, Jennifer Nolan has been an integral part of my life with her love, friendship, support, sense of humor and most importantly, her ability to give and love unconditionally and without the slightest trace of judgment. It is amazing that she is still relatively sane after putting up with me for such a long time.

My sister, Niki, deserves special thanks for never losing faith in me and for passively reminding me of what is important.

Most of all, I want to thank my parents for their unconditional love and support, and the pride they took in my education. The integrity with which they live their lives and the many sacrifices they made for me and my sister have served as guideposts in any venture I have taken. Mom and Dad, with all my heart, I thank you.

ABSTRACT

Zeolite molecular sieves have found extensive applications in ion-exchange, separation and catalytic processes, particularly in the chemical and petroleum industries. Currently, the state-of-the-art in synthesis of high-silica zeolites involves the use of complex organic molecules to direct the formation of zeolitic materials with novel pore structures. While efforts towards preparation of new zeolites using organic molecules as structure-directing agents continues, synthesis of calcium and other alkaline-earth zeolites has not received much attention since the inception of the systematic investigation of zeolite synthesis some 35 years ago. Of the approximate 50 natural zeolites discovered to date, over 20% have eluded synthesis and another 10% have proven exceedingly difficult to synthesize at typical hydrothermal conditions. The overwhelming majority of these zeolites are calcium-dominant. The difficulty encountered in the synthesis of these alkaline-earth zeolites is in direct contrast to their natural occurrence as alteration products of volcanic glasses. Thus, the objective of this work is developing practical methodolgies for the synthesis of alkaline-earth zeolites.

Hydrothermal transformation of perlite (a natural rhyolitic glass) to calcium zeolites is investigated as a first step towards developing synthesis procedures for the preparation of calcium and other alkaline-earth zeolites from pure starting reagents. In particular, synthetic analogues of the calcium zeolites gismondine, heulandite and epistilbite are obtained as alteration products of perlite glass reacting with calcium-containing solutions. The influence of the solution phase species and their concentrations, the pH and the temperature on the distribution of the zeolite products obtained are discussed. It is observed that the crystallization of heulandite from perlite is preceded by the transient formation of a gismondine-type zeolite most similar to the synthetic zeolite P1. This information is exploited to devise methodology for the preparation of zeolite P1 from pure starting reagents and its subsequent conversion to

calcium and other alkaline-earth zeolites upon treatment with solutions containing alkaline-earth cations. Thus, a novel approach for the synthesis of alkaline-earth zeolites based on the hydrothermal conversion of zeolite P1 is developed. Details of the synthesis procedures are enumerated for the preparation of alkaline-earth zeolites CIT-3 (HEU), CIT-4 (BRE), epistilbite (EPI), harmotome (PHI), and yugawaralite (YUG). Transformation of zeolite P1 to alkaline-earth zeolites is governed by factors such as the Si/Al ratio of the starting P1 material, the composition of the solution phase and the presence or absence of seed crystals. The effects of these factors on the products obtained, i.e., phase selectivity, are discussed.

Table of Contents

List of Figures

Chapter One

Chapter Two

Chapter Three

Chapter Four

Chapter Five

Chapter Six

List of Tables

Chapter One

Chapter Two

Chapter Three

Chapter Four

Chapter Five

Chapter Six

List of Publications

"Characterization of the Extra-Large Pore zeolite UTD-1" R. F. Lobo, M. Tsapatsis, C. C. Freyhardt, S. Khodabandeh, P. Wagner, C-.Y. Chen, K. Balkus Jr. S. I. Zones and M. E. Davis, *J. Am. Chem. Soc.* (accepted).

"CIT-4: the First Synthetic Analogue of Brewsterite" S. Khodabandeh, G. Lee and M. E. Davis, *Microporous Mater.* (in press).

"Alteration of Perlite to Calcium Zeolites" S. Khodabandeh and M. E. Davis, *Microporous Mater.* 9 (1997) 161.

"Synthesis of CIT-3: a Calcium Aluminosilicate with the Heulandite Topology" S. Khodabandeh and M. E. Davis, *Microporous Mater.* 9 (1997) 149.

"VPI-8: A High-Silica Zeolite with a Novel 'Pinwheel' Building Unit and its Implications for the Synthesis of Extra-Large Pore Molecular Sieves" C. C. Freyhardt, R. F. Lobo, S. Khodabandeh, J. E. Lewis Jr., M. Tsapatsis, M. Yoshikawa, M. Camblor, M. Pan, M. M. Helmkamp, S. I. Zones and M.E. Davis, *J. Am. Chem. Soc.* **1996**, (118) 7299.

"Synthesis of a Heulandite-Type Zeolite by Hydrothermal Conversion of Zeolite P1" S. Khodabandeh and M. E. Davis, *Chem. Commun.* **1996**, (10) 1205.

"Synthesis of Pure Alumina Mesoporous Materials" F. Vaudry, S. Khodabandeh and M. E. Davis, *Chem. Mater.* **1996**, (8) 1451.

"First-Principles-Derived Dynamics of F_2 Reactive Scattering on Si(100)-2x1" L. E. Carter, S. Khodabandeh, P. C. Weakliem and E. A. Carter, *J. Chem. Phys.* **1994**, (100) 2277.

"Methyl Substitution in Carbenes: Lack of Steric or Hyperconjugative Stabilization Effects on the CH_3CH Singlet-Triplet Splitting" S. Khodabandeh and E. A. Carter, *J. Phys. Chem.* **1993**, (97) 4360.

CHAPTER ONE

Introduction and Objectives

1.1 Introduction

Zeolites are microporous, crystalline, hydrated aluminosilicates with a three-dimensional framework structure composed of TO_4 tetrahedra where T = Si, Al. These tetrahedra are the primary building units in all zeolite structures, and are linked to each other by sharing all of their oxygen atoms. The result is a framework structure exhibiting regularly arrayed pores and cages. The size of the pore opening of zeolites is typically in the range of the size of small molecules (3 - 10 Å) and is often classified using the notation of "n-member" ring, where n = the number of tetrahedral atoms comprising the pore opening. Zeolites possessing 8-, 10-, and 12-member ring pores are well-known and are typically classified as small-, medium-, and large-pore zeolites, respectively. The ring-size of the pore opening is not necessarily limited to 8, 10 or 12, and zeolites possessing 9 and 14-member ring pores are also known. Scheme 1 shows the structure of the natural zeolite, faujasite, which is a large-pore zeolite with a pore openning of about 7 Å and an inside cage diameter of 13 Å.

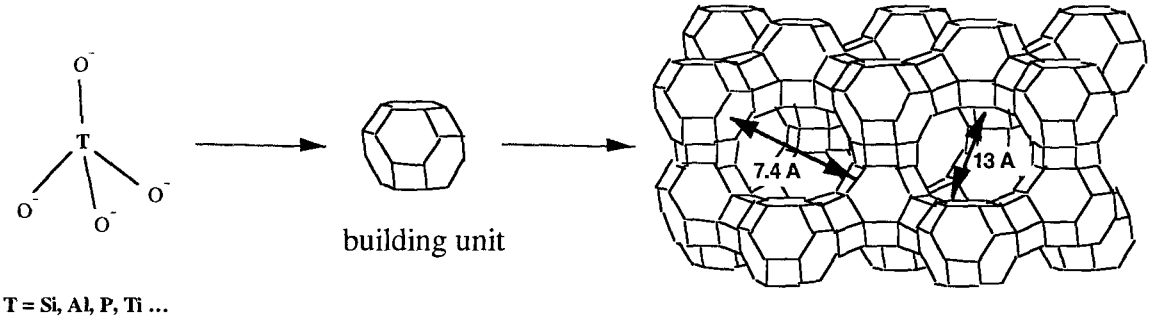

Scheme 1

This scheme illustrates how an extended three-dimensional network of silica and alumina tetrahedra can be pictured as consisting of smaller building units, which themselves can be thought of as a combination of the primary tetrahedra.

All zeolite frameworks are negatively charged due to the substitution of aluminum for silicon in the framework. This negative charge is typically balanced by an extra-framework alkali or alkaline-earth metal cation. Since these cation have a high affinity for water, zeolites are commonly hydrated with mobile water molecules occupying the void space afforded by the pores and cages. Thus, the generic composition of a zeolite is given by

$$M_z N_y[Al_{x+2y}Si_{n-(x+2y)}O_{2n}].mH_2O$$

where, M is a cation of charge 1+ and N is a cation of charge 2+.

Upon heating, the water is desorbed from the framework. The removal of the water from the framework structure of zeolites is often accomplished without any structural change. However, there are some cases when the removal of the zeolitic water results in the collapse of the structure or a phase transformation to a denser material.

Strictly speaking, zeolites are aluminosilicates. On the other hand, a number of framework structures (mostly synthetic) are known also where elements such as Zn, P, Ge, Ga or Be replace some of the Si tetrahedra. The term "molecular sieve" is typically used to denote zeolite-like structure that are not composed entirely of silica and alumina tetrahedra.

Currently, there are about 90 distinct framework structures known. These structures are differentiated solely on the basis of various spatial arrangements of TO_4 tetrahedra and not their chemical composition. A three-letter code is designated by the International Zeolite Association to each distinct molecular sieve framework. Within each framework topology, various chemical compositions may be possible. In Scheme 2, four distinct framework topologies are illustrated. The name of the molecular sieve appears above the structure and the three-letter code identifying the framework topology appears below it. $ALPO_4$-5 is a synthetic aluminophosphate molecular sieve while faujasite is a natural aluminosilicate zeolite. ZSM-5 and zeolite A are two synthetic

aluminosilicate zeolites used extensively for catalysis and ion-exchange applications, respectively.

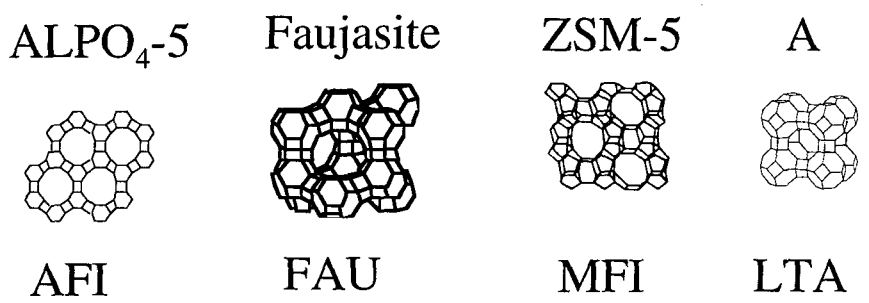

Scheme 2

Due to their high degree of porosity, zeolites and molecular sieves have effective internal surface areas of 300 - 700 m^2/g and sorption capacities in the range of 40 to 160 cc(STP)/g. Because of their well-defined pore openning, zeolites are able to discriminate between molecules of different sizes and allow diffusion of only molecules of appropriate size inside their framework structure. This "molecular sieving" property coupled with the high thermal and chemical stability of zeolites has imparted upon them their importance in a variety of chemical and physical processes. Since 1960, zeolites have found widespread uses in industrial processes such as ion-exchange, separation of gases, and catalysis. Synthetic zeolites are the single most important catalysts in the oil industry, and since their incorporation in the refinery processes, have resulted in an estimated added product value of $15-20 billion per year in the petrochemical industries [1]. A number of reviews on zeolites and molecular sieves and their applications can be found in references [2-4].

Zeolites are naturally occurring minerals and crystallize commonly as a result of alteration of volcanic ashes and glasses as well as clay materials in the presence of saline/alkaline ground water at temperatures ranging from 40 to 300°C. Transformation

of volcanic glasses or clay minerals to zeolites proceeds via dissolution of these materials to produce a solution that is rich in Al, Si, alkali metal, and alkaline-earth metal cations. The supersaturation of this solution with dissolved aluminosilicate species results in the nucleation and precipitation of zeolite crystals. The particular zeolite or zeolites that will crystallize from such a system is determined by such factors as the composition of the starting glass or clay, the composition of the aqueous phase, pH, temperature and the crystallization time.

Nomenclature in the field of natural zeolites is complicated and somewhat controversial. Typically, natural zeolites have been named as minerals bearing the name of a mineralogist or a locality. Often, similar materials with the same framework structure but different composition or locality have been named differently. For example, the two natural minerals heulandite and clinoptilolite have the same framework topology but differ in their chemical composition. Currently, there are over fifty different natural zeolites featuring about 30 distinct structures. Table 1.1 lists the natural zeolites discovered to date along with their typical compositions and the three-letter code that designates their structure. Notice, for example, that garronite, gobbinsite, amicite, and gismondine are all related zeolites with the same maximum framework topology but different chemical compositions. The Si/Al ratio and the dominant extra framework cation are the two characteristics typically used to classify zeolites in terms of their composition. The bold face entries in Table 1.1 denote natural zeolite that have not been synthesized previously.

1.2 Zeolite Synthesis

Synthetic zeolites are commonly prepared from gels or solutions of aluminates and silicates in basic conditions at temperatures ranging from 100 to 200°C. In a typical synthesis, a source of aluminum (e.g. sodium aluminate, aluminum hydroxide, etc.)

and a source of silicon (e.g. amorphous silica, sodium silicate, etc.) are mixed in the presence of a base resulting often in the formation of a gelatinous phase. This gel is subsequently heated at elevated temperatures until it crystallizes into a zeolite. The time required for the formation of zeolites at these conditions ranges from a few hours to a few days. Typical bases used are alkali metal hydroxides as well as organic bases such as quaternary alkyl ammonium hydroxides.

Crystallization of zeolites in hydrothermal systems is affected by factors such as the composition of the initial gel, pH, temperature and the reaction time. The effect of these factors can be both kinetic and thermodynamic. Most of the early work in zeolite synthesis is attributable to Barrer who essentially pioneered systematic zeolite synthesis and devised synthesis methodology for the preparation of synthetic analogues of natural zeolites as well as novel zeolites with no natural counterparts. The bulk of the early work on zeolite synthesis concentrated on preparation methods in the presence of alkali metal cations (Li, Na, K), and numerous experiments mapping out most of the phase space in terms of the composition of the gel, temperature and the reaction time were carried out.

One of the most significant parameters determining the final zeolite obtained (i.e. phase selectivity) is the nature of the cationic species in the solution. It is well-established that the presence of various alkali metal cations in otherwise identical gels results in the crystallization of different zeolites with particular structures being favored by certain cations or a combination thereof [6-8]. For example, the presence of Na^+, K^+, Cs^+ in otherwise identical aluminosilicate gels results in the crystallization of zeolites A, chabazite, and edingtonite, respectively [7].

In 1961, Barrer et al. reported the first synthesis of a zeolite in the presence of an organic base, tetramethylammonium hydroxide [5]. Since then, various organic substances (either bases or neutral molecules) have been used in the synthesis mixture

to crystallize molecular sieve structures. Currently, the state-of-the-art in zeolite synthesis appears to be arriving at novel molecular sieves with structures featuring unique pore sizes and geometries. It is now generally believed that the use of alkali metals such as Li, Na, and K as the sole cations in the synthesis mixture in hope of arriving at new structure is likely to be futile since the early work on zeolite synthesis has essentially covered all simple variations in terms of the composition of the starting mixture, the reaction temperature, and the crystallization time. Rather, the forefront of zeolite synthesis is outlined by efforts utilizing specifically prepared organic molecules to affect the crystallization of zeolites. Organic additives are attractive agents in zeolite synthesis since unlike the inorganic cations, they can be "designed" to have certain properties in terms of their shape and charge-to-size ratio. Hundreds of different organic molecules have been used in zeolite synthesis to date in the hope of crystallizing novel molecular sieves with unique properties. The subtle interactions between various negatively charged silicate, aluminate, and aluminosilicate species in the solution phase and the cations are extremely important in determining what final zeolite will crystallize from a given gel. The organic cations have the ability to organize silicate and aluminosilicate species in the solution phase and thus affect the final framework structure obtained [9-11]. The ability of the cationic species to favor one zeolite structure over another (i.e. phase selectivity) is termed "structure-direction" and the organic molecules that demonstrate this ability are denoted as structure-directing agents (SDA's). Figure 1.1 lists some organic molecules used to crystallize novel zeolites and molecular sieves. This figure is intended merely to give the reader an impression of some typical structure-directing agents (SDA's) and the difficulty inherent in their synthesis. The number of different organic additives used in zeolites synthesis far exceeds the few shown in Figure 1.1.

When synthetic zeolites are made in the presence of organic molecules, after crystallization, the organic is occluded in the cages and/or channels of the framework and must be removed in order for the void space to be accessible for application. The removal of the organic from the framework structure is often only possible by calcination, i.e., heating the zeolite to high temperatures, since the organic-inorganic interactions are often too strong to allow extraction of the organic molecule. Typically, the organic additive is expensive and its preparation requires multistep procedures. As a result, the calcination step after the zeolite synthesis step presents a substantial economic constraint on the type and the amount of zeolite that can be synthesized. Also, the rapid emergence of stricter environmental regulations poses another economic limitation on zeolite synthesis in the presence of organics. As a result, production of zeolites on industrial scales is significantly complicated if an organic additive is needed for the successful synthesis.

Work on synthesis of zeolites using organic structure-directing agents (SDA's) has yielded a number of novel molecular sieves and resulted in a better understanding of the mechanisms of zeolite formation in the presence of organic additives. However, work on "organic-free" synthesis of zeolites is far from complete. Research efforts on the synthesis of novel zeolites in the presence of alkali metal cations has plateaued due to the justifiable belief that it is unlikely to obtain a new structure in the presence of these cations alone. However, very few reports of synthesis in the presence of *alkaline-earth* metal cations are found in the literature. Interestingly, of all natural zeolites known to date, about 30% have either defied synthesis in the laboratory or proven exceedingly difficult to synthesize reproducibly. Some of these zeolites (such as boggsite) are so rare that a rock containing about 0.1 mg of zeolite crystals can cost over $100 while others (such as heulandite) are quite abundant and are readily found in rocks and altered volcanic tuff deposits. What all of these natural zeolites have in

common is that the dominant cation in their composition is an alkaline-earth cation. The crystallization of these structures in nature in the absence of organic molecules clearly suggests the possibility of obtaining them synthetically in the presence of calcium or other alkaline-earth cations without the use of organic additives. Only a handful of studies have been reported on zeolite synthesis from pure starting reagents in the presence of alkaline-earth cations, and some of the most original work can be found in references [13-17].

I believe there are two major reasons why zeolite synthesis in the presence of alkaline-earth cations has not been given much attention in the past. 1) The feasibility of zeolite synthesis in the presence of organic SDA's has offered a new arena for zeolite scientist to engage in efforts towards rational zeolite synthesis. These efforts are justified by recent understanding of some of the mechanisms of zeolite formation involving organization of the inorganic silicate and aluminate species around the organic molecule [11,12]. 2) Synthesis of zeolites at typical hydrothermal conditions in the presence of alkaline-earth cations such as calcium is usually unsuccessful due to the low activity of calcium in basic conditions. In other words, the low solubility of calcium hydroxide (0.74g/l) in water presents a fundamental limit on the alkalinity of the synthesis mixture (roughly a pH of about 12). At low alkalinity conditions, dissolution of the silicon and aluminum sources is considerably slower than it is the case in the presence of alkali metal cations, and this poses a significant obstacle in the synthesis of calcium zeolites under typical hydrothermal conditions. Typical previous work on the synthesis of alkaline-earth zeolites from pure reagents has been carried out under pneumatolytic conditions, requiring pressures as high as 4000 atm and temperatures as high as 450°C. These conditions, although not practical by any means, appeared to circumvent the problem of low solubility of calcium hydroxide encountered in typical hydrothermal syntheses.

1.3 Objectives

As mentioned in the previous section, laboratory synthesis of alkaline-earth zeolites from pure starting reagents has been problematic. While research efforts continue on the synthesis of novel zeolites in the presence of complex structure-directing agents, about 20% of natural zeolites found to date remain unsynthesized. Another 10% have proved exceedingly difficult to synthesize reproducibly. The development of reliable and practical synthesis procedures for the preparation of alkaline-earth zeolites allows for their extended use in separation and catalysis applications. Use of the natural zeolite rather than its synthetic analogue for these applications is limited by i) extreme rarity of some natural zeolites; ii) difficulty inherent in extraction and separation of even those for which a natural supply exists; iii) presence of impurities such as Fe and Ti that can act as poisons in a number of catalysis applications; iv) the almost inevitable presence of salts and oxides within the framework of natural zeolites that render the void space inaccessible unless they are extracted.

The major objective of this work is to develop a practical synthesis procedure for the preparation of the synthetic analogues of alkaline-earth zeolites under "typical" hydrothermal conditions. Conventional methodology utilizing an alkaline-earth-containing aluminosilicate gel has not been successful in the synthesis of calcium and other alkaline-earth zeolites. A new approach for the synthesis of these zeolites is necessary and is presented here. This methodology utilizes zeolite P1, which is a sodium zeolite, as a precursor material for the synthesis of calcium, strontium and barium zeolites. By carefully tailoring the composition of zeolite P1 in terms of its Si/Al ratio and the dominant cation, an appropriate starting material is prepared. Then, this zeolite is treated hydrothermally with aqueous solutions containing alkaline-earth cations. The final product obtained is determined by factors such as the composition of

the starting zeolite P1, the solution composition, pH, reaction time and the presence or absence of seed crystals. Using this approach synthetic analogues of alkaline-earth zeolites heulandite, epistilbite, harmotome, brewsterite and yugawaralite are prepared.

The idea to use zeolite P1 as a starting phase for the preparation of alkaline-earth zeolites originated following an initial investigation on the transformation of volcanic glasses to zeolites. Natural zeolites are very often alteration product of volcanic glasses, and an understanding of the factors that determine what zeolites will crystallize from the glass serves as a first step toward developing synthesis procedures for the preparation of alkaline-earth zeolites. This work is discussed in Chapter 2. In this chapter, alteration of a siliceous volcanic glass to calcium zeolites is discussed. It is observed that during the transformation of the glass to zeolites, a transient zeolite is observed very similar to the synthetic zeolite P1.

In Chapter 3, zeolite P1 is converted to a synthetic analogue of heulandite referred to as CIT-3. Although heulandite is the most abundant zeolite found in nature, it has proven exceedingly difficult to synthesize reproducibly in the laboratory. Chapter 4, further extends this work to the first synthesis of a zeolite with the brewsterite topology, named CIT-4. Chapter 5 presents an overall summary and more details of the conversion of zeolite P1 to various alkaline-earth zeolites, and outlines the most significant factors determining the final product obtained. In Chapter 6, a small group of zeolites (including CIT-3 and CIT-4) that exhibit structural similarities are investigated using infrared spectroscopy in order to determine whether the existence of topological similarities between various zeolites can be deduced a priori from the IR spectra.

1.4 References

[1] J. B. Higgins, *Reviews in Mineralogy*, 29 (1994) 507.

[2] J. M. Newsam, in A. K. Cheetham and P. Day (Eds.), *Solid State Chemistry: Compounds*; Oxford University Press, 1992, pp 234-280.

[3] M. E. Davis, *Ind. Eng. Chem. Res.*, 30 (1991) 1675.

[4] M. E. Davis, *Accounts of Chemical Research*, 26 (1993) 111.

[5] R. M. Barrer and P. J. Denny, *J. Chem. Soc.*, (1961) 971.

[6] A. V. McCormick and A. T. Bell, *Catal. Rev. Ser. Eng*, 31 (1988) 97.

[7] P. K. Dutta, M. Pur and D. C. Shieh, *Mater. Res. Soc. Symp. Proc.*, 111 (1988) 101.

[8] D. E. W. Vaughan, in G. Ohlmann (Ed.), *Catalysis and adsorption by Zeolites*; Elsevier, Amsterdam, 1991, pp 275-285.

[9] S. L. Burkett and M. E. Davis, *Micropor. Mater.*, 1 (1993) 265.

[10] S. L. Burkett and M. E. Davis, *J. Phys. Chem.*, 98 (1994) 4647.

[11] S. L. Burkett and M. E. Davis, *Chem. Mater.*, 7 (1995) 920.

[12] S. L. Burkett and M. E. Davis, *Chem Mater.*, 7 (1995) 1453.

[13] L. L. Ames and L. B. Sand, *Am. Miner.*, 43 (1958) 476.

[14] R. M. Barrer and D. J. Marshal, *J. Chem. Soc.*, 485 (1964).

[15] D. B. Hawkins, *Mat. Res. Bull.*, 2 (1967) 951.

[16] U. Wirsching, *Clays and Clay Miner.*, 29 (1981) 171.

[17] M. Koizumi and R. Roy, *Geology*, 68 (1960) 41..

Table 1.1 Natural zeolites known to date and their three-letter designation.

Zeolite	Composition	Structure-code
Amicite	$K_2Na_2[Al_4Si_4O_{16}].5H_2O$	GIS
Analcime	$Na_2[Al_2Si_4O_{12}].2H_2O$	ANA
Barrerite	$Na_8[Al_8Si_{28}O_{72}].26H_2O$	**STI**
Bikitaite	$Li[AlSi_2O_6].H_2O$	BIK
Boggsite	$Ca_{2.5}Na[Al_6Si_{26}O_{64}].23H_2O$	**BOG**
Brewsterite	$(Sr,Ba)[Al_2Si_6O_{12}].5H_2O$	**BRE**
Chabazite	$(Ca,Na_2,K_2)[Al_2Si_4O_{12}].6H_2O$	CHA
Clinoptilolite	$(Na,K)_6[Al_6Si_{30}O_{72}].20H_2O$	HEU
Cowelsite	$Ca[Al_2Si_3O_{10}].5H_2O$	**unknown**
Dachiardite	$(Ca,Na_2,K_2)[Al_4Si_{20}O_{48}].14H_2O$	DAC
Edingtonite	$(Ba,Ca)_2[Al_4Si_6O_{20}].8H_2O$	EDI
Epistilbite	$Ca[Al_2Si_6O_{16}].5H_2O$	EPI
Erionite	$(Na,K_2,MgCa_{1.5})[Al_8Si_{28}O_{72}].28H_2O$	ERI
Faujasite	$(Ca,Na_2)_{3.5}[Al_7Si_{17}O_{48}].32H_2O$	FAU
Ferrierite	$(Na_2,K_2,Mg,Ca)_3[Al_6Si_{30}O_{72}].18H_2O$	FER
Garronite	$Ca_5Na_2[Al_{12}Si_{20}O_{64}].26H_2O$	GIS
Gismondine	$Ca_2[Al_4Si_4O_{16}].9H_2O$	GIS
Gmelinite	$(Na_2,Ca)_4[Al_2Si_4O_{12}].6H_2O$	GME
Gobbinsite	$Na_3Ca_{1.5}[Al_6Si_{10}O_{32}].12H_2O$	GIS
Gonnardite	$(Na_2Ca)_9[Al_9Si_{11}O_{40}].10H_2O$	NAT
Goosecreekite	$Ca[Al_2Si_6O_{16}].5H_2O$	**GOO**
Harmotome	$Ba_2(Ca_{0.5}, Na)[Al_5Si_{11}O_{32}].12H_2O$	PHI
Heulandite	$(Na,K)Ca_4[Al_9Si_{27}O_{72}].24H_2O$	HEU
Laumontite	$Ca_4[Al_8Si_{16}O_{48}]15.H_2O$	LAU
Levyne	$(Ca,Na_2,K_2)_3[Al_6Si_{12}O_{36}].18H_2O$	LEV
Mazzite	$(K_2,Na_2,Ca)_5[Al_{10}Si_{26}O_{72}].28H_2O$	MAZ
Merlinoite	$(K,Na)_5(Ca,Ba)_2[Al_9Si_{23}O_{64}].24H_2O$	MER
Mesolite	$Na_2Ca_2[Al_6Si_9O_{30}].8H_2O$	NAT
Montesommaite	$(K,Na)_9[AlSi_{23}O_{64}].10H_2O$	MON
Mordenite	$(Na_2,Ca,K_2)[Al_2Si_{10}O_{24}].7H_2O$	MOR
Natrolite	$Na_2[Al_2Si_3O_{10}].2H_2O$	NAT
Offretite	$(Ca,K_2,Mg)_{2.5}[Al_5Si_{13}O_{36}].16H_2O$	OFF
Paranatrolite	$Na_2[Al_2Si_3O_{10}].3H_2O$	NAT
Partheite	$Ca_8[Al_{16}Si_{16}O_{60}(OH)_8].16H_2O$	**PAR**
Paulingite	$(K_2,Ca,Na_2)_5[Al_{10}Si_{32}O_{84}].34\text{-}44H_2O$	**PAU**
Perlialite	$K_9NaCa[Al_{12}Si_{24}O_{72}].15H_2O$	similar to LTL
Phillipsite	$(K_2,Ca,Na_2)_{2.5}[Al_5Si_{11}O_{32}].13H_2O$	PHI
Pollucite	$Ca[AlSi_2O_6].nH_2O$	ANA
Roggianite	$Ca_{16}[Be_8Al_{16}Si_{32}O_{104}(OH)_{16}].19H_2O$	**ROG**
Scolecite	$Ca[Al_2Si_3O_{10}].3H_2O$	NAT
Stellerite	$Ca_4[Al_8Si_{28}O_2].28H_2O$	**STI**
Stilbite	$NaCa_4[Al_9Si_{27}O_{72}].30H_2O$	**STI**
Thomsonite	$Ca_2Na[Al_5Si_5O_{20}].6H_2O$	THO
Tschernichite	$Ca[Al_2Si_6O_{16}].8H_2O$	**BEA**
Wariakite	$(Ca,Na_2)[Al_2Si_4O_{12}].2H_2O$	ANA
Yugawaralite	$Ca[Al_2Si_6O_{16}].4H_2O$	YUG

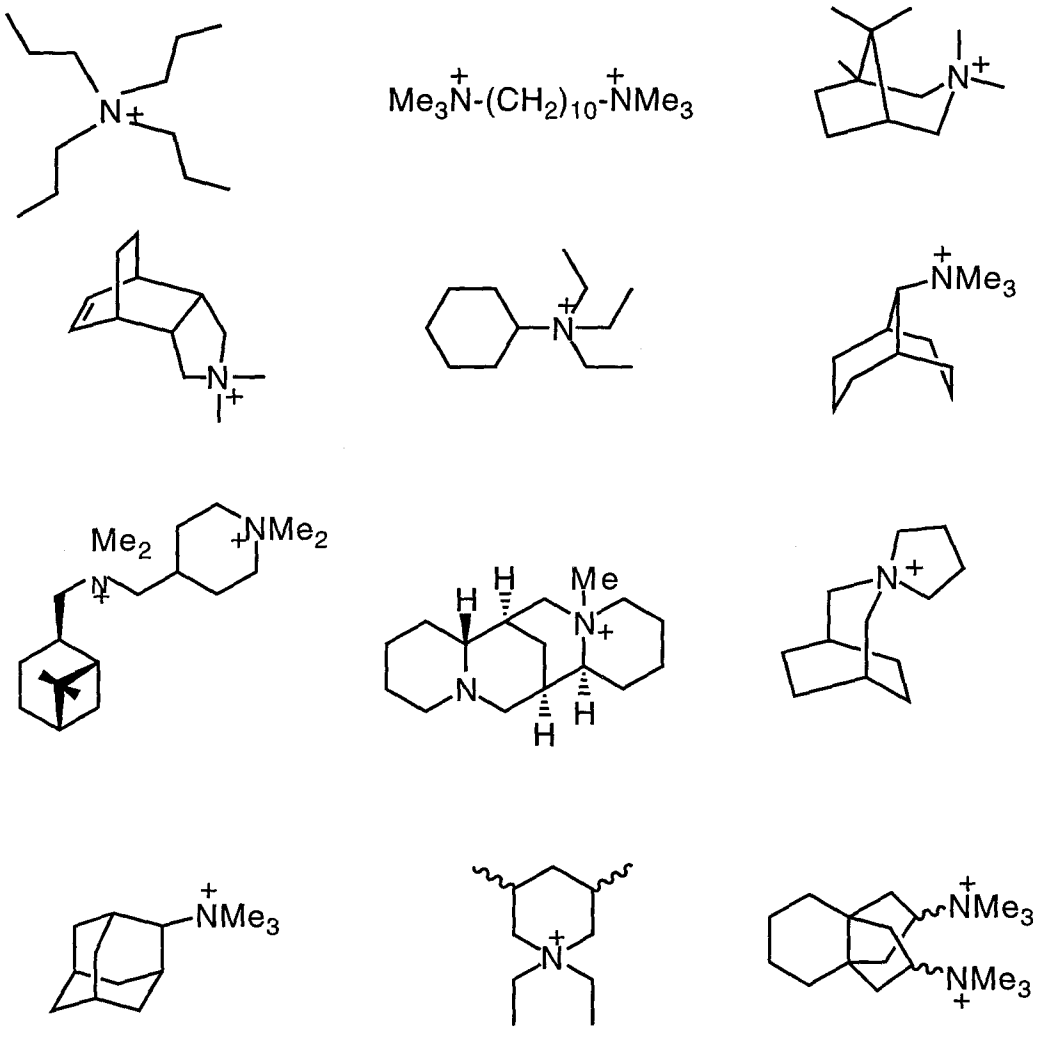

Figure 1.1 Some organic structure-directing agents (SDA's) used in zeolite synthesis.

CHAPTER TWO

Alteration of Perlite to Calcium Zeolites

Reprinted with permission from the article
[S. Khodabandeh and M. E. Davis, *Microporous Mater.* 29 (1997) 161]

Alteration of Perlite to Calcium Zeolites

Shervin Khodabandeh and Mark E. Davis*

Chemical Engineering
California Institute of Technology
Pasadena, CA 91125 USA
Phone: (818)395-4251
Fax: (818)568-8743

Abstract

Hydrothermal synthesis of calcium zeolites via the alteration of perlite (a rhyolitic glass) is presented. Synthetic versions of the zeolites gismondine, epistilbite and heulandite are synthesized from perlite using calcium-containing solutions, and the effects of the solution phase, pH and temperature on the distribution of the zeolitic products obtained are discussed. Transient formation of a gismondine-type zeolite during transformation of perlite to heulandite suggests a novel synthesis route for the crystallization of heulandite-type zeolites from synthetic zeolite P1.

2.1 Introduction

Zeolite molecular sieves have found extensive applications in catalytic and separation processes, particularly in the petrochemical industry [1]. Of over ninety distinct zeolitic structures known today, about 60 arise from synthetic zeolites and phosphate-based molecular sieves with no natural counterparts, while the remainder are structures featured in natural zeolites. If differences in composition (Si/Al ratio, cation type, water content) are considered, over fifty natural zeolites have been identified and, at least partially, characterized [2,3]. Of all the natural zeolites known, a considerable number remain unsynthesized. Table 2.1 lists the natural zeolites that have eluded laboratory synthesis to date. Noteworthy entries are Boggsite [4] which possesses intersecting 10-12 channels and is the only natural zeolite that has pore structure like the synthetic molecular sieves SSZ-26/SSZ-33/CIT-1 [5,6] and tschernichite [7] which is the aluminum-rich, natural analogue of zeolite beta. Synthesis of zeolites featuring 10-12 pore systems in the absence of organic structure-directing agents is likely to allow industrial-scale applications of such molecular sieves.

As evident from the entries in Table 2.1, the majority of unsynthesized, natural zeolites contain calcium as the dominant cation. Although it is conceivable that calcium is incorporated in the void structure of these zeolites via ion-exchange mechanisms after their formation, the possibility that calcium ions play a role in the crystallization of these zeolites can not be ruled out.

Most natural zeolites result from alteration of volcanic glasses at temperatures between 75° and 250°C. Although analogues of most natural zeolites have been synthesized hydrothermally in the laboratory in the presence of alkali metals cations and/or organic structure-directing agents, the synthesis of calcium zeolites, particularly from pure oxides, at typical hydrothermal conditions has been difficult. For example, heulandite-type zeolites (heulandite and clinoptilolite) are the most common natural

zeolites and are widely found in volcanic rocks, altered volcanic rock deposits and deep-sea sediments [3]. However, synthesis of heulandite-type zeolites in the laboratory has proven exceedingly difficult (vide infra). Several analogues of natural zeolites have been synthesized in their calcium form, however these syntheses generally have involved pneumatolytic conditions utilizing temperatures as high as 400°C and pressures in excess of 1000 atm [8-10]. One of the major difficulties related to the synthesis of calcium zeolites is the low activity of calcium ions in basic conditions. Whereas most zeolite syntheses occur at conditions of high alkalinity (pH >13,14), low solubility of calcium hydroxide in water (0.74 g/L) presents a limit (about 12) to the pH of the solution. In highly alkaline systems, formation of an aluminosilicate gel in which the aluminum is incorporated tetrahedrally in the second coordination sphere of silicon often precedes zeolite crystallization. On the contrary, at the lower pH ranges encountered in a calcium system, dissolution of the metal oxides (particularly oxides of aluminum) is considerably slower than it is the case in the presence of alkali metal cations. Therefore, synthesis of calcium zeolites at typical hydrothermal conditions from a physical mixture of metal oxides appears not to be a viable synthesis route due to the low activity of calcium in basic conditions. On the other hand, aluminosilicate glasses provide a substrate in which the alumina and silica are already polymerized into a tetrahedral network. To circumvent problems resulting from low activity of calcium, an "open system" can be used as demonstrated by Wirsching [11]. The idea is to react natural glasses with solutions containing Ca^{2+} and to frequently replace the solution phase so as to replenish the Ca^{2+} ions in the solution and thus mimic the natural formation of zeolites due to the action of flowing saline/alkaline water on glassy tuffs.

Formation of zeolites from glasses at hydrothermal conditions has been the subject of a number of previous studies [11-16]. Here, we focus on the use of perlite glass as a starting material in synthesis of calcium zeolites. An open system is

employed and the effects of solution concentration, pH and temperature on the final alteration products of the glass is discussed. Formation of synthetic versions of the zeolites garronite, epistilbite, heulandite and gismondine, as well as the calcium aluminosilicate, tobermorite are reported. Furthermore, based on the experimental results from the transformation of perlite to heulandite, a novel synthesis route for the crystallization of heulandite-type zeolites is suggested.

2.2 Experimental Section

2.2.1 Phases

Perlite

Perlite is a rhyolitic glass with the molar composition $9.4SiO_2 : Al_2O_3 : 0.5 Na_2O : 0.39 K_2O : 0.12 CaO : 1.2 H_2O + (0.016MgO : 0035 Fe_2O_3 : 0.013TiO_2)$ [17].

Epistilbite

Epistilbite, $Ca_3(Al_6Si_{18}O_{48}).16\ H_2O$, is a calcium-dominant zeolite possessing intersecting channels bound by 10- and 8-ring pores [18]. Epistilbite occurs commonly in vugs of volcanic rocks, and the framework composition of natural samples is very close to the general formula given above [2]. The first report of a synthesis of epistilbite is by Barrer and Denny [19]. Wirsching also obtained epistilbite by simulating an open system during hydrothermal treatment of a rhyolitic glass with $CaCl_2$ solutions [11].

Heulandite

Heulandite is a calcium dominant zeolite with the general formula $(Na,K)Ca_4(Al_9Si_{27}O_{72}).24\ H_2O$, although the Si/Al ratio can vary from 2.5 to 4. Heulandite zeolites feature a two-dimensional pore system consisting of intersecting channels in distinct crystallographic directions bounded by 8 and 10 tetrahedral atoms

[18]. Clinoptilolite is a heulandite-type zeolite that has a Si/Al ratio greater than 4, and a sodium and potassium content such that (Na+K)>Ca [20,21]. Since the natural conditions under which these zeolites are formed, as well as their physical properties, are considerably different, when speaking of their synthesis or their physical properties (as opposed to their topology), heulandite and clinoptilolite should be distinguished from each other.

To date, there are two reported synthesis routes to heulandite. In 1960, Koizumi and Roy reported the synthesis of heulandite from the composition $CaO:Al_2O_3:7SiO_2:5H_2O$ at temperatures between 250°C and 360°C and a pressure range of 15000 to 37000 psi [8]. In 1981, Wirsching obtained heulandite by hydrothermal alteration of rhyolitic glass under the action of $CaCl_2$ solutions at temperatures of 200°C to 240°C and reaction times of around 40 to 80 days [11]. In addition, several syntheses for clinoptilolite have been reported [9,10,22-25].

P1, Garronite and Gismondine

All three of these zeolites have the gismondine (GIS) topology which has a three-dimensional channel system consisting of 8-ring pores [18]. The typical formula for natural garronite is $NaCa_{2.5}(Al_6Si_{10}O_{32}):13H_2O$, while gismondine refers to the calcium form [2]. P1 is the synthetic sodium analogue of the gismondine-type zeolites and typically crystallizes with a Si/Al ratio of 1.5 - 2.7 in a sodium system [26].

Tobermorite

Tobermorite is a calcium-silicate-hydroxide-hydrate with the general formula $Ca_5(OH)_2[Si_6O_{16}].4H_2O$, although Al-containing tobermorite is also common. Tobermorite typically crystallizes in the system $CaO\text{-}SiO_2\text{-}H_2O$ or $CaO\text{-}Al_2O_3\text{-}SiO_2\text{-}H_2O$ [27].

2.2.2 Synthesis

Perlite glass (PA-1000, Johns-Manville) was used as the starting glass phase. Perlite was ground to a particle size of about 50 μm. For the conversion of the glass into zeolites an "open system" was used as discussed by Wirsching [11]. The pulverized glass was reacted with a solution phase in Teflon-lined autoclave reactors at autogenous pressures. After 8 days, the reaction was stopped by quenching the autoclave in cold water. The solid phase was removed by filtration and dried at room-temperature. After analysis (XRD, SEM, NMR, etc.) the solid was placed again in the autoclave and a fresh volume of solution was added. These cycles were repeated generally 8 to 12 times. The solution-to-solid ratio was maintained at 3 : 1 (mL/g). From here on, a "cycle" will refer to an 8-day interval in which the glass and the liquid react at hydrothermal conditions.

For the direct conversion of P1 to heulandite, Ca-P1 was used as the starting material. Ca-P1 was obtained by ion exchange of the sodium form of P1 with 1.0 N $CaCl_2$ solutions (1g zeolite/100 ml solution) at 70 - 80°C overnight (conducted 2x). A typical reaction for the conversion of P1 to heulandite involves reacting 0.2 g of P1 with 10 ml of solution in Teflon-lined autoclaves at 240°C for 16 days. Seeds used were natural clinoptilolite from Hector, CA.

2.2.3 Characterization

X-ray diffraction patterns were recorded on a Scintag XDS 2000 diffractometer using Cu-K$<\alpha>$ radiation. The diffracted beam was detected by a liquid-nitrogen-cooled germanium solid-state detector. The samples were analyzed in the 2θ range 2-51° in steps of 0.03°. Thermogravimetic analyses (TGA) were performed on a Du Pont

951 thermogravimetric analyzer. Typically 10 - 20 mg of sample was heated in air, and the temperature ramp was 1 °C/min. Ion chromatography was performed using a Dionex DX-500 equipped with a CS12 cation column. The scanning electron micrographs (SEM) were recorded on a Camscan series 2-LV scanning electron microscope using an accelerating voltage of 15 kV.

Solid-state NMR spectroscopy was performed on a Bruker AM 300 spectrometer. Samples were packed into 7mm ZrO_2 rotors and spun in air. ^{29}Si (59.63 MHz) NMR spectra were obtained using magic angle spinning (MAS) at spinning rates of 3 - 4 kHz, pulse widths of 4 μs (40° pulse), and recycle delay times of 10 - 30 seconds. Tetrakis(trimethylsilyl)silane was used as the external reference material for ^{29}Si NMR chemical shift determination, and all chemical shifts are reported in ppm relative to TMS. ^{27}Al NMR (78.2 MHz) spectra were measured on samples packed in 4 mm rotors spinning at 8 kHz using 4 μs pulses ($\pi/12$ flip angle). ^{27}Al NMR chemical shifts were referenced to 1M $Al(NO_3)_3$ solution (δ = 0.00 ppm) and are not corrected for second order quadruple effects. Spectral simulation was performed using Bruker Linesim and QNMR software packages.

2.3 Results and Discussions

Zeolitization of glasses reacting in hydrothermal systems is a solution-mediated process and occurs via multiple dissolution-reprecipitation stages. Yang and Kirkpatrick studied reactions of water with glasses and showed that the alteration of the glass is preceded by the incorporation of molecular water into bulk glass and that the dissolution of the glass occurs mainly at the glass-water interface [28,29]. Additionally, three distinct steps of: 1) glass hydration, 2) glass dissolution and 3)

zeolite crystallization have been identified in calorimetric studies of glass alteration [30,31]. Condensation of the aluminosilicate species released into the solution phase during dissolution of the glass results in the formation and precipitation of zeolite crystallites. This process continues until the entire glass has dissolved and converted to zeolite material. The structure and composition of the glass affects its reactivity ,thus, the distribution of the aluminosilicate species in the solution phase. Similarly, the cation composition of the solution phase, the pH and the temperature have strong bearing on the type and the distribution of zeolites obtained.

Zeolitization of perlite under the action of aqueous calcium and sodium results in the formation of synthetic versions of the zeolites of epistilbite, garronite, tobermorite, gismondine, and heulandite phases depending on the concentration of the solutions, pH and temperature as discussed below.

2.3.1 Formation of epistilbite from perlite

Figure 2.1 shows a typical series of XRD patterns illustrating the zeolitization of perlite in contact with a 0.01 N $CaCl_2$ and 0.9 mN NaCl solution over 9 cycles (72 days) at 240°C. Perlite was allowed to react with the solution phase in 8-day intervals. After each 8-day cycle, the solution phase was analyzed by ion-chromatography and the reaction resumed with freshly-prepared solution of the original composition. As illustrated by the data in Figure 2.1, the glass remains XRD-amorphous for the first 24 days of the treatment. By the end of the fourth cycle (32 days), some crystallinity is observed. From that time forward, the XRD peak positions remain the same while the peaks increase in intensity, and the broad amorphous peak from the glass gradually disappears as the glass is converted to zeolite. The greatest change in the extent of crystallinity of the solid phase is observed between the 40th and 48th days (5th and 6th

cycle). The alteration product for this case is a mixture of two phases, epistilbite and garronite, as identified by XRD.

During the hydrothermal treatment of glasses with saline/alkaline waters, considerable transfer of cations between the solution phase and the solid phase may take place. An example of such transfer for the case discussed above is given in Figure 2.2a which shows the ion-composition of the solution phase after each cycle. These data essentially depict an ion-exchange process whereby the composition of the solid phase changes substantially over each 8-day cycle. The exchange of sodium and potassium in the solid phase for calcium in the solution phase is evident. The incorporation of calcium into the solid phase is most pronounced between the 2nd and 5th cycles, and is approaching completion by the 10th cycle. By the end of the 5th cycle, the sodium and potassium contents of the solid phase have been reduced to about 30 and 50% of their initial values, respectively [32]. After the 5th cycle, the concentration of Ca^{2+} in the solution phase begins to increase, and this is coincident with the sudden increase in the crystallinity of the solid phase observed in Figure 2.1. These results appear to indicate that a substantial precipitation of epistilbite and garrontie crystallites occurs when both the solution and the solid phases are dominated by calcium rather than sodium or potassium.

Since perlite initially contains near-equal amounts of K^+, Na^+, and Ca^{2+} and considering that the initial concentration of the solution phase is only 0.01 N in $CaCl_2$, the great extent of exchange of calcium during the first 5 cycles (as evidenced by relatively low concentration of Ca^{2+} in the solution phase) indicates a higher affinity of the solid phase for this cation as compared to sodium and potassium. This is in contrast to the case where the solution phase is 0.01 N in NaCl as shown in Figure 2.2b. A comparison of Figures 2a and 2b reveals that the extent of removal of K^+ and Na^+ from the glass is much higher when the solution phase is $CaCl_2$.

If the calcium concentration of the solution phase is raised to 0.1 N or to 1.0 N while the pH is maintained below 8, epistilbite is obtained as the only crystalline phase. Figure 2.3 shows a series of XRD patterns depicting the transformation of perlite to epistilbite via reaction with 0.1 N solutions of $CaCl_2$. Figure 2.4a gives the ^{29}Si NMR spectrum of synthetic epistilbite. The spectrum contains three relatively broad resonances and strong spinning sidebands indicating a greater degree of local disorder relative to the other zeolitic phases synthesized here (vide infra). The ^{29}Si NMR spectrum of perlite is shown in Figure 2.4d, and is characterized by a broad resonance which envelopes the spectra of the zeolitic phases. The ^{27}Al NMR spectrum of epistilbite (not shown) has a single resonance ca. 55 ppm which corresponds to tetrahedral coordination of aluminum in aluminosilicate materials.

A scanning electron micrograph of the epistilbite obtained from perlite is shown in Figure 2.5a. The bulk of the sample is aggregates of very small crystallites that do not exhibit a clearly definable morphology, although small prismatic crystallites of epistilbite 2 - 3 μm in size can also be observed.

2.3.2 Formation of P1 (gismondine-type) zeolite from perlite

Under the influence of sodium, perlite is typically converted to single or a mixture of phases of analcime (ANA), mordenite (MOR) and P1 (GIS). For low concentrations of Na^+ (< 0.05 N) and low pH values (< 11), P1 is the only alteration product of perlite and the transformation takes place over a period of 6 to 8 cycles (48 to 64 days). At higher sodium concentrations (0.4 to 6.0 N) and pH values higher than 11.0 (11.3 to 12.85), the transformation of perlite to zeolites occurs at much faster rates (2 hrs. to 10 days) such that no replacement of the solution phase is necessary. Table 2.2 summarizes the effects of temperature, sodium concentration, and the pH on

the alteration products of perlite in a sodium-rich environment. As evidenced by the entries in Table 2.2, P1 typically crystallizes at milder conditions while higher temperatures, higher pH ranges, and higher sodium contents favor the formation of mordenite and analcime. The SEM of P1 synthesized from perlite at 120°C is given in Figure 2.5b. In addition to aggregates of P1 crystallites, few elongated mordenite prisms are also observed. The XRD pattern of this phase is shown in Figure 2.6a. The ^{29}Si NMR spectrum of this phase is given in Figure 2.4b and is characterized by 4 well-resolved Q^4 resonances (Q^4 stands for silicon atoms connected to 4 other tetrahedral atoms via bridging oxygens). The 4 observed NMR resonances correspond to silicon atoms with second-neighboring aluminum populations ranging from Si(0Al) through Si(3Al). Simulation of the NMR spectrum using 4 peaks at -93.2 (6.7%), -98.6 (30.5%), -104.0 (48.4%) and -109.8 (14.3%) ppm yields a Si/Al ratio of 3.2±0.1. The ^{27}Al NMR spectrum (δ = 55 ppm) indicates that all the aluminum is tetrahedrally coordinated in this phase. Elemental analysis yields a Si/Al ratio of 3.2 for this material which is consistent with the NMR results.

2.3.3 Formation of heulandite

Perlite was treated with a solution 0.01N in $CaCl_2$ and 0.92 mN in NaOH at 240°C. The small amount of added NaOH raises the pH of the solution to a value of 10.95. Figure 2.7 contains the series of XRD patterns that show the alteration of perlite in this case. Again, no crystallinity observable by XRD is detected until the 4th cycle. By the 5th cycle (40D), a gismondine-like phase can be identified by the XRD peaks. From then on, the position of the peaks remain essentially unchanged until the end of the 7th cycle as the transformation of the glass to this phase goes to completion. By the end of the 8th cycle, minor changes in the two-theta ranges 8-10° and 21-26° are

observable in the XRD pattern. At the end of the ninth cycle (72 D), all of the gismondine-like phase has disappeared and a new phase has emerged. This phase is a heulandite-type zeolite. The ^{29}Si NMR spectrum of the heulandite synthesized from perlite (Figure 2.4c) is characterized by 4 resolved peaks and a small shoulder downfield. The spectrum is simulated using 5 gaussian peaks at -90.0 (1.4%), 94.5 (7.7%), -100.0 (39.3%), -106.5 (43.7%), and -112.3 (7.8%) ppm. These 5 resonances are assigned to Si(3Al), Si(2Al), Si(1Al), Si(1Al), Si(0Al), respectively. Again, no octahedral coordination of aluminum is detected by ^{27}Al NMR spectroscopy (δ = 55 ppm) and the Si/Al ratio of 3.8 determined by elemental analysis is consistent with a value of 3.9±0.1 determined from ^{29}Si NMR spectroscopy. The SEM photographs for heulandite synthesized from perlite at 240°C are given in Figure 2.5c-d. Small flattened crystallites (1 - 3 μm) of heulandite are observed in the electron micrograph. About 95% of the sample reveals a morphology similar to that observed in Figure 2.5c, although scarce larger crystals (10 x10 μm) are also found as shown in Figure2.5d. The coexistence of few larger crystals with the abundant smaller crystals that comprise the bulk of the sample, may indicate variable nucleation times for heulandite during the transformation of perlite. This may suggest that while the majority of the heulandite crystals result from the alteration of the gismondine-type phase, earlier crystallization of heulandite directly from perlite occurs also.

2.3.4 Effects of pH and temperature

To investigate the role of pH and temperature on the distribution of alteration products of perlite, experiments were performed at temperatures ranging from 130 to 240°C using saturated $Ca(OH)_2$ as the solution phase (pH = 12.3). A typical series of XRD patterns showing the reaction of perlite with saturated $Ca(OH)_2$ at 200°C is given

in Figure 2.8. Transformation of the glass to crystalline products proceeds at a faster rate at pH = 12.3 as compared to previously discussed cases where the pH < 11. By the 3rd or 4th cycle, even for the experiments carried out at 175 or 200°C, the broad XRD peak characteristic of the amorphous glass is not observed any longer. Table 2.3 summarizes the results obtained from such experiments. At low temperatures, a gismondine-type phase (G) and tobermorite (T) are detected along with small amounts of calcite (C). Furthermore, for the experiments performed at 200 and 240°C, between the 4th and the 6th cycles (32 days to 48 days), small amounts of heulandite (H) are observed by XRD (Figure 2.8). However, heulandite does not remain in the solid phase with further treatment, and by the end of the 7th cycle, completely disappears (based on the XRD patterns only). This is in contrast to the case shown in Figure 2.7 where it is observed that the gismondine-like phase is fully converted to heulandite in the presence of Ca^{2+} at a pH of 10.9. Thus, although nucleation/crystallization of heulandite from perlite (or gismondine) is possible in the presence of calcium at temperatures of 200 to 240°C, the transformation of gismondine to heulandite as observed in Figure 2.7 does not occur at high pH. At higher pH, tobermorite appears to be the stable phase, and by the ninth cycle it is the dominant phase at all temperatures explored except at 130°C (probably due to slower kinetics at lower temperatures).

The alteration products of perlite at 240°C with different concentrations of Ca^{2+} and Na^{+} are presented in Table 2.4. Formation of heulandite is observed in two instances but the complete conversion of the gismondine phase to heulandite is only obtained at a pH value of 10 - 11. Epistilbite forms from perlite at higher calcium activities and near-neutral pH. We note that although the pH of the solution has an effect on the final alteration products, varying the pH from 7 to 11 does not result in a significant increase in the rate of the alteration; the transformation of the amorphous glass to crystalline zeolite at 240°C generally takes about 8 to 10 cycles. On the other

hand, for experiments carried out at pH = 12.3, the rate of conversion of glass to crystalline products is faster (compare Figure 2.8 with Figures 1, 3 or 7). This indicates that the rate of dissolution of perlite does not appreciably change when the pH is varied from 7 to 11. This interpretation is consistent with the solubility curves of quartz and amorphous silica as a function of pH [33]. These curves typically show a constant low value of solubility at low pH and a sharp increase of several orders of magnitude in the solubility at a critical pH value (between 10 and 12) depending on the nature of the silica polymorph.

2.3.5 Synthesis of a heulandite-type zeolite from P1

The transformation of the gismondine-like phase to heulandite as shown in Figure 2.7 is interesting. If the phase preceding heulandite can be synthesized via an alternate route at shorter times, then conversion of this phase to heulandite could provide a new synthetic route to heulandite. Based only on the XRD pattern (Figure 2.7), the phase preceding the formation of heulandite is identified as a gismondine-type phase most similar to the synthetic zeolite P1. Thus, we attempted synthesis of a P1-type zeolite from perlite and the subsequent conversion of this phase to heulandite. Synthesis of a P1-type zeolite from perlite can be accomplished under a variety of experimental conditions with excellent reproducibility as summarized in Table 2.2. Synthesis times as short as 2 hours can be sufficient for the preparation of P1 from perlite using 0.8 M sodium carbonate with a liquid to solid ratio of 10 ml/0.5 g. However, it was found that longer synthesis times and lower temperatures (pH~11.3, T = 110 to 120°C) resulted in materials with higher degrees of crystallinity. Figure 2.6 shows the XRD pattern of a P1 phase synthesized at 120°C compared to the phase preceding heulandite.

The conversion of the P1-type phase to heulandite was attempted as follows. First, P1 was ion-exchanged to its calcium form as detailed in the experimental section. Ca-P1 obtained from perlite was then reacted with a solution of 0.01N $CaCl_2$ and 0.92 mN NaOH at a temperature of 240°C in order to obtain heulandite. No conversion of Ca-P1 to heulandite was observed in the absence of seeds after four 8-day cycles.

The observation that P1 is not converted to heulandite in the absence of seeds is in contrast to the results from perlite that show the conversion of a gismondine-like phase to heulandite without any added seed (section 3.3, Figure 2.7). Given that P1 readily converts to heulandite in the presence of seeds, the above observation may indicate that during alteration of perlite to heulandite, some heulandite crystallites actually formed from unreacted perlite and functioned as seeds for further nucleation and crystal growth. This is consistent with the SEM results presented in Figures 5c and 5d showing the coexistence of larger crystals with well-defined crystal faces and smaller aggregates with less definition. The large crystals could presumably correspond to heulandite formed directly (and slowly) from perlite, while the smaller aggregates represent heulandite crystallized later from the gismondine-type phase. This conjecture also seems consistent with the results given in section 3.4 where heulandite crystallites were observed during alteration of perlite in the presence of $Ca(OH)_2$, but did not continue to grow at the high pH of the system. The hypothesis that part of perlite was converted to heulandite while the rest went on to form P1 is not unreasonable considering the compositional heterogeneity expected for a glass material of natural origin. Thus, it appears that nucleation of heulandite directly from perlite is possible in the presence of calcium and a relatively alkaline environment. In a calcium-dominant system at lower pH, these seeds probably provide nucleation and crystal growth sites promoting the conversion of P1 to heulandite while at higher pH,

tobermorite is the favored product. A more detailed investigation on the crystallization of a heulandite-type zeolite directly from P1 is presented elsewhere [34].

2.4 Summary

Reactions of perlite with calcium-containing solutions results in the crystallization of synthetic versions of calcium zeolites such as epistilbite, gismondine, heulandite, and the dense aluminosilicate mineral, tobermorite. A P1-type zeolites (GIS) is formed at high sodium activities and pH values between 11.0 and 11.5; higher alkalinity typically favors mordenite and analcime in sodium-rich systems, as does higher temperatures. Epistilbite forms from perlite glass at higher calcium activities and pH values below 8. Heulandite is formed also from perlite glass in a calcium-containing system but at a higher pH value of 10.9. Crystallization of heulandite from perlite is preceded by the formation of a gismondine-like phase similar to the synthetic zeolite P1. Based on this observation, a P1-type zeolite is synthesized directly from perlite in a relatively alkaline, sodium-rich system. This phase is subsequently transformed to heulandite via treatment with calcium-containing solutions and added seeds and represents a new route for the synthesis of heulandite-type zeolites.

It appears that the rate of conversion of the glass to zeolite is not substantially influenced by the pH of the system as long as the pH < ~11, although the alkalinity of the solution influences the final zeolites obtained. At 240°C, for the pH range of 7 -11, the first evidence of crystallinity by XRD is typically not observed until the 3rd or 4th cycle. Furthermore, the complete transformation of perlite to zeolite typically takes 8 to 10 cycles at these pH ranges. At the higher pH of 12.3, the alteration of perlite proceeds at a faster rate and by the 3rd or 4th cycle at 175 - 200°C, a substantial portion of the glass has reacted. Note that at the higher alkalinity of the saturated $Ca(OH)_2$ solution, the final product for a range of temperatures is tobermorite whereas for cases

featuring comparable calcium activities but lower hydroxide concentrations, zeolites are always obtained. This may imply a practical limit on the alkalinity of the reaction mixtures used to crystallize calcium zeolites from glasses.

Given the difficulties associated with the crystallization of calcium zeolites at typical hydrothermal conditions, the use of a calcium-rich aluminosilicate glass as a starting phase along with the incorporation of an open reaction system represents a promising route to the synthesis of calcium zeolites. Perlite and other natural glasses contain relatively large amounts of impurities such as iron and titanium. Furthermore, the cation composition and the Si/Al ratio of natural glasses are fixed. Thus, use of synthetic calcium aluminosilicate glasses, where the Si/Al and Ca/Al ratios can be tailored, may prove a viable approach to the manufacture of those calcium zeolites which have defied synthesis to date. We are currently exploring this approach.

Acknowledgement

The authors wish to thank Akzo Nobel for financial support

2.5 References

[1] M. E. Davis, *Ind. Eng. Chem. Res.*, 30 (1991) 1675.

[2] G. Gottardi and E. Galli, *Natural Zeolites*, Springer-Verlag, Heidelberg, 1985.

[3] R. W. Tschernich, *Zeolites of the World*, Geoscience Press Inc., Arizona, 1992.

[4] J. J. Pluth and J. V. Smith, *Am. Miner.*, 75 (1990) 501.

[5] R. L. Lobo, M. Pan, I. Chan, H. X. Li, R. C. Medrud, S. I. Zones, P. A. Crozier and M. E. Davis, *Science*, 262 (1993) 1543.

[6] R. L. Lobo and M. E. Davis, *J. Am. Chem. Soc.*, 117 (1994) 3764.

[7] J. V. Smith, J. J. Pluth, R. C. Boggs and D. G. Howard, *J. Chem. Soc., Chem. Commun.*, 6 (1991) 363.

[8] M. Koizumi and R. Roy, *Geology*, 68 (1960) 41.

[9] D. B. Hawkins, *Mat. Res. Bull.*, 2 (1967) 951.

[10] D. B. Hawkins, R. A. Sheppard and A. J. Gude, in L. B. Sand and F. A. Mumpton (Eds.), *Natural Zeolites: Occurrence, Properties, Use*, Pergamon, Oxford, 1978, pp. 337-343.

[11] U. Wirsching, *Clays and Clay Minerals*, 29 (1981) 171.

[12] P. L. Antonucci, M. L. Crisafulli, N. Giordano and N. Burriesci, *Mater. Lett.*, 3 (1985) 302.

[13] G. Larsen, K.-H. Plum and H. Forster, *Eur. J. Miner.*, 3 (1991) 933.

[14] M. de'Gennaro and C. Colella, *N. Jb. Miner. Mh.*, 8 (1991) 355.

[15] M. de'Gennaro, C. Colella and M. Pansini, *N. Jb. Miner. Mh.*, 3 (1993) 97.

[16] U. Barth-Wirsching, H. Höller, D. Klammer and B. Konrad, *Mineralogy and Petrology*, 48 (1993) 275-294.

[17] Elemental analysis data for perlite is provided by Johns Manville Company.

[18] S. M. Meier and D. H. Olson, *Atlas of Zeolite Structure Types*; 3rd. ed., Butterworth, London, 1992.

[19] R. M. Barrer and P. J. Denny, *J. Chem. Soc.* (1961) 983.

[20] B. Mason and L. B. Sand, *Am. Miner.*, 45 (1960) 341.

[21] J. R. Boles, *Am. Miner.*, 57 (1972) 1463.

[22] L. L. Ames and L. B. Sand, *Am. Miner.*, 43 (1958) 476.

[23] Y. Goto, *Am. Miner.*, 62 (1977) 330.

[24] C. H. Chi and L. B. Sand, *Nature*, 304 (1983) 255.

[25] S. Satokawa and K. Itabashi *Eur. Pat. Appl.* 681 991 (1995).

[26] For a review of P1 syntheses see a) R. Szostak, *Handbook of Molecular Sieves*, Van Nostrand Reinhold, New York, 1992, pp. 351-352. b) D. W. Breck, *Zeolite Molecular Sieves*, John Wiley & Sons, New York, 1973, pp. 276-277.

[27] For more discussion on the formation of tobermorite in calcium aluminosilicate systems see a) T. Mitsuda and H. F. W. Taylor, *Cement and Concrete Researh*, 5 (1975), 203. b) M. W. Barnes and B. E. Scheetz, in B. E. Scheetz, A. G. Landers, I. Older and H. Jennings, *Specialty Cements with Advanced Properties, Proceedings of Materials Research Society Symposium*, Boston, MA, Nov. 1989, MRS, Pittsburgh, PA, 1991, pp. 243-272.

[28] W.-H. A. Yang and R. J. Kirkpatrick, *Geochimica et Cosmochimia Acta*, 53 (1989) 805.

[29] W.-H. A. Yang and R. J. Kirkpatrick, *Am. Miner.*, 75 (1990) 1009.

[30] G. N. Kirov and N. Petrova, in J. Weitkamp, H. G. Karge, H. Pfiefer and W. Holderich (Eds.),*Studies in Surface Science*, Vol. 84, Elsevier, 1994, pp 291-298.

[31] N. Petrova and G. N. Kirov, *Thermochim. Acta.*, 269 (1995) 443.

[32] The cation content of the solid phase after each cycle is estimated by performing a mass balance on the solution phase considering the changes in the concentration of the cations before and after each cycle.

[33] P. M. Dove and J. D. Rimstidt, in P. J. Heany (Eds.), *Reviews in Mineralogy*, Vol. 29, Bookcrafters Inc., Chelsea, MI, 1994, pp. 259-308.

[34] S. Khodabandeh and M. E. Davis, "Synthesis of CIT-3: a calcium aluminosilicate with the heulandite topology," *Microporous. Mater.*, 9 (1997) 149.

Table 2.1 Unsynthesized zeolites.[a]

Name	Structure Code	Composition
Tschernichite	BEA	$Ca_8(Al_{16}Si_{48}O_{128}).64H_2O$
Boggsite	BOG	$Na_3Ca_{7.5}(Al_{18}Si_{78}O_{192}).69H_2O$
Brewsterite	BRE	$(Sr,Ba)_2(Al_4Si_{12}O_{32}).10H_2O$
Goosecreekite	GOO	$Ca_2(Al_4Si_{12}O_{32}).10H_2O$
Roggianite	ROG	$Ca_{16}[Al_{16}Si_{32}O_{88}(OH)_{16}](OH)_{16}.26H_2O$
Stilbite	STI	$NaCa_4(Al_9Si_{27}O_{72}).30H_2O$
Stellerite	STI	$Ca_4(Al_8Si_{28}O_{72}).28H_2O$
Barrerite	STI	$Na_8(Al_8Si_{28}O_{72}).26H_2O$
Paulingite	PAU	$Na_{12}K_{65}Ca_{41}(Al_{162}Si_{500}O_{1344}).705H_2O$
Cowlesite	unknown	$Ca_6(Al_{12}Si_{18}O_{60}).36H_2O$
Partheite	PAR	$Ca_8(Al_{16}Si_{16}O_{64}).16H_2O$

[a] Compositions and the three letter structure codes are taken from W. M. Meier, D. H. Olson and Ch. Baerlocher, *Atlas of Zeolite Structure Types*, 4th ed. Elsevier, 1996, and references therein.

Table 2.2 Alteration products of perlite in a sodium-rich environment.[a]

Na_2CO_3 Conc. (M)	pH[b]	Temperature (°C)	Duration	Results[c]
0.8	11.47	150	5 D	GIS + (MOR)
0.8	12.00	150	5 D	GIS + (MOR)
0.8	12.50	150	5 D	GIS + (MOR)
0.8	12.65	150	5 D	GIS + (ANA)
0.8	12.85	150	5 D	ANA + GIS
0.8	11.47	110	10 D	GIS + amorphous
0.8	11.47	120	10 D	GIS
0.8	11.47	175	5 D	ANA + (GIS)
0.8	11.47	240	2 hr	GIS
0.8	11.47	240	10 hr	GIS + ANA
0.8	11.47	240	1 D	ANA
0.2	11.17	150	5 D	GIS + (MOR)
0.4	11.35	150	5 D	GIS + (MOR)
1.5	11.60	150	5 D	GIS + (ANA)
1.5	11.60	175	5 D	ANA
3.0	11.80	175	5 D	ANA

[a] Reactions were carried out on 0.5 g perlite and 10 ml of solution.
[b] Initial pH of the solution phase. For the case where the sodium carbonate concentration is 0.8 M, pH values higher than 11.47 were achieved by the addition of few drops of NaOH solution.
[c] The phase appearing first is the major phase. Minor phases are denoted in parentheses.
GIS = zeolite P1, ANA = analcime, MOR = mordenite

Table 2.3 Alteration products of perlite reacting with saturated $Ca(OH)_2$ solutions.[a]

Number of Cycles	T = 130°C	T = 150°C	T = 175°C	T = 200°C	T = 240°C
1	---	---	---	---	(G)
2	---	---	---	(G)	G + (T)
3	(C)	(C)	G + (C)	G	G + (T)
4	(C)	(G) + (C)	G + (T) + (C)	G + (T)	G + (T) + (H)
5	C	(G) + C + (T)	G + (T) + (C)	G + (H) + (T)	G + (H) + (T)
6	C + G	G + C + (T)	G + T + (C)	G + T + (H)	G + T + (H)
7	G + (C)	G + C + T	G + T	T + G	T + G
8	G + (C)	T + G	T + G	T + G	T + (G)
9	G + (C)	T + G	T + G	T + (G)	T

[a] Phases given in descending order of abundance. G = gismondine, C = calcite, T = tobermorite, H = heulandite.

Table 2.4 Alteration products of perlite at 240°C.

Ca^{2+} Conc. (mN)	Na^{+} Conc. (mN)	pH	Result[a]
10	---	6.2	EPI + GIS
10	0.9	6.7	GIS + EPI
10	0.9	10.9	GIS--> HEU
26	---	12.3	T + (GIS) + (HEU)
100	---	6.7	EPI
1000	---	6.7	EPI
---	10	10.9	GIS

[a] Phases appear in descending order of abundance. EPI = epistilbite, GIS = gismondine-type zeolite similar in XRD pattern to natural garronite or synthetic zeolite P1, HEU = heulandite, T = tobermorite.

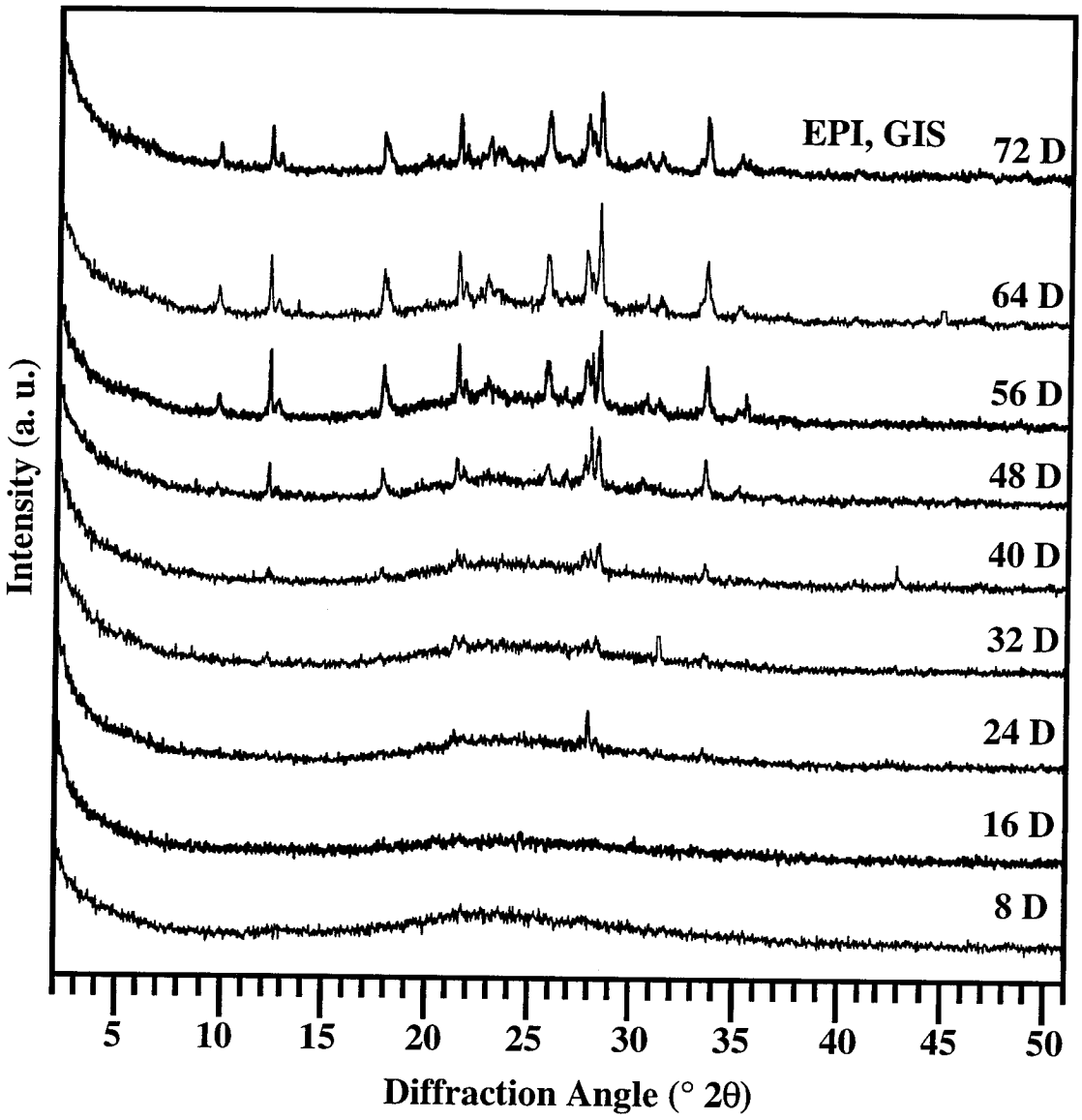

Figure 2.1 XRD patterns showing the transformation of perlite to a mixture of garronite and epistilbite; solution phase: 0.01 N CaCl2 + 0.9 mN NaCl (pH = 6.7). D = days of reaction.

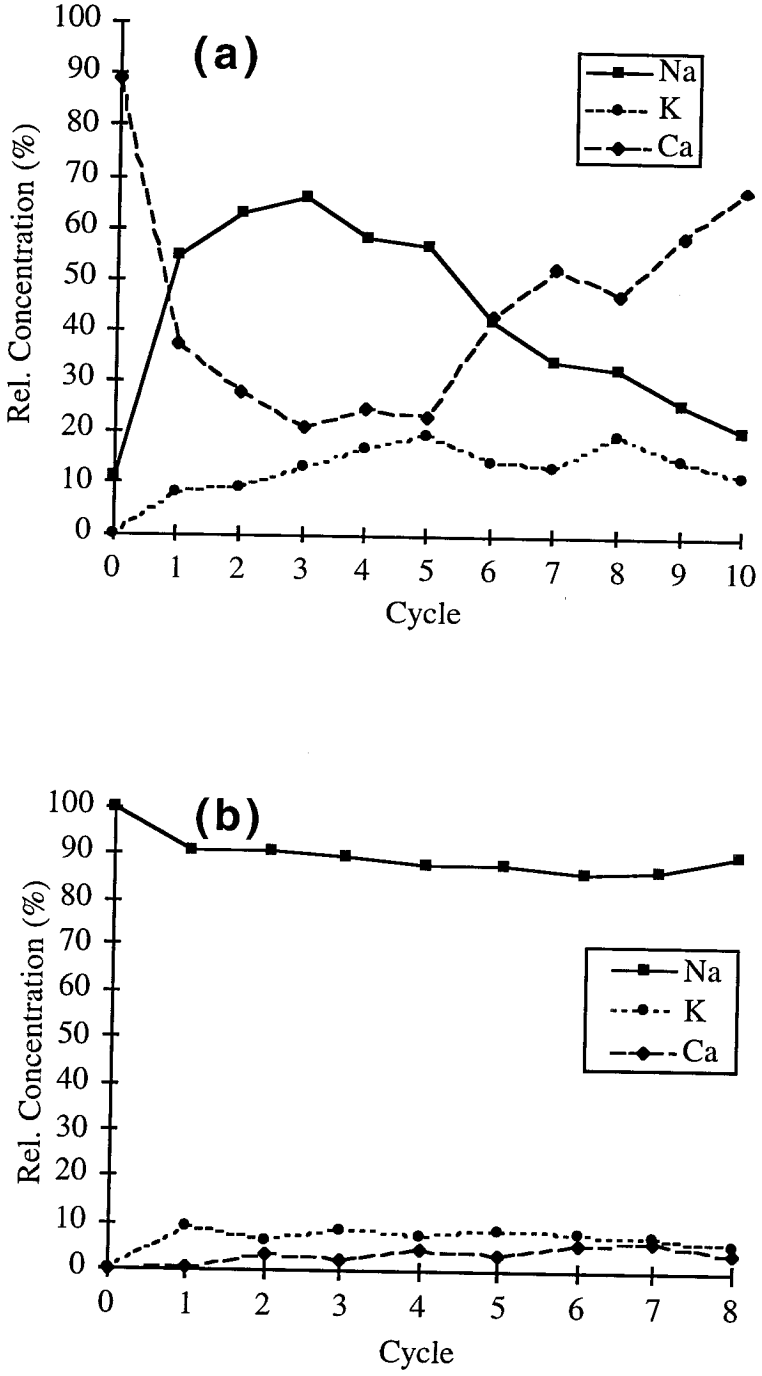

Figure 2.2 Ion concentrations for the solution phase as a function of treaction time of perlite with (a) 0.01 N $CaCl_2$ + 0.9 mN NaCl and (b) with 0.01 N NaCl.

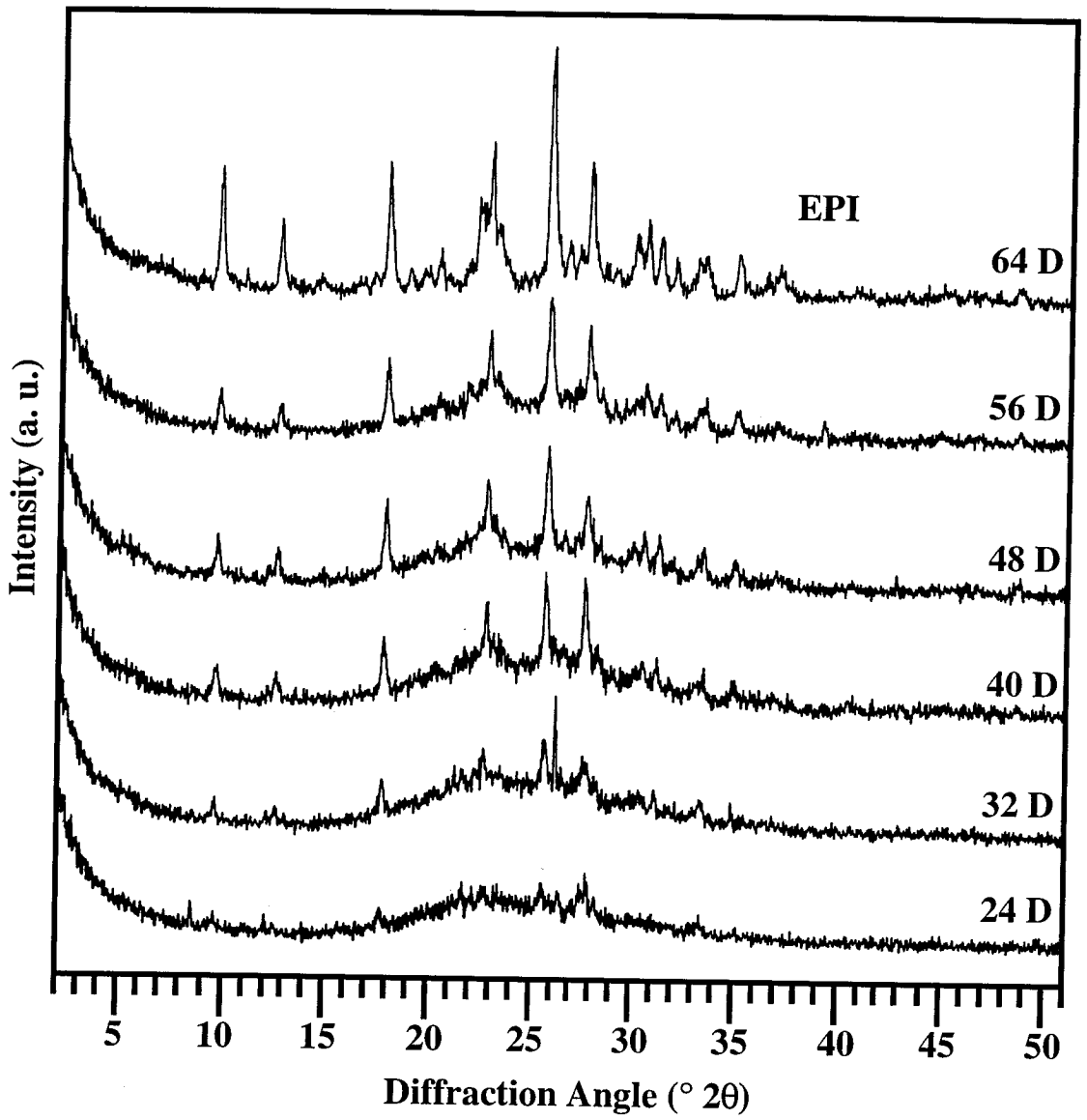

Figure 2.3 XRD patterns showing the transformation of perlite to epistilbite; solution phase: 0.1 N $CaCl_2$. D = days of reaction.

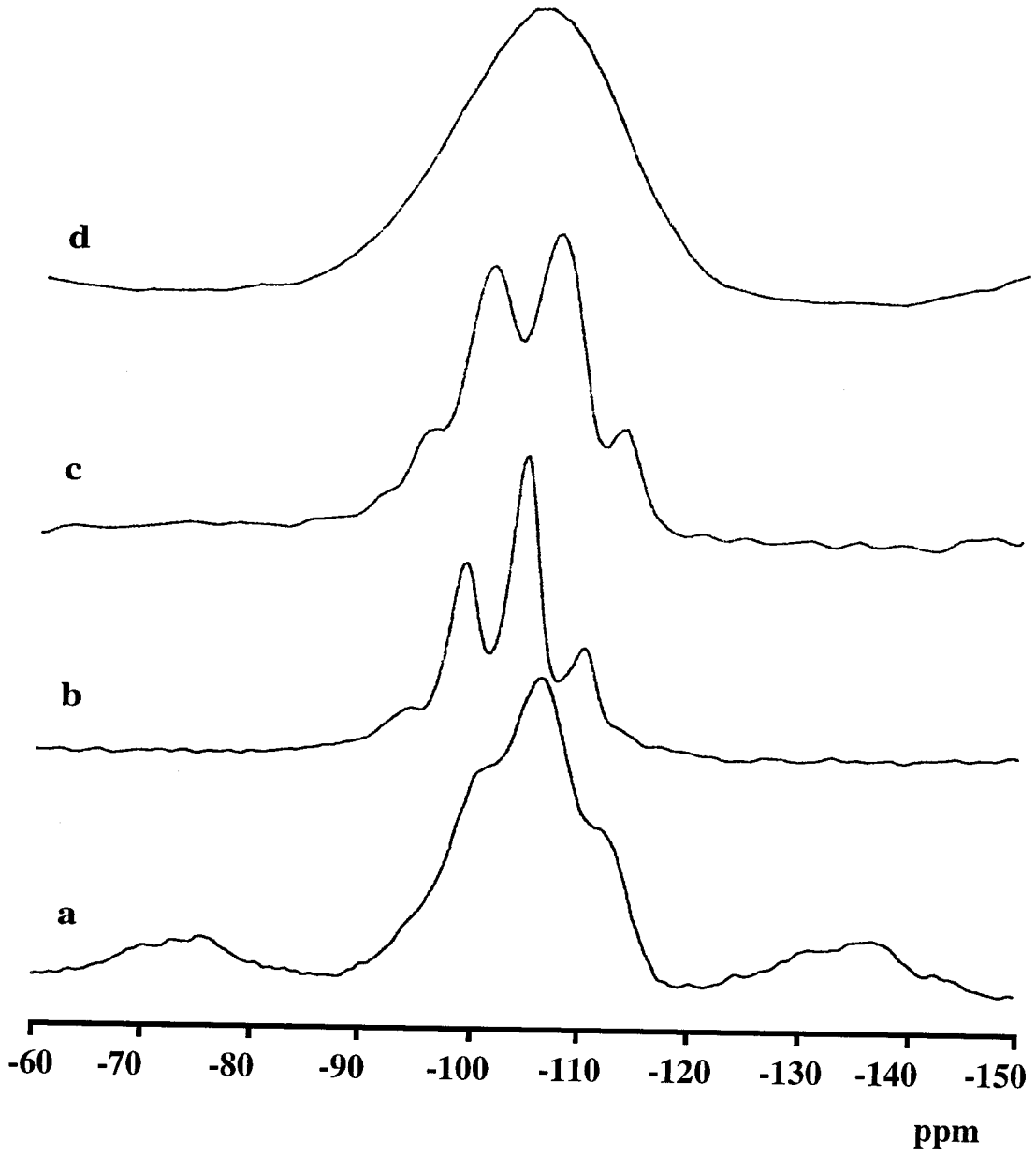

Figure 2.4 ^{29}Si MAS NMR spectra (arbitrary intensity units) for (a) epistilbite, (b) P1, (c) heulandite zeolites synthesized from perlite and (d) unreacted perlite.

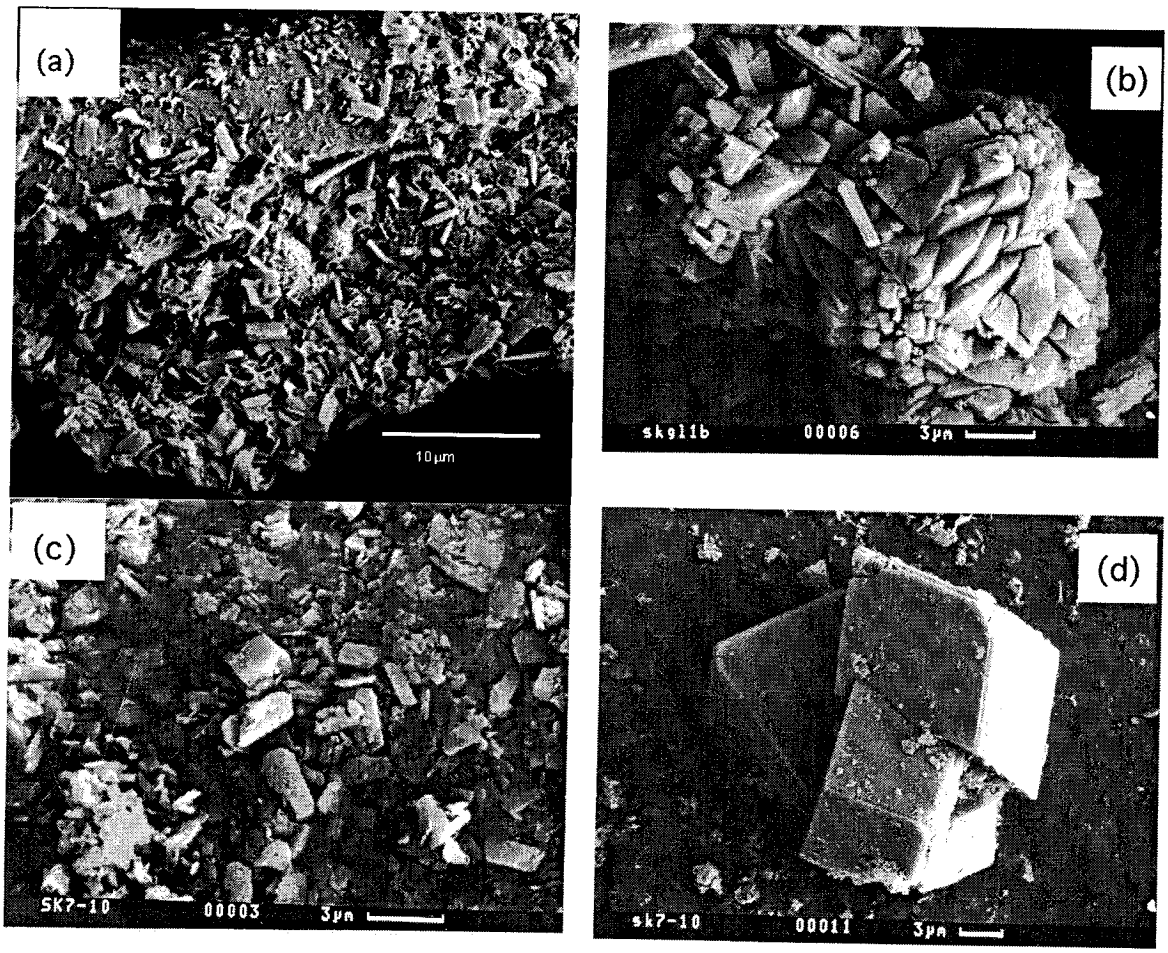

Figure 2.5 Scanning electron micrographs of (a) epistilbite, (b) P1 and (c, d) heulandite synthesized from perlite.

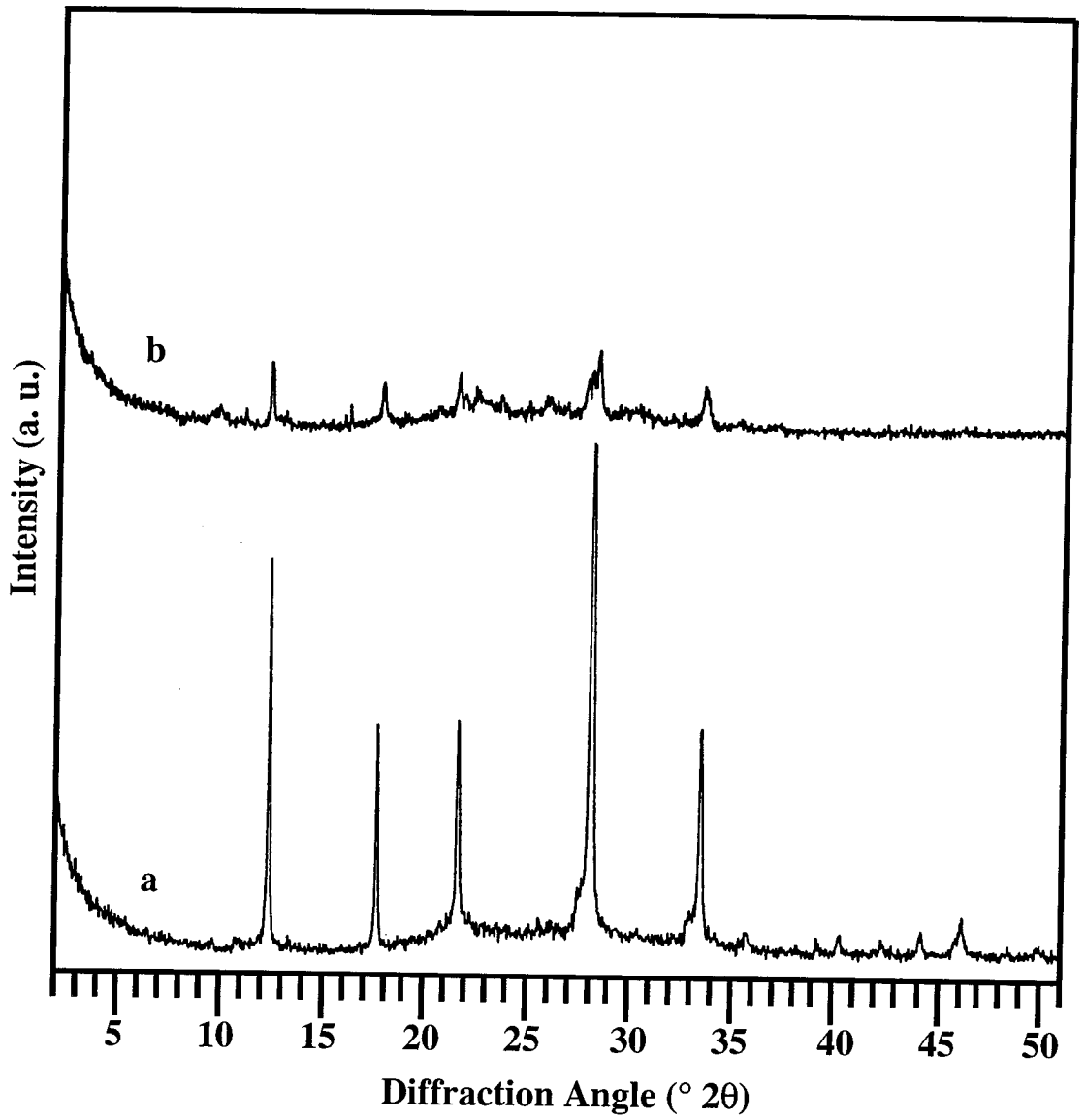

Figure 2.6 XRD pattern of (a) P1 synthesized from perlite and (b) the gismondine-type phase preceeding crystallization of heulandite.

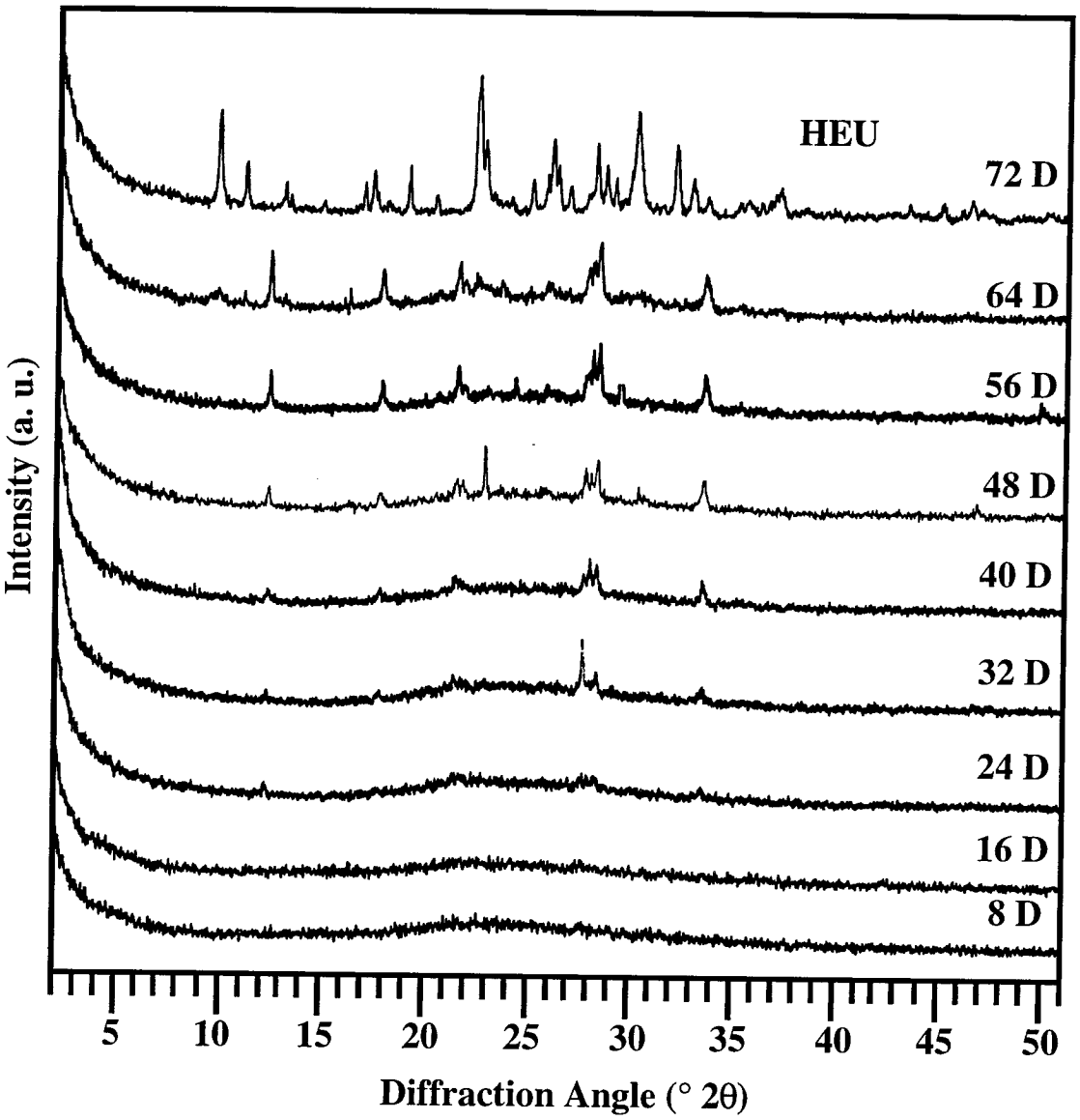

Figure 2.7 XRD patterns showing the transformation of perlite to heulandite; solution: 0.01 N $CaCl_2$ + 0.92 mN NaOH (pH = 10.95). D = days of reaction.

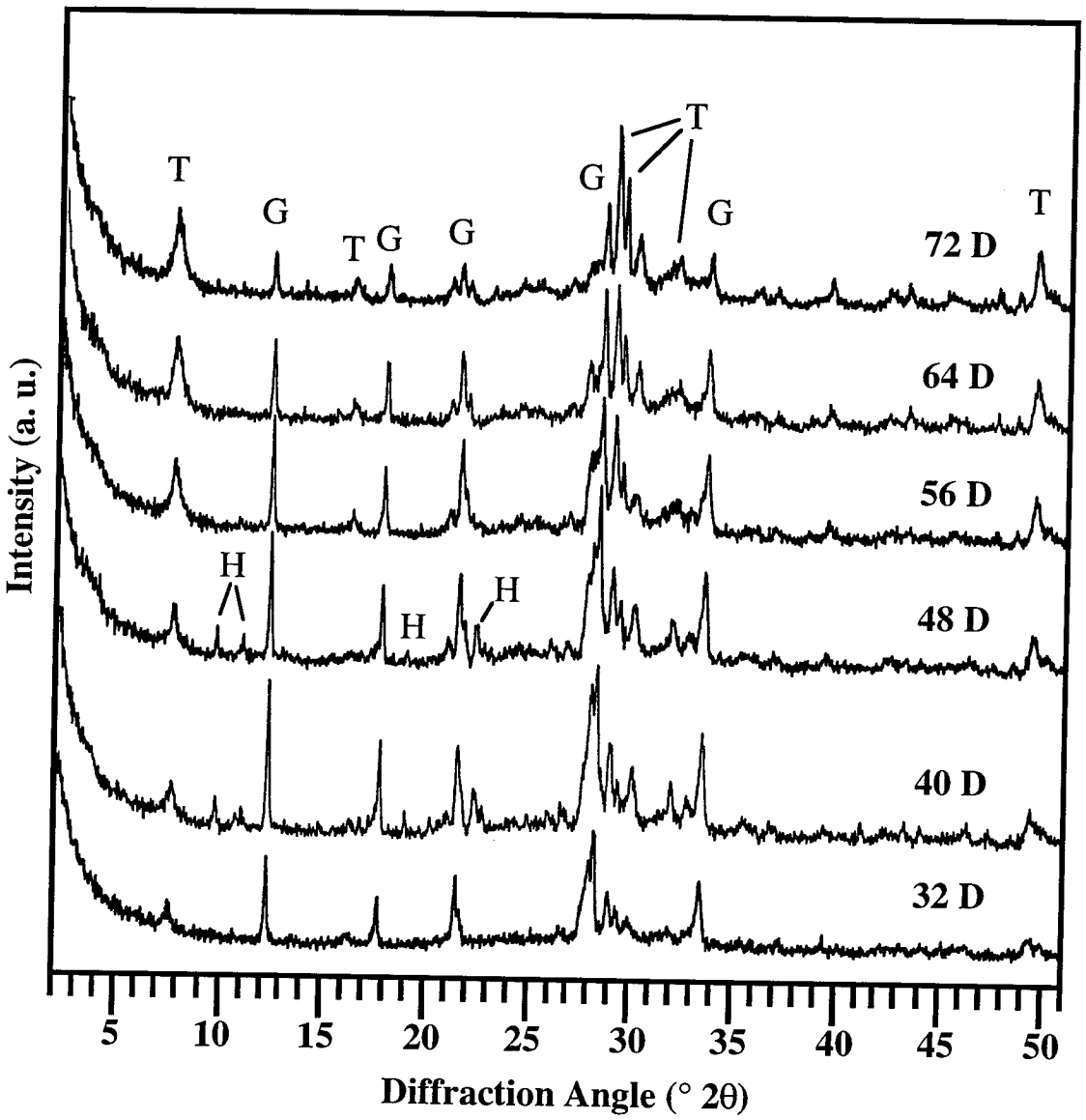

Figure 2.8 XRD patterns showing the alteration of perlite reacting with saturated $Ca(OH)_2$ solutions at 200C°C (pH = 12.3). T = tobermorite, G = gismondine, H = heulandite. D = days of reaction.

CHAPTER THREE

Synthesis of CIT-3: a Calcium Aluminosilicate with the Heulandite Topology

Reprinted with permission from the article
[S. Khodabandeh and M. E. Davis, *Microporous Mater.* 9 (1997) 149]

Synthesis of CIT-3: a Calcium Aluminosilicate with the Heulandite Topology

Shervin Khodabandeh and Mark E. Davis*

Chemical Engineering
California Institute of Technology
Pasadena, CA 91125 USA
Phone: (818)395-4251
Fax: (818)568-8743

Abstract

The synthesis of CIT-3, a calcium aluminosilicate zeolite of composition $CaO : Al_2O_3 : 7 - 7.2\ SiO_2 : 6\ H_2O$ possessing the HEU topology is accomplished by hydrothermal transformation of a specifically-prepared zeolite P1 using calcium-containing solutions and HEU seeds. In the absence of seeds, a synthetic epistilbite phase is obtained. Details of the synthetic methodology necessary for the preparation of CIT-3 are enumerated.

3.1 Introduction

Heulandite-type zeolites (heulandite and clinoptilolite) are the most abundant natural zeolites and are frequently found in volcanic rocks, altered volcanic tuff deposits and deep-sea sediments [1]. However, in spite of their great abundance in nature, synthesis of heulandite zeolites at laboratory conditions has generally been very difficult. The topology of heulandite-type zeolites is characterized by a two-dimensional void structure consisting of pores composed of 8 tetrahedral atoms in the [100] direction that intersect pores composed of 10 tetrahedral atoms in the [001] direction [2]. Heulandite can be distinguished from clinoptilolite on the basis of chemical composition. If the Si/Al ratio ≤ 4 and the cation content is such that Ca > (Na + K), then the zeolite is referred to as heulandite; otherwise, it is called clinoptilolite [3]. Although heulandite and clinoptilolite have the same maximum framework topology, the natural conditions under which they are formed, as well as their physical and thermal properties are markedly different. Natural heulandites and clinpotilolites have found applications in ion-exchange and separation processes [4-7]. However, their use as a catalyst is limited by the presence of relatively large amounts (on the order of 0.5 weight %) of impurities such as iron [3,8] and titanium [9]. Such impurities are commonly found in natural samples as oxides and hydroxides both in the zeolite framework and as other crystalline phases or amorphous tuffs associated with a particular occurrence of the zeolite.

One potential catalytic application of an impurity-free synthetic zeolite with the heulandite topology is that of the isomerization of 1-butene to isobutene as suggested by the recent work of Woo et al.[10]. The development of an efficient catalyst for the production of isobutene could have great industrial implications due to the versatility of isobutene in the manufacture of a number of chemicals particularly that of methyl tert.-butyl ether (MTBE) as an octane booster for gasoline [11].

To date, there are two published synthesis routes to heulandite. In 1960, Koizumi and Roy reported the synthesis of a heulandite-type zeolite from the composition $CaO:Al_2O_3:7SiO_2:5H_2O$ at temperatures between 250°C and 360°C and a pressure range of 15000 to 37000 psi [12]. In 1981, Wirsching obtained heulandite by hydrothermal alteration of rhyolitic glass under the action of $CaCl_2$ solutions at temperatures of 200°C to 250°C and reaction times of around 80 days [13]. Additionally, a few syntheses for clinoptilolite zeolites have also been reported [14-19].

Recently, we have been able to synthesize a heulandite-type zeolite from a natural glass of perlite composition [20]. Perlite (a rhyolitic glass) was converted to a heulandite-type zeolite as a result of periodic treatments with solutions containing Ca^{2+} and Na^{+} at a pH of 10.95. The transformation of perlite to heulandite was carried out in a semi-batch system where after predetermined intervals, the reaction was stopped and the solution phase was renewed. The idea to replace periodically the solution phase in a synthesis mixture with fresh volumes was originally proposed by Wirsching who also reported crystallization of heulandite from a rhyolitic glass [13]. In our work, it was established that the formation of the heulandite-type zeolite from perlite was preceded by the crystallization of a gismondine-type zeolite most similar to the synthetic zeolite P1. The observation of the transformation (glass -> gismondine -> heulandite) led us to pursue synthesis of zeolite P1 from perlite and the subsequent conversion of this zeolite to a heulandite-type phase. Thus, a synthesis route for the preparation of P1 from perlite and the conversion of P1 to heulandite was developed [20]. However, since the starting P1 material was prepared from perlite, it contained the impurities commonly found in natural zeolitic tuffs, and these impurities were found to have been incorporated in the synthetic heulandite-type phase.

In addition to our work on converting perlite to a heulandite-type phase, we were able to synthesize a pure synthetic heulandite-type zeolite by conversion of a

specifically-prepared zeolite P1 [21]. Here, we report the synthetic details on how to prepare the calcium aluminosilicate zeolite with the heulandite topology, denoted CIT-3 (for California Institute of Technology number 3). The synthesis is accomplished via hydrothermal conversion of a specially-prepared P1-type zeolite under the influence of calcium-containing solutions. The effect of solution phase, pH, temperature and seeding are discussed, and it is shown that formation of CIT-3 from another zeolite is specific to zeolite P1 with a very limited range of Si/Al ratios.

3.2 Experimental

3.2.1 Synthesis of the aluminosilicate gel

An amorphous sodium aluminosilicate gel was prepared with the composition 1.0-3.7Na_2O : Al_2O_3 : 9.4 SiO_2 : x H_2O using SiO_2 (Cab-O-Sil, M5) sodium aluminate (Na_2O : Al_2O_3 : $3H_2O$, EM) and NaOH as follows. Two grams of sodium aluminate were dissolved in 60 ml of distilled water. Four grams of a 50% w/w solution of NaOH were added and the resulting mixture was stirred until a clear solution was obtained. 5.2 grams of Cab-O-Sil were slowly added with stirring. The resulting gel was stirred at room temperature for 2 days after which the stirring was stopped and the gel allowed to dry at room temperature for 7 to 10 days. The resulting amorphous aluminosilicate obtained in this way is referred to as "gel-E".

3.2.2 Synthesis of P1 zeolites

Numerous experiments were performed in attempts to prepare a P1 zeolite with Si/Al ratio ≥ 3. P1 was synthesized in two different ways. 1) In a series of syntheses, gel-E (as prepared above) was reacted with 0.4-0.8 M sodium carbonate solutions at temperatures of 110-150°C for 1 to 10 days. The reactions were carried out using

0.30 - 1.0 g of gel-E and 5 - 15 ml of solution in Teflon-lined autoclave reactors at autogenous pressures. 2) An alternate synthesis of P1 with Si/Al $\geq$ 3 was accomplished by adding 0.40 g aluminum trihydroxide (Reheis, F2000) to a solution containing 2.0 grams of 50% w/w NaOH in 10.5 g water. The Si/Al ratio of the starting mixture was controlled by the addition of the appropriate amount of colloidal silica (Ludox, AS-40). The mixture was stirred at room temperature for 3 hours. The resulting gel was transferred to a Teflon-lined autoclave reactor and heated at 150°C for 3-5 days. Using this method, P1 with Si/Al = 3.0 was synthesized from a starting composition of $5.5Na_2O : Al_2O_3 : 15.8\ SiO_2 : 370\ H_2O$ while P1 with Si/Al = 3.2 was made from a starting composition of $5.5Na_2O : Al_2O_3 : 17.5\ SiO_2 : 380\ H_2O$.

Ion-exchange of zeolite P1 was carried out (1g zeolite/100mL solution) using 1.0 N chloride solutions of the desired cation at 70 - 80°C overnight (performed 2x).

CIT-3 was synthesized by the reaction of P1 with calcium-containing solutions at a temperature of 200 to 270°C and a pH of 6.2 - 11.5 in Teflon-lined autoclave reactors for 8 to 24 days. Typically, 0.20 g of P1 was used with 10 ml of the calcium chloride solution. The concentration of the chloride solution was varied between 0.01 and 1.0 N. The pH of the solution phase was typically adjusted by adding a few drops of concentrated NaOH, NH_4OH or $Ca(OH)_2$ solutions. For some experiments, an open system was used as discussed in our recent publication [20] and as first introduced by Wirsching [13]; after each 8-day interval, the solid phase was removed by filtration, the reacting solution phase renewed and the mixture heated again for another 8 days. Seeds used for the synthesis of CIT-3 were natural clinoptilolite from Hector, CA, or CIT-3 prepared from previous syntheses.

3.2.3 Characterization

X-ray diffraction patterns were recorded on a Scintag XDS 2000 diffractometer using Cu-K<α> radiation. The diffracted beam was detected by a liquid nitrogen-cooled germanium solid-state detector. For routine analysis and identification of phases, the samples were analyzed in the 2θ range 2-51° in steps of 0.03°. For the calculation of the unit cell parameters, a long step-scan was taken in the range of 8-60° 2θ with a step size of 0.02° and radiation time of 10 minutes per step. Indexing of the X-ray powder diffraction patterns were performed using the TREOR program.

Thermogravimetic analysis (TGA) was performed on a Du Pont 951 thermogravimetric analyzer. Five to 10 mg of sample was heated in air with a temperature ramp of 10 °C/min. Ion concentrations in the solution phases were determined using a Dionex DX-500 ion chromatography instrument equipped with a CS12 cation column. Elemental analysis was performed by Galbraith Laboratories Inc., TN.

Solid-state NMR spectroscopy was performed on a Bruker AM 300 spectrometer. Samples were packed into 7-mm ZrO_2 rotors and spun in air. ^{29}Si (59.63 MHz) NMR spectra were obtained using magic angle spinning (MAS) at spinning rates of 3.5-4 kHz, pulse widths of 4 μs (40° pulse), and recycle delay times of 10-60 seconds. Tetrakis- (trimethylsilyl) silane was used as the external reference material for ^{29}Si NMR chemical shift determination, and all chemical shifts are reported in ppm relative to TMS. ^{27}Al NMR spectra were recorded at a frequency of 78.2 MHz on samples packed in 4-mm ZrO_2 rotors spinning at 8 - 9 kHz. A pulse width of 4 μs corresponding to a flip angle of 15° along with a recycle delay time of 1 s was used.

^{27}Al NMR chemical shifts are referenced to 1.0 M $Al(NO_3)_3$ solution (δ = 0.00 ppm), and are not corrected for second order quadrupolar effects. Exponential line-broadening of 20 Hz and 50 Hz were applied to the ^{29}Si and ^{27}Al NMR data, respectively. Spectral deconvolution and simulation was performed using both the Bruker Linesim and the QNMR software packages.

3.3 Results and Discussions

3.3.1 Synthesis of P1 with Si/Al ≥ 3.0

For the synthesis of CIT-3 it is crucial that the Si/Al ratio of the starting P1 phase be at least 3.0 (vide infra). Therefore, a substantial portion of this work was devoted to the development of synthesis procedures utilizing reagent grade materials in order to obtain a P1-type zeolite with Si/Al ≥ 3. In general, zeolite P1 is synthesized in a sodium aluminosilicate system from gels or clear solutions. This zeolite typically crystallizes with a Si/Al ratio of ca. 1.6 although syntheses have been reported for this zeolite with a Si/Al = 1.0 to 2.6 [22] and Si/Al = 2.5-3.0 [23]. Our efforts to synthesize a suitable P1 phase as the starting material for the synthesis of CIT-3 involved two synthesis routes. In one approach, a sodium aluminosilicate amorphous gel was prepared as explained in the experimental section. This gel, referred to as gel-E, was reacted with sodium carbonate solutions at temperatures ranging from 110 to 150°C for 1 to 10 days. Table 3.1 summarizes the results obtained from these experiments. Analcime and mordenite commonly crystallized with P1 and this has been noted previously [23,24]. As observed from the data shown in Table 3.1, minor variations in the reaction conditions result in the emergence of small amounts of analcime and mordenite crystallites detectable by XRD. It is extremely crucial that the P1 sample used to synthesize CIT-3 not have any analcime impurities. This is because

at the high temperatures (200-240°C) used to crystallize CIT-3 (vide infra) formation of analcime from P1 is also favored; any impurities of analcime will function as seeds for further growth of analcime and will suppress the formation of CIT-3.

For the cases where P1 is obtained as the only XRD-detectable phase, small variations in the Na content and reaction time or temperature affect the Si/Al ratio of the final zeolite produced. In general, conditions featuring higher sodium contents or higher temperatures along with longer crystallization times lead to higher amounts of impurities. Appropriate conditions for the synthesis of P1 zeolite with Si/Al $\geq$ 3 are given in the last three rows of Table 3.1.

Figure 3.1a shows the XRD pattern of P1 synthesized from gel-E. The ^{29}Si NMR spectrum of this phase is shown in Figure 3.2a and is characterized by 4 well-resolved resonances at -93.3 (8%), -98.6 (32.1%), -104.1(46.9%), and -109.7(14%) ppm. These resonances arise from Q^4 silicon atoms (silicon atoms connected tetrahedrally to 4 other tetrahedral atoms via bridging oxygens). The four resonances observed are assignable to crystallographically identical silicon atoms with various second neighboring aluminum populations as Si(3Al), Si(2Al), Si(1Al) and Si(0Al), respectively. The framework Si/Al ratio can then be calculated by considering the relative intensity of each resonance. For the P1 whose NMR spectra is shown in Figure 3.2a, the Si/Al ratio is 3.0.

Figure 3a shows the ^{27}Al spectrum for Na-P1 made from gel-E. Only one resonance at 55 ppm is observed corresponding to tetrahedrally coordinated aluminum atoms in the framework. Elemental analysis of this material yields a Si/Al ratio of 3.0 consistent with the results from NMR. The agreement between the Si/Al ratios calculated from ^{29}Si NMR and elemental analysis suggests that for this material reliable Si/Al ratios can be determined from ^{29}Si NMR spectroscopy provided that no extra framework aluminum atoms are detected in the ^{27}Al NMR spectra.

An alternate synthesis of zeolite P1 was carried out without the use of a dried gel and utilized colloidal silica as the silicon source and aluminum trihydroxide as the aluminum source (see the experimental section). Zeolite P1 typically crystallized from sodium aluminosilicate gels with composition 5-6Na_2O : Al_2O_3: 14-17 SiO_2 : 370-400 H_2O. The framework Si/Al ratio of zeolite P1 synthesized via this method is 2.8 to 3.2, and varies with the silica content of the starting gel. The XRD pattern for zeolite P1(Si/Al = 3.2) made via this approach is illustrated in Figure 3.1b. The ^{29}Si NMR spectrum of this material is shown in Figure 3.2b and features 4 resonances at: -93.3 (4.9%), -98.6 (31.8%), -104.1 (47.3%), and -109.7 (16%), corresponding to Q^4 silicon atoms with Si(3Al), Si(2Al), Si(1Al) and Si(0Al) coordinations, respectively. The framework Si/Al ratio of this material based on ^{29}Si NMR is 3.2. Figure 3.3b shows the ^{27}Al NMR spectrum for this material, confirming exclusively tetrahedral aluminum atoms in the structure.

3.3.2 CIT-3

CIT-3 is a calcium aluminosilicate that has the heulandite topology. In nature, a continuous series of materials exists between heulandite and clinoptilolite (all possessing the same framework topology) where both the Si/Al ratio and the type and number of cations vary. At one end of the series are heulandite zeolites, which typically feature Si/Al <4 and Ca > (Na + K), while the opposite end is occupied by clinoptilolite zeolites with Si/Al > 4 and Ca < (Na + K) [8]. CIT-3 is a synthetic calcium endmember of the heulandite-type zeolites.

Figure 3.4 shows the powder X-ray diffraction pattern of CIT-3. All reflections are assignable to a zeolite with a heulandite (HEU) structure [3,25]. However, the peak intensities are somewhat different from typical natural heulandite samples which exhibit the highest intensity for the 020 reflection (8.98 Å or 9.84 ° two-

theta). Such minor variations in the peak intensities are probably due to differences in the composition of the CIT-3 compared to the natural heulandite samples. Based on 40 of its most intense reflections, CIT-3 is indexed to a monoclinic unit cell with a = 17.71, b = 17.94, c = 7.42 Å and β = 116°24'. The morphology of CIT-3 is characterized by rhombic prismatic crystals 1-3 microns in size as shown in Figure 3.5.

TGA and DTG data for CIT-3 are shown in Figure 3.6 and are remarkably similar to typical thermal curves obtained from natural heulandite samples featuring a broad DTG peak ca 120°C and a sharper peak ca. 300°C, corresponding to two distinct water losses. This type of thermal behavior is characteristic of natural heulandites and is not observed in natural clinoptilolite which shows a single broad DTG peak centered around 100°C [8]. The overall weight loss up to 620°C for CIT-3 is 13.5%.

Figure 3.7 shows the ^{29}Si NMR spectrum of CIT-3. Four well-resolved resonances and a small downfield shoulder are observed. This spectrum exhibits much better resolution as compared to previously reported NMR spectra for natural heulandite and clinoptilolite zeolites [26,27]. The spectrum is simulated using 5 Gaussian peaks at -88.5 (2.1%), -93.95 (13.3%), -99.62 (34.5%), -105.70 (40.8%) and -111.87 (9.3%) ppm. A zeolite with the (HEU) structure will have a maximum topological symmetry characterized by 5 crystallographically distinct tetrahedral atoms. In theory, each T-site can have a second nearest neighbor coordination ranging from 0 to 4 aluminum atoms. Existence of multiple T-sites, particularly in aluminum-containing zeolites, makes the interpretation and assignment of NMR spectra for these zeolites difficult and ambiguous as compared to the much simpler case with structures featuring only one T site such as zeolites Y, A, and P1.

^{27}Al NMR spectrum for CIT-3 is shown in Figure 3.3c and contains a single resonance at 55 ppm corresponding to tetrahedral coordination of aluminum atoms.

Elemental analysis of CIT-3 yields a bulk Si/Al ratio of 3.6 and a Ca/Al ratio of 0.5. Given the bulk Si/Al ratio, a high concentration of Si(3Al) and Si(4Al) coordinations is not probable and the 5 observed resonances in the ^{29}Si NMR spectrum most likely arise from Si(0Al), Si(1Al) and Si(2Al) environments. In light of the results from elemental analysis and the absence of extra framework aluminum atoms, the ^{29}Si NMR spectrum of CIT-3 can be assigned as presented in Table 3.2. Previously published data for natural heulandite and clinoptilolite are also included for comparison. The framework Si/Al ratio of 3.6-3.7 for CIT-3 determined from ^{29}Si NMR agrees well with the bulk Si/Al ratio of 3.6 from elemental analysis.

3.3.3 Conversion of P1 to CIT-3

The P1 zeolite synthesized with Si/Al $\geq$ 3.0 as discussed above can be converted to CIT-3 via hydrothermal treatment with a calcium-containing solution at temperatures between 200 and 270°C and a pH of 6 - 11.5. A typical synthesis of CIT-3 from zeolite P1 is accomplished using Na-P1 or Ca-P1 (Ca-P1 obtained by ion exchanging the as-made zeolite P1 (Na-P1) with $CaCl_2$) in the presence of seed crystals as reported in the experimental section. For some reactions, an open system was employed as described also in the experimental section. These preparations are denoted in the table as (n x 8-day) where n is the number of times the solution phase was renewed. The renewal of the solution phase is done to replenish the calcium content of the solution phase, particularly for cases where the initial solution concentration is 0.01. Results from a number of experiments carried out at 240°C on Na-P1 and Ca- P1 are summarized in Table 3.3. The XRD data from a typical conversion of P1 to CIT-3 is shown in Figure 3.8 which illustrates the transformation of Ca-P1 to CIT-3 at 240°C using a solution 0.1 N in $CaCl_2$ and 0.002 N in NaOH (overall initial pH = 11) with 5% seeds. It is observed from the XRD patterns in Figure 3.8 that after 8 days, a

substantial amount of CIT-3 is formed from P1 and by the 16th day no P1 is observable by XRD. From the data in Table 3.3, it is clear that CIT-3 crystallizes in relatively calcium-rich systems. When calcium is not present in the reaction mixture, even when 20% seed is used, no CIT-3 is formed and P1 begins to convert to analcime after about 24 days. Furthermore, it is observed that an increase in the total sodium content of the mixture hinders the formation of CIT-3 and promotes the transformation of P1 to analcime, mordenite, or a mixture of both. This is shown in experiments 3, 15 and 16 where even in the presence of 20% seeds no CIT-3 is formed from P1 due to the high relative sodium content of the reacting mixture. No conversion of P1 to CIT-3 is observed in the absence of seeds, although the amount of seeds can be as small as 3%. For lower amount of seeds, crystallization of CIT-3 is completed at longer times (24 to 30 days). Transformation of Ca-P1 to CIT-3 typically takes 16 days at 240°C at a pH between 9 and 11. Renewal of the solution phase is not necessary when the initial calcium concentration in the solution phase is between 0.1 and 1.0 N (experiments 9, 10). When the calcium concentration in the solution phase is reduced to 0.01 N, Ca-P1 is still converted to CIT-3 with one replacement of solution (two 8-day cycles). Without seeds, Na-P1 typically begins to convert to a mixture of mordenite and analcime if the sodium content of the solution is high. Ca-P1 in the absence of seeds is converted to an epistilbite-type zeolite if the calcium concentration is high (experiments 13, 14). Transformation of P1 to epistilbite, a calcium-dominant zeolite for which only few syntheses are reported [13,28], is interesting and will be investigated further elsewhere.

Table 3.4 shows data that illustrate the extents of conversion of Ca-P1 and Na-P1 to CIT-3 after 8 days under various calcium concentrations and Na^{+}/Ca^{2+} equivalence ratios (one mole of calcium is regarded as two equivalents). The extent of conversion is determined as the ratio of the intensity of the (020) reflection of CIT-3 to that of the (110) reflection of P1. The extents of conversion for Na-P1 and Ca-P1 are

different depending on the solution phase and the overall Na^+/Ca^{2+} ratio as shown in data presented in Table 3.4. As evidenced by these data, no marked affect on the extent of conversion of Ca-P1 to CIT-3 is observed when the calcium concentration in the solution phase is varied from 0.01 to 1.0 N while maintaining the initial pH at 11. On the other hand, the extent of conversion of Na-P1 to CIT-3 depends on the calcium concentration in the solution phase. No CIT-3 is formed from Na-P1 when the calcium concentration in the solution phase is 0.01 N. This corresponds to an overall Na/Ca equivalence ratio of 6.5, and as mentioned above, presents too high a sodium concentration for the synthesis of CIT-3. When the calcium concentration is increased to above 0.1 N, the extent of reaction for Na-P1 after 8 days is roughly half of that of Ca-P1. Finally, when the calcium concentration is 1.0 N, the extent of reaction for Na-P1 and Ca-P1 is essentially the same. These results suggest that the conversion of Na-P1 to CIT-3 is preceded by the ion-exchange of calcium for sodium. This hypothesis is supported by the observation that for the conversion of Na-P1 to CIT-3, one renewal of the solution is necessary when the solution phase used is 0.1 N in Ca^{2+} while no replacement of solution is necessary for the case of 1.0 N Ca^{2+} (Table 3.3, expt. 18, 19). For the latter case, the total calcium content of the system is high enough (as evidenced by a Na^+/Ca^{2+} ratio for the complete reaction mixture of 0.07, shown in Table 3.4) to provide a sufficient excess of Ca^{2+} for substantial ion-exchange of Na-P1 to Ca-P1. On the other hand, when the Ca^{2+} concentration of the solution is 0.1 N, the overall contents of sodium and calcium are similar (Table 3.4). Thus, the ion-exchange of Na-P1 to Ca-P1 in this case is probably not as complete within the first 8 days of reaction. After the first 8 days, the solution phase is renewed and thus the overall Na^+/Ca^{2+} ratio is expected to be low enough for the conversion of (Na,Ca)-P1 to CIT-3.

In Table 3.5, various conditions leading to the crystallization of CIT-3 from Ca-P1 are presented. It is shown that the conversion of Ca-P1 to CIT-3 can be accomplished at initial pH values between 6.2 and 11.5. Also, the source of hydroxide ions can be either NaOH, $Ca(OH)_2$ or NH_4OH. Conversions are slower for the cases when the pH is below 9, but do not vary when the pH is changed from 9 to 11.5. Very little conversion of Ca-P1 to CIT-3 is detected in 16 days when the initial pH is increased beyond 12, even though the total calcium content of the solution is such that the overall ratio of calcium to monovalent cations is below 0.01. When the solution phase is saturated $Ca(OH)_2$ at a pH of 12.3, only small amounts of CIT-3 along with some analcime are obtained after 16 days. Given that the concentration of the saturated solution is 0.026 N and recalling that calcium concentrations for the conversion of Ca-P1 to CIT-3 can be as low as 0.01 N (Table 3.3), the low conversion of Ca-P1 to CIT-3 cannot be attributed to the low calcium activity of the $Ca(OH)_2$ solution. In fact, Table 3.5 shows that even when the solution phase is distilled water, a substantial amount of CIT-3 is formed after 16 days suggesting that the overall calcium content in the system is sufficient for the transformation to occur. Thus, it appears that an increase in the pH beyond 12 suppresses the crystallization of CIT-3. One possible explanation for this observation is that there is a dynamic equilibrium between the solid P1 phase and the dissolved aluminate, silicate and aluminosilicate ionic species in the solution (represented by "dissolved species").

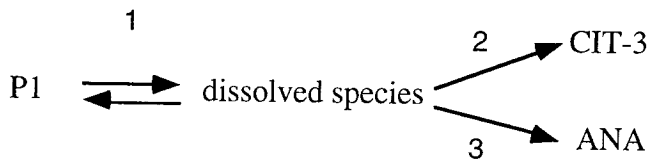

It is reasonable to assume that equilibrium (1) will be shifted more to the right with increasing pH. On the other hand, for the nucleation or crystal growth of CIT-3,

condensation of these species is required and this is represented by reaction (2). Furthermore, analcime also competes with P1 and CIT-3, particularly at higher pH, and this is shown by reaction(3). It is not unlikely that the degree by which the extent of these three reactions are affected as a result of a change in the hydroxide concentration is different. This yields an optimum range of pH values within which dissolution of P1 and its conversion to CIT-3 proceeds to completion.

The effect of temperature in the synthesis of CIT-3 has not yet been thoroughly investigated. Under the same conditions that yield CIT-3 in 16 days at 240°C, CIT-3 crystallizes from Ca-P1 in 24 days at 200°C and in 6-8 days at 270°C. However, CIT-3 obtained at 270°C is typically of lower crystallinity as compared to CIT-3 synthesized at 240°C.

Thus far, we have not been able to successfully carry out the conversion of P1 to CIT-3 when the starting P1 phase has a Si/Al < 3. Table 3.6 summarizes results for CIT-3 synthesis attempts using various starting phases, e.g., P1 with different Si/Al, etc. The synthesis of CIT-3 at the conditions explored here appears to require a starting P1 phase with Si/Al ≥ 3.0. When Ca-P1 or Ca-Y with a framework Si/Al < 3 are used, no CIT-3 is obtained even when the overall Si/Al ratio is increased by the addition of amorphous silica. A faujasite-type phase with a Si/Al =3.5 [29] was also used as a starting material. No conversion of this phase to CIT-3 or any other phases is discerned after three 8-day cycles. Thus, it appears that P1 with a framework Si/Al ≥ 3 is particularly suitable for the synthesis of CIT-3.

Calcium zeolites generally have proven exceedingly difficult to synthesize at laboratory conditions despite their abundance in nature. Typical syntheses of calcium zeolites given in the literature are accomplished either under pneumatolytic conditions (utilizing high temperatures, high pressures and low water content) or via alteration of glasses. Conversion of P1 to a pure calcium endmember heulandite-type zeolite

represents a new approach to the synthesis of calcium zeolites. Transient formation of zeolite P1 in the synthesis of other zeolites has previously been observed in the synthesis of SSZ-13 (a high-silica chabazite), and direct conversion of P1 to SSZ-13 has been accomplished [23]. Currently, we are attempting to extend the transformations of high-silica P1 to other zeolites and to explore the influence of other alkaline-earth metals on the conversion products of P1. Additionally, work on the adsorption, ion-exchange and catalytic properties of CIT-3 is presently under way.

3.4 Conclusions

A calcium aluminosilicate zeolite with the heulandite topology has been synthesized and named CIT-3. CIT-3 has a composition of CaO : Al_2O_3 : 7-7.2 SiO_2 : 6 H_2O and crystallizes via hydrothermal alteration of zeolite P1 using calcium-containing solutions at pH values between 6 and 11.5. Crystallization of CIT-3 is very sensitive to the structure and the Si/Al ratio of the starting phase. Only P1 with Si/Al $\geq$ 3 has been transformed to CIT-3. Seeds of a (HEU) phase are necessary for the conversion of P1 to CIT-3. Additionally, an epistilbite-type zeolite has been synthesized from Ca-P1 in the absence of seeds. Crystallization of this zeolite from P1 suggests that the approach used here to crystallize CIT-3 may prove viable for the synthesis of other calcium zeolites that either have proved difficult to synthesize or have eluded synthesis altogether.

Acknowledgement

The authors wish to thank Akzo Nobel for financial support.

3.5 References

[1] R. W. Tschernich, *Zeolites of the World*, Geoscience Press Inc., Arizona, 1992.

[2] S. M. Meier and D. H. Olson, *Atlas of Zeolite Structure Types*; 3rd. ed., Butterworth, London, 1992.

[3] G. Gottardi and E. Galli, *Natural Zeolites*, Springer-Verlag, Heidelberg, 1985.

[4] L. Predescu, F. H. Tezel and P. Stelmack, in L. Bonneviot and S. Kaliaguine (Eds.), *Studies in Surface Science*; Vol. 97, Elsevier Science, 1995, pp. 507-512.

[5] B. Srinivas and K. Srininvasulu, *J. Indian Chem. Soc.*, 70 (1993) 853.

[6] B. Srinivas and K. Srinivasulu, *J. Indian Chem. Soc.*, 71 (1994) 711.

[7] M. W. Ackley, R. F. Giese and R. T. Yang, *Zeolites*, 12 (1992) 780.

[8] A. Alietti, *Am. Mineral.*, 57 (1972) 1448.

[9] F. Grejták, J. Krajcovic and P. Komadel, *Geologica Carpathica- clays*, 45 (1994) 99.

[10] H. C. Woo, K. H. Lee and J. S. Lee, *Appl. Catal. A*, 134 (1996) 147.

[11] G. J. Hutchings, C. P. Nicolaides and M. S. Scurrell, *Catal. Today*, 15 (1992) 23.

[12] M. Koizumi and R. Roy, *Geology*, 68 (1960) 41.

[13] U. Wirsching, *Clays and Clay Minerals*, 29 (1981) 171.

[14] Ames, L. L., *Am. Miner.*, 48 (1963) 1374.

[15] C. H. Chi and L. B. Sand, *Nature*, 304 (1983) 255.

[16] Y. Goto, *Am. Miner.*, 62 (1977) 330.

[17] D. B. Hawkins, R. A. Sheppard and A. J. Gude, in L. B. Sand and F. A. Mumpton (Eds.), *Natural Zeolites: Occurrence, Properties, Use*; Pergamon, Oxforfd, 1978, pp. 337-343.

[18] S. Satokawa and K. Itabashi,*Eur. Pat. Appl., 681 991* (1995).

[19] D. B. Hawkins, *Mat. Res. Bull.*, 2 (1967) 951.

[20] S. Khodabandeh and M. E. Davis, *Microporous Mater.*, 9 (1997) 161 .

[21] S. Khodabandeh and M. E. Davis, *Chem. Commun.*, 10 (1996) 1205.

[22] For a review of P1 syntheses see a) R. Szostak, *Handbook of Molecular Sieves*, Van Nostrand Reinhold, New York, 1992, pp. 351-352. b) D. W. Breck, *Zeolite Molecular Sieves*, John Wiley & Sons, New York, 1973, p. 276.

[23] S. I. Zones and R. A. Van Nordstrand, *Zeolites*, 8 (1988) 166.

[24] S. Ueda, N. Kageyama and M. Koizumi, *J. Phys. Chem.*, 88 (1984) 2128.

[25] R. von Ballmoos and J. B. Higgins, *Zeolites*, 10 (1990) 414S.

[26] E. Lippmaa, M. Magi, A. Samoson, M. Tarmak and G. Engelhardt, *J. Am. Chem. Soc.*, 103 (1981) 4992.

[27] R. L. Ward and H. L. McKague, *J. Phys. Chem.*, 98 (1994) 1232.

[28] R. M. Barrer and P. J. Denny, *J. Chem. Soc. (Lond)*, (1961) 983.

[29] S. L. Burkett and M. E. Davis, *Microporous Mater.*, 1 (1993) 265.

Table 3.1 Reactions of aluminosilicate gel-E with sodium carbonate solutions[a]. Molar composition of the complete reaction mixture is x Na_2O : Al_2O_3 : 9.4 SiO_2 : y H_2O.

T (°C)	time (d)	conc.[b] (M)	Na_2O	H_2O	Results[c]
110	11	0.8	43	2768	amorphous
130	11	0.8	24	1386	P1 + ANA (10%)
130	11	0.8	43	2768	P1 + ANA (30%)
130	10	0.8	19.6	1110	P1(Si/Al = 2.7)[d]
130	7	0.8	19.6	1110	P1 + amorphous
150	5	0.8	17	926	P1 + ANA (5%)
150	5	0.8	11.7	558	P1 + MOR(3%) + ANA (3%)
150	2	0.8	19.6	1110	P1 + amorphous
150	2	0.4	11.7	1110	amorphous + P1
150	5	0.4	11.7	1110	P1 (Si/Al = 3.0)[d]
150	5	0.4	10.3	926	P1 (Si/Al = 3.0)[e]
150	5	0.4	9.7	834	P1(Si/Al = 3.2)[e]

[a] Reactions were carried out using 0.3 to 1.0 g of gel-E and 5 to 15 ml of Na_2CO_3 solution. Relative Na_2O concentration was controlled by varying the concentration and/or the solid/solution ratio of the reaction mixture.

[b] Starting concentration of the solution phase.

[c] Final products are given in decreasing order of relative abundance based on XRD. ANA = analcime, MOR = mordenite. For quantification of relative amount of impurities, the characteristic XRD intensities of the phases were compared: (211) for ANA, (200) for MOR and (110) for P1.

[d] Si/Al ratio determined by ^{29}Si NMR spectroscopy (no extra framework aluminum is detected by ^{27}Al NMR spectroscopy).

[e] Si/Al ratio determined by ^{29}Si NMR spectroscopy and elemental analysis (no extra framework aluminum is detected by ^{27}Al NMR spcetroscopy).

Table 3.2 ^{29}Si isotropic chemical shifts (vs TMS) for CIT-3, heulandite and clinoptilolite.

Zeolite	$(Si/Al)_{n}$	$(Si/Al)_{bu}$	Si(3Al)	Si(2Al)	Si(1Al)	Si(0Al)
CIT-3	3.6-3.7[a]	3.6	-88.2	-93.5	-99.6 -105.7	-111.9
heulandite[b]	---	3.5	---	-95.0	-99.0 -105.3	-108
clinoptilolite[b]	---	5	---	---	-100.6	-106.9 -112.8

[a] Calculated framework Si/Al ratio varied between 3.6 and 3.7 based on number of spectral simulations with minor variations in peak parameters.
[b] From reference 26.

Table 3.3 Representative synthesis conditions leading to CIT-3.[a]

Expt.	P1 (Si/Al > 3)[b]	Ca^{2+} Conc.[c] (mN)	Na^{+} Conc. (mN)	pH[d]	Seed (% w/w)	Result[e,f]
1	Ca-P1	0	0.9	11	0	P1 + (ANA)+ (MOR)
2	Ca-P1	0	10	12	0	P1 + ANA + (MOR)
3	Ca-P1	0	10	12	10-20	P1 + ANA
4	Ca-P1	10	0.9	11	5-10	CIT-3 (2x8-day)
5	Ca-P1	10	0	6.7	10	CIT-3 (3x8-day)
6	Ca-P1	100	0	6.7	10	CIT-3 (3x8-day)
7	Ca-P1	1000	0	6.2	10	CIT-3 (3x8-day)
8	Ca-P1	10	0.9	11	10	CIT-3 (2x8-day)
9	Ca-P1	100	2.4	11	10	CIT-3 (16-day)
10	Ca-P1	1000	8	11	10	CIT-3 (16-day)
11	Ca-P1	1000	8	11	3 - 5	CIT-3 (16-day)
12	Ca-P1	10	0.9	11	0	P1
13	Ca-P1	100	2.4	11	0	EPI
14	Ca-P1	1000	8	11	0	EPI
15	Na-P1	0	10	11	10-20	P1 + ANA
16	Na-P1	10	0.9	11	10-20	P1 + ANA + MOR
17	Na-P1	100	2.4	11	10	P1 + CIT-3 (16-day)
18	Na-P1	100	2.4	11	10	CIT-3 (2x8-day)
19	Na-P1	1000	8	11	10	CIT-3 (16-day)

[a] In each case, 0.20 g of P1 was reacted with 10 ml of solution at 240°C.
[b] Si/Al = 3.0 to 3.2
[c] Source of Ca^{2+} is $CaCl_2$.
[d] Initial pH of the starting solution; pH adjusted by addition of NaOH.
[e] Phases are given in descending order of relative abundance; parentheses signify products obtained in trace amounts. ANA = analcime, MOR = mordenite, EPI = epistilbite.
[f] The reaction time is given in parentheses: (n x 8-day) represents n 8-day cycles where after each cycle, the solution phase was renewed and the reaction continued, e.g., 2x8-day means the solution was renewed after 8-days and the reaction was carried out for a total of 16 days. For cases where no CIT-3 is obtained, the reaction time is between two and four 8-day cycles.

Table 3.4 Extent of Conversion of P1 to CIT-3.[a]

Type of P1	Ca^{2+} Conc. (N)	pH	$(Na/Ca)_{sol.}$[b]	$(Na/Ca)_{tot.}$[c]	CIT-3/P1[d]
Ca-P1	0.01	11	0.09	0.012	1.2
Na-P1	0.01	11	0.09	6.5	0.0
Ca-P1	0.10	11	0.024	0.015	1.3
Na-P1	0.10	11	0.024	0.66	0.5
Ca-P1	1.00	11	0.008	0.008	1.2
Na-P1	1.00	11	0.008	0.073	1.4
Ca-P1	0.01	6.7	0.0	0.0	0.5
Ca-P1	0.10	6.7	0.0	0.0	0.6
Ca-P1	1.00	6.2	0.0	0.0	0.7
Ca-P1	1.00	9	10^{-6}	~0	1.2
Ca-P1	1.00	10	10^{-4}	~0	1.3

[a] Reactions were carried out at 240°C using 0.20 g of P1, 10% seeds, 10 ml of $CaCl_2$ solution as the source of calcium and few drops of concentrated NaOH solution to adjust the pH.

[b] Ratio of the normality of Na^+ to Ca^{2+} in the starting solution phase.

[c] Ratio of total sodium content to total calcium content in the complete reaction mixture based on equivalents, i.e. one atom of calcium is regarded as two equivalents.

[d] Ratio of the XRD peak arising from the (020) reflection of CIT-3 to that of the (110) reflection of P1.

Table 3.5 Conversion of Ca-P1 to CIT-3.[a]

Ca^{2+} Conc. (N)	Source of OH^-	pH[c]	Results [d]
---[b]	---	6.5	CIT-3 + P1
0.01	---	6.7	CIT-3 + P1
0.10	---	6.7	CIT-3 + P1
1.0	---	6.2	CIT-3 + P1
1.0	NaOH	8	CIT-3 + (P1)
1.0	NaOH	9	CIT-3
1.0	NaOH	10	CIT-3
1.0	NaOH	11	CIT-3
1.0	NaOH	11.5	CIT-3
1.0	NaOH	12.0	P1 + ANA + (CIT-3)
0.026[e]	$Ca(OH)_2$	12.3	P1 + ANA + (CIT-3)
0.10	$Ca(OH)_2$	11.0	CIT-3
0.10	NH_4OH	11.0	CIT-3
0.10	NH_4OH	11.4	P1 + (CIT-3)

[a] Reactions were carried out at 240°C using 0.20 g of Ca-P1, 10% seeds and 10 ml of $CaCl_2$ solution with or without the source of hydroxide.
[b] Distilled water was the solution phase.
[c] Initial pH of the solution phase was adjusted by adding few drops of a concentrated solution of the hydroxide source.
[d] Results are for solids obtained after 16 days of reaction. Phases are given in descending order of relative abundance. Parentheses signify trace amounts of crystalline material.
[e] Solution phase was saturated $Ca(OH)_2$.

Table 3.6 Effect of the structure and the Si/Al ratio of the starting phase on the synthesis of CIT-3.[a]

Starting Phase	$(Si/Al)_{zeolite}$	$(Si/Al)_{total}$	Result[d]
Ca-P1	1.0	1.0	P1
Ca-P1 + silica[b]	1.0	3.0, 3.2[c]	P1 + amorphous
Ca-P1	2.6	2.6	P1 + (ANA)
Ca-P1	2.7	2.7	P1 + (ANA)
Ca-P1 + silica[b]	2.7	3.0, 3.2[c]	P1 + amorphous + (ANA)
Ca-P1	3.0	3.0	CIT-3
Ca-P1	3.2	3.2	CIT-3
Ca-Y	2.4	2.4	Ca-Y
Ca-Y + silica[b]	2.4	3.0, 3.2, 3.5[c]	Ca-Y + amorphous
Ca-Y	2.8	2.8	Ca-Y
Ca-Y + silica[b]	2.8	3.0, 3.2, 3.5[c]	Ca-Y + amorphous
Ca-Y	3.5	3.5	Ca-Y

[a] Reactions were carried out on the starting material with 10% seeds at 240°C. Two reaction were performed for each case; one using 0.1 N $CaCl_2$ (pH = 11) and the other using 1.0 N $CaCl_2$ (pH =11). The pH was adjusted by the addition of concentrated NaOH solution.

[b] Extra silica was used to increase the bulk Si/Al ratio of the starting material. Source of silica was Syloid-63 or Cab-O-sil, M5.

[c] The bulk Si/Al ratio, adjusted by the addition of amorphous silica. For each value of the Si/Al ratio, two reactions were performed as described in a.

[d] Results are given after two 8-day cycles, where after each cycle, the solution phase is renewed.

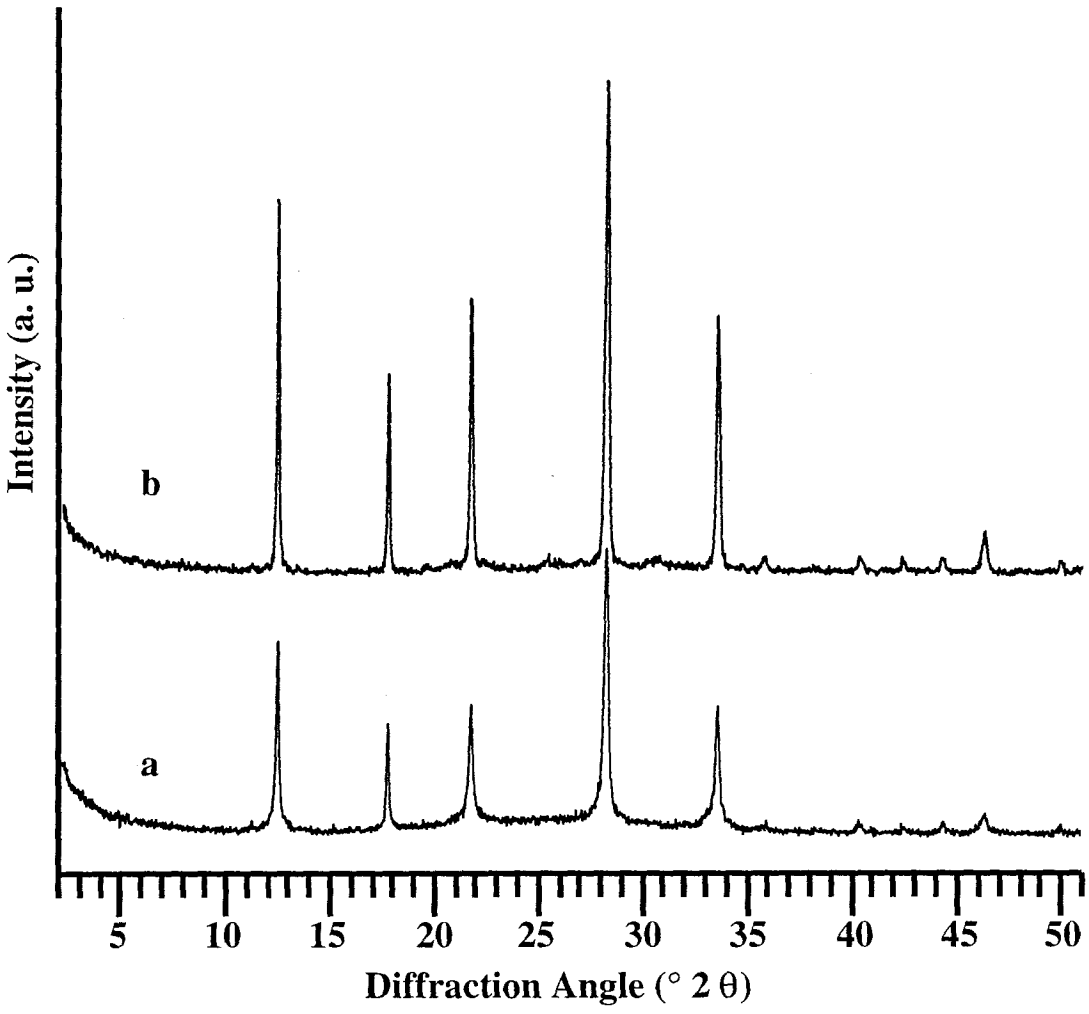

Figure 3.1 Powder X-ray diffraction pattern of (a) P1 synthesized from gel-E, and (b) P1 synthesized from colloidal silica.

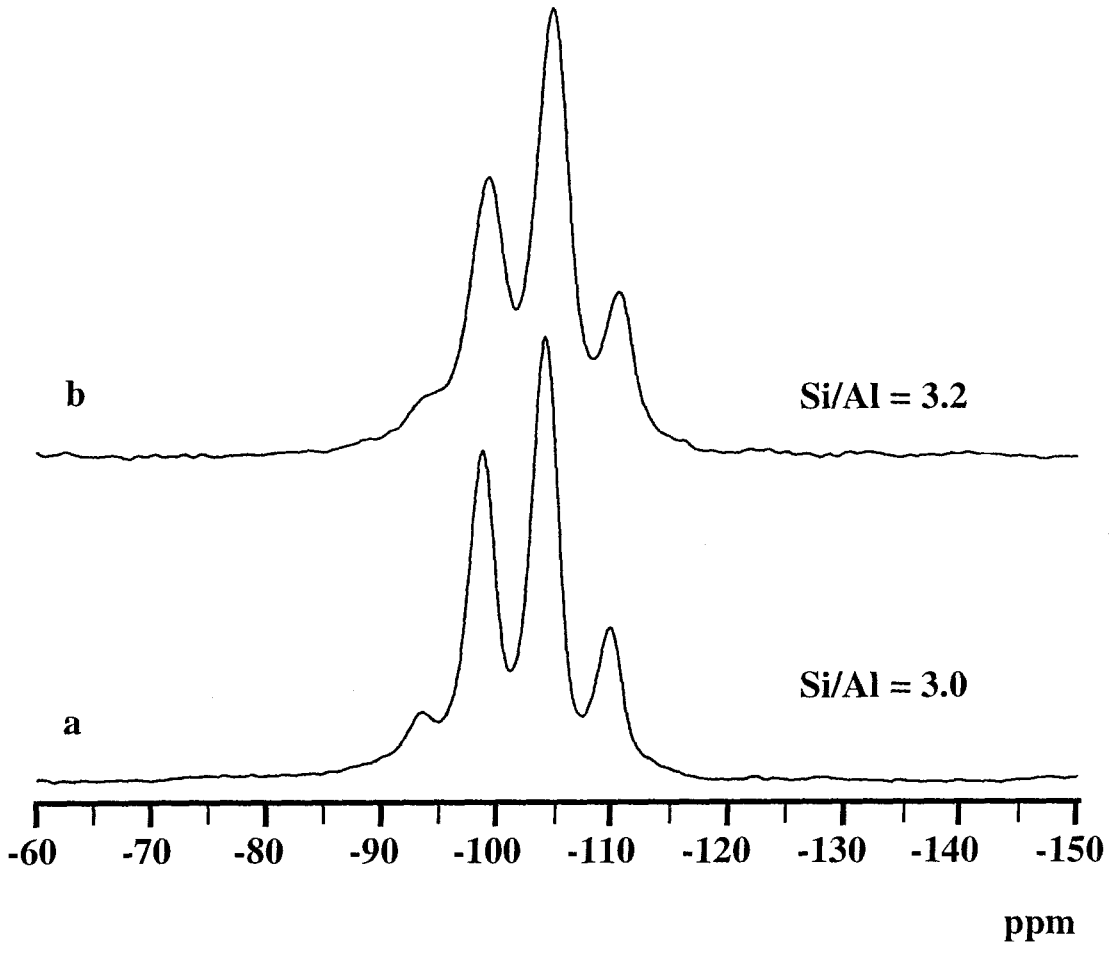

Figure 3.2 ^{29}Si NMR spectra (arbitrary intensity) of P1 prepared from gel-E (a), and from colloidal silica (b).

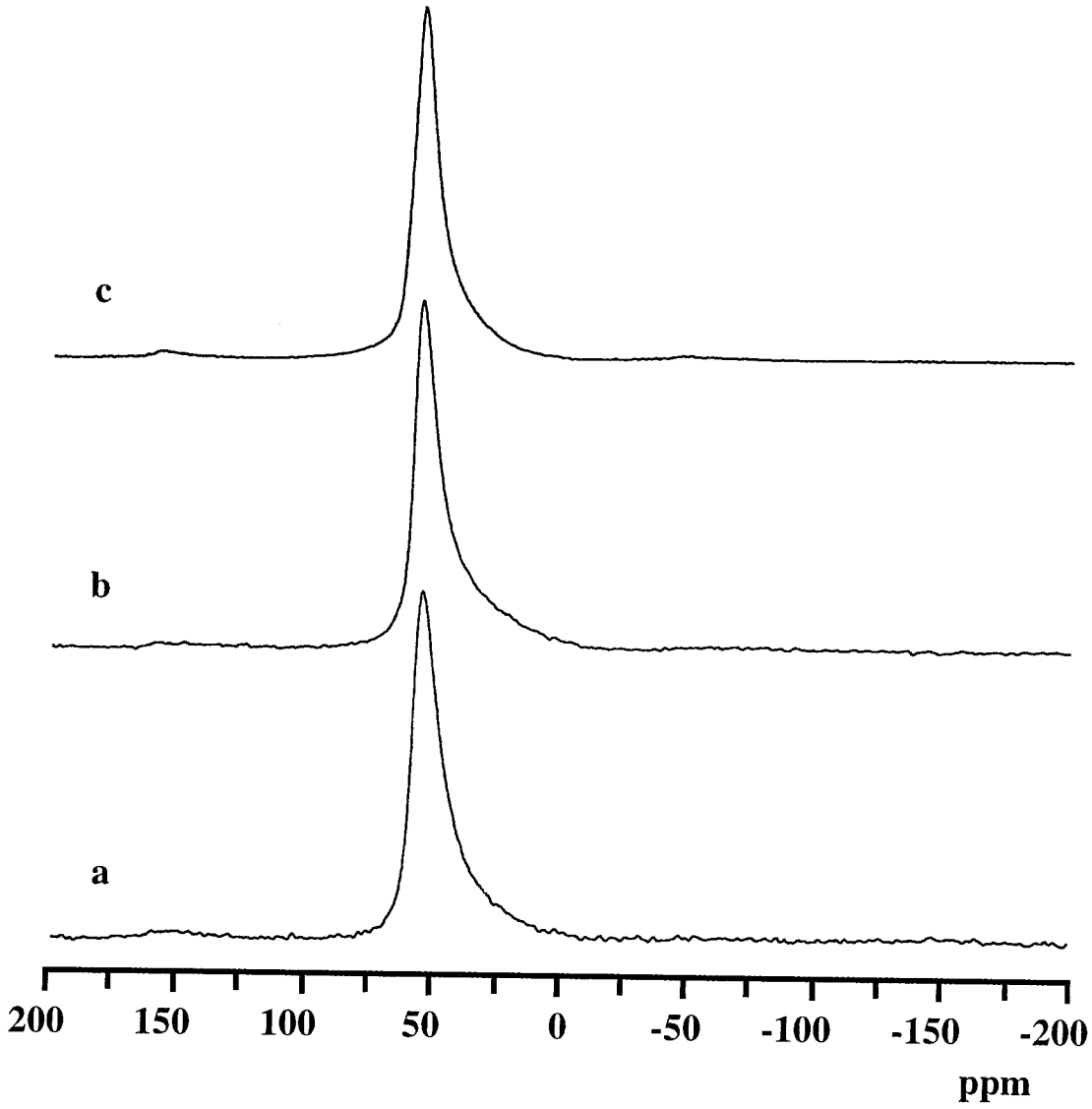

Figure 3.3 ^{27}Al NMR spectra (arbitrary intensity) of (a) P1 synthesized from gel-E, (b) P1 prepared from colloidal silica and (c) CIT-3.

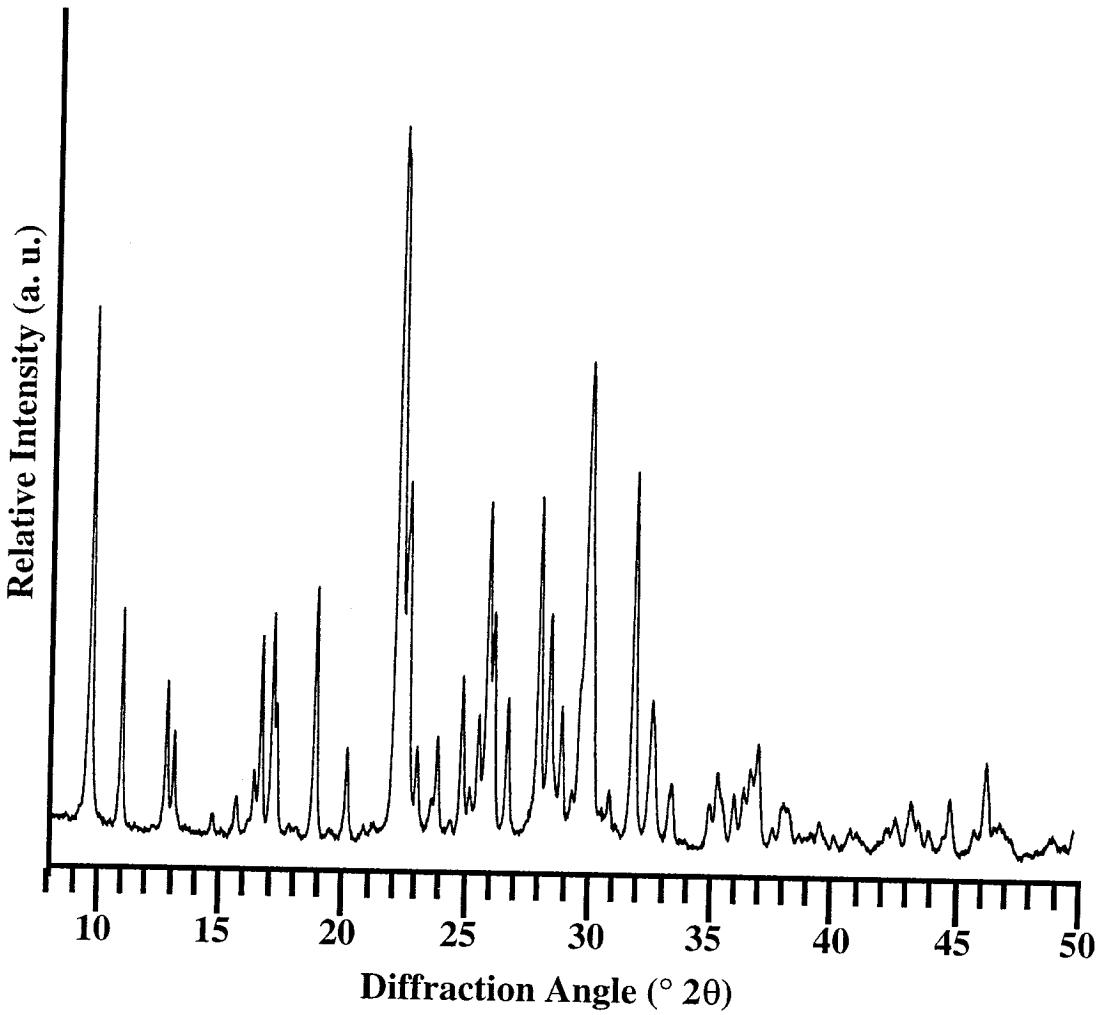

Figure 3.4 Powder X-ray diffraction pattern of CIT-3.

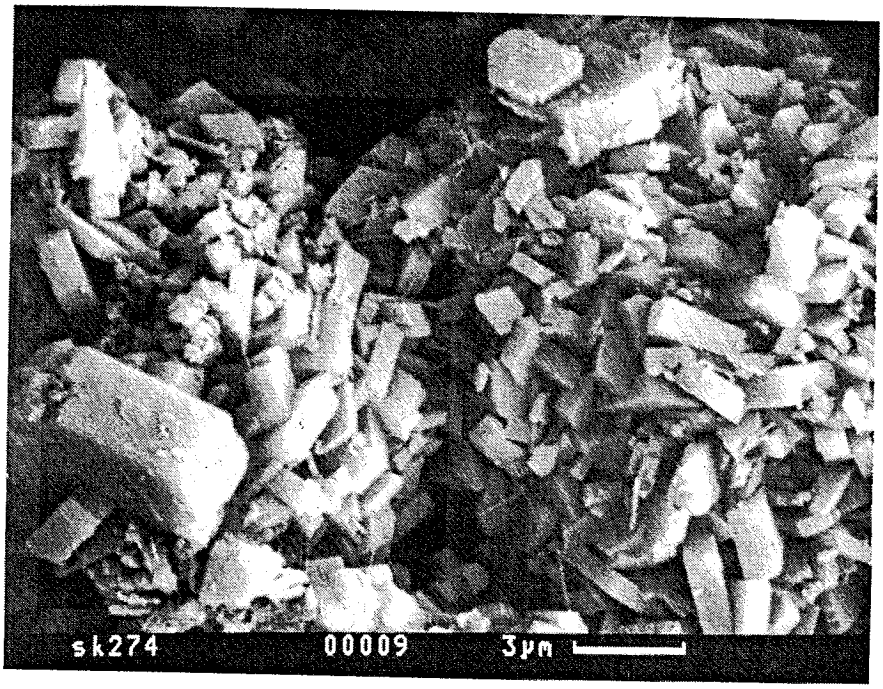

Figure 3.5 Scanning electron micrograph of CIT-3.

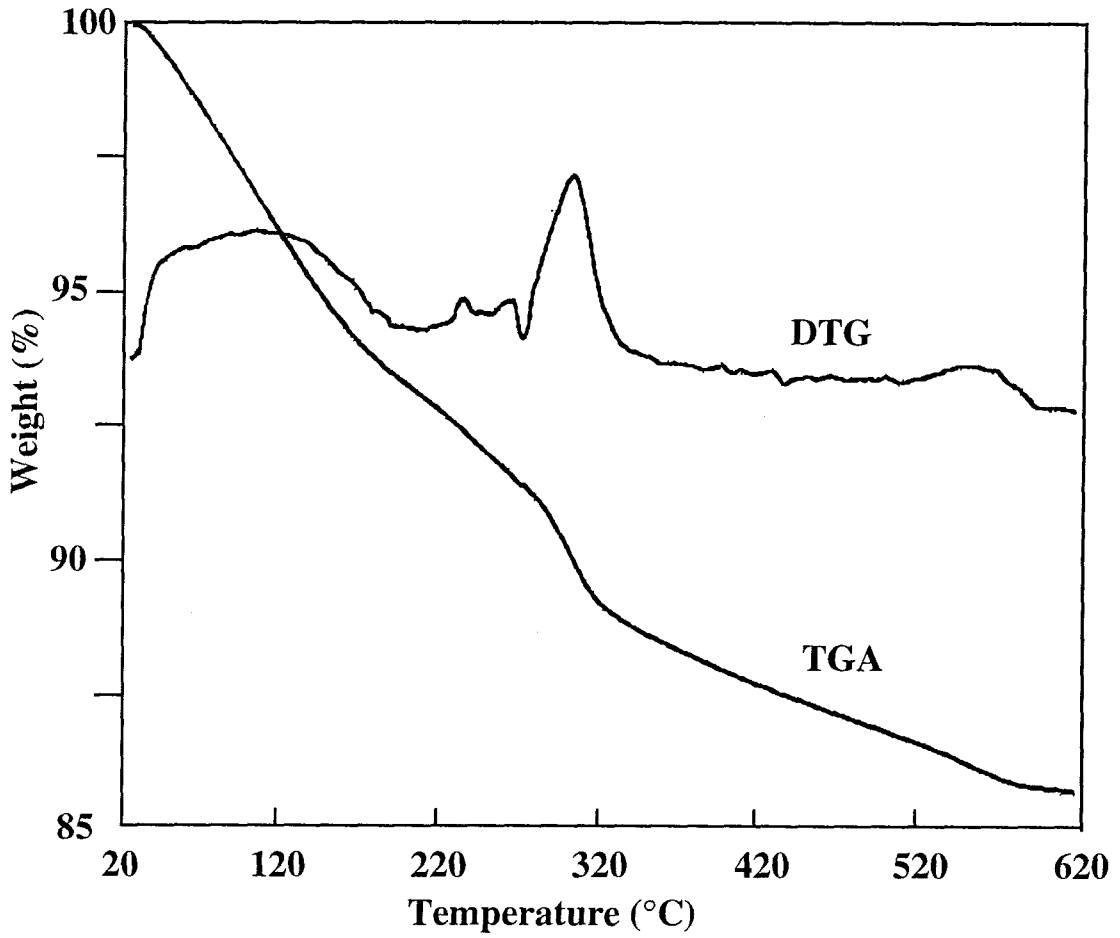

Figure 3.6 Thermogravimetric results for CIT-3.

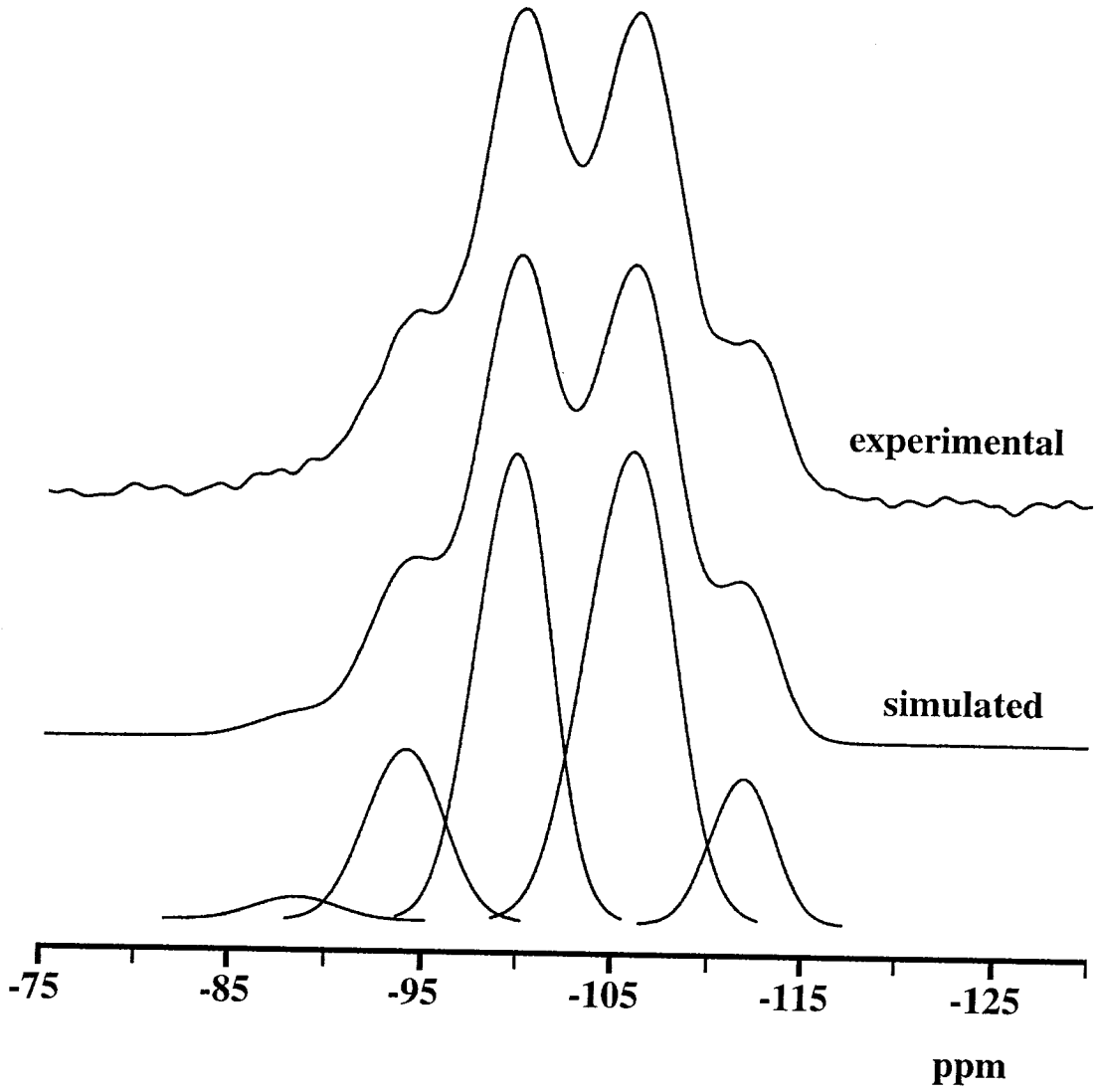

Figure 3.7 Experimental and simulated ^{29}Si NMR spectra of CIT-3.

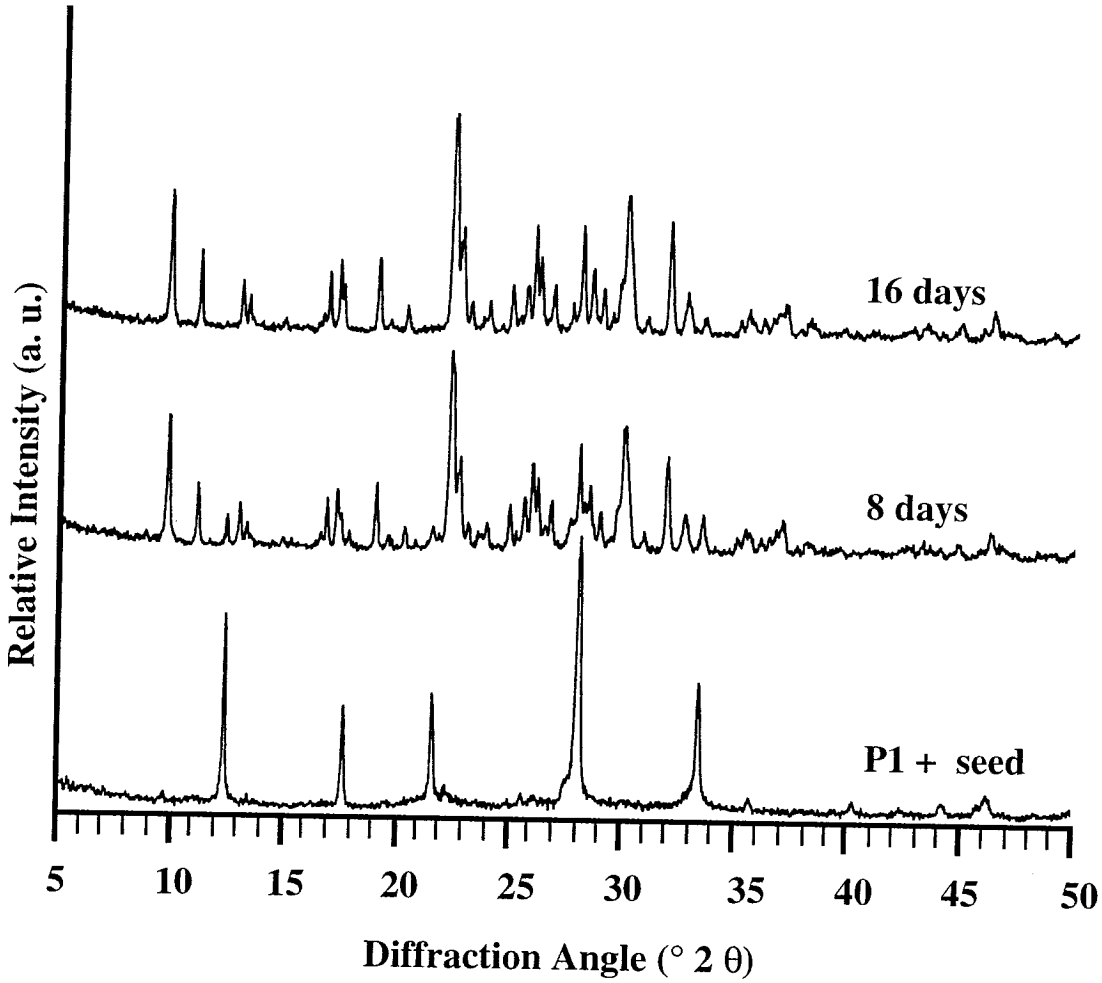

Figure 3.8 XRD patterns showing the crystallization of CIT-3 from P1 in 16 days.

CHAPTER FOUR

CIT-4: The First Synthetic Analogue of Brewsterite

Reprinted with permission from the article
[S. Khodabandeh, G. Lee and M. E. Davis, *Microporous Mater.* (In press)]

CIT-4: The First Synthetic Analogue of Brewsterite

Shervin Khodabandeh, Gary Lee and Mark E. Davis*

Chemical Engineering
California Institute of Technology
Pasadena, CA 91125 USA
Phone: (818)395-4251
Fax: (818)568-8743

Abstract

The first synthetic analogue of the rare natural zeolite brewsterite has been synthesized and named CIT-4. CIT-4 crystallizes with a composition SrO : Al_2O_3 : 5.8 - 6 SiO_2 : 4.5 H_2O and is prepared via hydrothermal alteration of zeolite P1 by strontium-containing solutions and in the presence of seed crystals of brewsterite.

4.1 Introduction

Brewsterite is the only natural strontium-dominant zeolite known to date. It is a rare zeolite of hydrothermal origin found mostly in veins of massive rocks [1,2]. The ideal composition of natural brewsterite is (Sr, Ba)$_2$ [$Al_4Si_{12}O_{32}$].10 H_2O. Natural brewsterite samples typically contain small amounts of Na and Ca and have Si/Al ratios ranging from 2.69 to 3.03 [2]. Although most occurrences of brewsterite have been strontium-dominant [1,2], two deposits of barium-dominant brewsterite have been reported also [3,4]. The structure of brewsterite consists of intersecting pores in the [100] and [001] directions each composed of 8 tetrahedral atoms [10]. There is only one cation site in the structure located in the middle of the volume created by the intersection of channels along the *a* and *c* directions. This site is occupied by either strontium or barium and is surrounded by five water molecules[5].

The framework structure of brewsterite is most similar to the zeolites heulandite and stilbite. As shown in Figure 4.1, brewsterite, stilbite and heulandite frameworks can be visualized in terms of different linkings of the rather rare 4-4-1-1 secondary building unit. In the heulandite and stilbite structures, the 4-4-1-1 units are connected via their vertices while in the brewsterite structure, the units share an edge.

To the best of our knowledge, no synthesis of a brewsterite-like phase has been reported previously. In this work, we present synthesis details for the preparation of a synthetic analogue of brewsterite, referred to as CIT-4 (for California Institute of Technology, number 4). CIT-4 can be prepared via hydrothermal alteration of zeolite P1 by strontium-containing solutions in the presence of seeds of brewsterite. Previously, we reported on the preparation of synthetic analogues of the calcium zeolites heulandite and epistilbite via conversion of zeolite P1 [6]. It is established by our previous work that the Si/Al ratio of the zeolite P1 and the overall composition of the reaction mixture are crucial factors in determining the products obtained. Similarly,

here, we observe that only P1 with a narrow range of Si/Al ratio and in a strontium-dominant reaction mixture can be converted to CIT-4.

4.2 Experimental Section

4.2.1 Synthesis

Zeolite P1 with a framework Si/Al ratio varying between 2.5 and 3.2 was synthesized from a gel of composition 4.5-5.5 Na_2O : Al_2O_3 : 11-18 SiO_2 : 370-400 H_2O by heating at 150 - 175°C for a period of 2 to 5 days. The aluminum source was aluminum trihydroxide (Reheis, F2000) and the silicon source was colloidal silica (Ludox, AS-40). For example, P1 with Si/Al of 3.0 was prepared as follows: 0.40 g of aluminum trihydroxide were added to a solution containing 2.0 grams of 50% w/w NaOH in 10.5 g water. 5.4 grams of colloidal silica were then added and the mixture stirred at room temperature for 3 hours. The resulting reaction mixture was transferred to a Teflon-lined autoclave reactor and statically heated at a temperature of 150 °C for 3.5 days.

Ion-exchange of zeolite P1 was carried out (1g zeolite/100mL solution) using 1.0 N chloride solutions of the desired cation at 70 - 80°C overnight (performed twice).

CIT-4 was synthesized by the reaction of P1 with strontium chloride solutions in a pH range of 10 to 12 (pH was adjusted by the addition of $Sr(OH)_2$). Typically, 0.15 to 0.20 g of P1 was used with 10 ml of the strontium-containing solution and 3 to 5% seeds by weight. The concentration of the chloride solution was varied between 0.01 and 1.0 N and the reaction temperature ranged from 200 to 270°C. Seeds used were natural brewsterite from Strontian, Scotland. In a typical synthesis, a 0.1 N $SrCl_2$ solution was prepared and the pH of the solution was adjusted to 11 by the addition of few drops of saturated $Sr(OH)_2$ solution. Ten ml of this solution was contacted with a physical mixture of 0.20 g of Ca-P1 and 0.01 g (5%) of brewsterite seeds in a Teflon-

lined autoclave. The autoclave was heated for 14 days at 240°C in order to crystallize CIT-4.

4.2.2. Characterization

X-ray diffraction patterns were recorded on a Scintag XDS 2000 diffractometer using Cu-K<α> radiation. The diffracted beam was detected by a liquid nitrogen-cooled germanium solid-state detector. For routine analysis and identification of phases, the samples were analyzed in the 2θ range 2-51° in steps of 0.03°. For the calculation of the unit cell parameters, a long step-scan was taken in the range of 8-50° 2θ with a step size of 0.02° and radiation time of 10 seconds per step.

Thermogravimetric analysis (TGA) was performed on a Du Pont 951 thermogravimetric analyzer. About 10 mg of sample were heated in air with a temperature ramp of 5 °C/min. Elemental analysis was performed by Galbraith Laboratories Inc., TN.

Solid-state NMR spectroscopy was performed on a Bruker AM 300 spectrometer equipped with solids accessories. Samples were packed into 7-mm ZrO_2 rotors and spun in air. ^{29}Si (59.63 MHz) NMR spectra were obtained using magic-angle spinning (MAS) at spinning rates of 3 - 4 kHz, pulse widths of 4 μs (40° pulse), and recycle delay times of 30-60 seconds. Tetrakis- (trimethylsilyl) silane was used as the external reference material for ^{29}Si NMR chemical shift determination, and all chemical shifts are reported in ppm relative to TMS. ^{27}Al NMR spectra were recorded at a frequency of 78.2 MHz on samples packed in 4-mm ZrO_2 rotors spinning at 8 - 9 kHz. A pulse width of 4 μs corresponding to a flip angle of 15° along with a recycle

delay time of 1 s were used. ^{27}Al NMR chemical shifts are referenced to a 1.0 M $Al(NO_3)_3$ solution (δ = 0.00 ppm), and are not corrected for second-order quadrupolar effects. Exponential line-broadening of 10-30 Hz for ^{29}Si and 50 Hz for ^{27}Al were applied to the data. Spectral deconvolution and simulation was performed using both the Bruker Linesim and the MacFID software packages.

4.3 Results and Discussion

4.3.1. CIT-4

CIT-4 is the synthetic analogue of zeolite brewsterite. Elemental analyses performed on typical samples yield the composition SrO : Al_2O_3 : 5.8 - 6 SiO_2 : 4.5 H_2O. The Si/Al ratio of 2.9 - 3.0 is in the higher end of the range found for natural samples [2]. Also, typical natural samples contain amounts of Ba, Ca, and Na while CIT-4 can be prepared with strontium as the only cation.

The powder X-ray diffraction pattern of a CIT-4 sample (Si/Al = 3.0) is shown in Figure 4.2a. Based on 48 strongest reflections, the pattern is indexed to a monoclinic unit cell with a = 6.776 $\pm$ 0.001 Å, b = 17.469 $\pm$ 0.003 Å, c = 7.731 $\pm$ 0.001 Å, β = 94.32 $\pm$ 0.002° and V = 912.52 Å^3. These parameters are in the range found for natural brewsterite samples [2] although they tend more towards the smaller unit cell sizes, consistent with a Si/Al ratio higher than that found for a typical deposit. For example, a Ba-dominant and a Sr-dominant natural sample with Si/Al = 2.90 give unit cell volumes of 919.9 [4] and 923.3 [5] Å^3, respectively. The unit cell volume for a CIT-4 sample with Si/Al = 2.9 was calculated to be 918.1 Å^3.

Table 4.1 lists the powder X-ray diffraction intensities for CIT-4 (Si/Al = 3.0). Although the structure of natural brewsterite has been refined in the monoclinic space group $P2_1/m$, it has been proposed by Akizuki that the actual space group is triclinic

[7]. By studying the extinctions of the {610}, {010}, and {011} sectors of a natural sample, Akizuki observed slight distortions from a monoclinic unit cell, e.g., a distortion of 0.5° from the c-axis. He attributed this distortion to the ordering of Si and Al during the crystal growth. Also, the structure solution of natural brewsterite yields an average T-O bond length of 1.607 Å for one of the crystallographic sites (compared with 1.645, 1.664 and 1.660 Å for the other three)[5] suggesting the exclusive occupation of that site by silicon atoms. Furthermore, natural brewsterite samples exhibit piezoelectric character inconsistent with the $P2_1/m$ space group [1]. No evidence of triclinicity is observed in the X-ray diffraction pattern of CIT-4 although it is certainly possible that the triclinicity is too slight to be observed by X-ray diffraction.

A SEM image of CIT-4 is given in Figure 4.3. Crystals of CIT-4 exhibit a flattened, blocky morphology. One common morphology of natural brewsterite is prismatic with {010}, {100}, {001}, {011} and {610} as the most common forms [2]. The CIT-4 crystals synthesized here exhibit a dominance of the {010}, {100}, and {001} forms as do some natural specimen, hence their blocky appearance. The crystal sizes range from about 10 to 50 microns. The majority of the sample is characterized by the smaller size crystals.

The larger crystals in Figure 4.3 are not the initial seed crystals since the natural seeds used were all ground to a crystal size of 1 - 2 micron before synthesis. In addition to the crystals of CIT-4, a small quantity of aggregates with no clear morphology also appears in the SEM. Since no other crystalline phase is detected by XRD, these aggregates are likely to arise from an amorphous aluminosilicate phase (vide infra).

The TGA and DTG curves for CIT-4 appear in Figure 4.4. The TGA curve shows a weight loss of up to 12.5% by 800°C which corresponds to the complete loss of water from the framework. The DTG curve exhibits three distinct weight losses at 150, 235 and 315°C and a shoulder at around 70 °C consistent with the loss of water

from four distinct water sites in the structure. The TGA curve for natural Strontian brewsterite used as seed (not shown) is very similar, and its DTG curve reveals three peaks at 144, 220 and 315°C as well. A similar thermal curve for natural brewsterite has been observed by Gottardi and Galli [1].

^{29}Si NMR spectra for CIT-4 (Si/Al = 3.0) are shown in Figures 5a and 5b. The spectrum from a synthetic heulandite (CIT-3, Si/Al = 3.5) is shown for comparison in Figure 4.5c and remarkably resembles that of the synthetic brewsterite suggesting similarities in the short-range structural features of BRE and HEU (see Figure 4.1).

Five distinct resonances are observed in the ^{29}Si NMR spectrum of CIT-4. The small intensity observed around -80 ppm arises from a small amount of impurity phase (not observable by XRD) and probably corresponds to an amorphous aluminosilicate with Si/Al = 1. This is consistent with the observation that in the cross-polarization spectrum shown in Figure 4.5b, this resonance exhibits no intensity. If the resonance ca. -80 ppm were in fact arising from a Si(4Al) framework site, it would be highly unlikely for this site not to exhibit a resonance in the cross-polarization spectrum. This interpretation is also consistent with small non-crystalline aggregates observed in the SEM (Figure 4.3).

The NMR spectrum is deconvoluted (Figure 4.6) into five peaks at -89.6 (7%), -94.1 (15.7%), -99.5 (41.3%), -105.5 (28.2%) and -111.6 (7.9%) ppm. Given the multiple T-sites in the structure of brewsterite, the assignment of these resonances to particular T-sites is not unambiguously possible. However, considering the NMR chemical shift ranges and the similarity of the BRE and HEU NMR spectra, the observed resonances are likely to arise from the following second neighbor coordinations of framework silicon atoms: -89.6 (Si3Al), -94.1 (Si2Al), -99.5 (Si1Al), -105.5 (Si1Al) and -111.6 (Si4Si). This yields a calculated Si/Al ratio of 3.3 (assuming a completely random distribution of aluminum in the framework), which is

likely to be flawed considering the likely Si-Al ordering in the structure. All of the aluminum atoms in CIT-4 are in tetrahedral coordination as confirmed by a single resonance at 55 ppm in the ^{27}Al NMR spectrum appearing in Figure 4.7.

4.3.2. Synthesis of CIT-4

CIT-4 is obtained by hydrothermal treatment of zeolite P1 with Sr-containing solutions at pH values ranging from 10 to 12 and temperatures ranging from 200 to 270 °C. Table 4.2 lists typical synthesis conditions for the preparation of CIT-4 from the calcium form of zeolite P1. As seen from the entries in Table 4.2, seeds are necessary for the transformation of P1 to CIT-4; in the absence of seeds, a crystalline hydrated strontium aluminosilicate phase results as the final product. The X-ray powder diffraction pattern of this material appears in Figure 4.2b and is remarkably similar to that of the synthetic strontium aluminosilicate referred to as Sr-Q (JCPDS 18-1267) by Barrer and Marshall [8,9]. It is believed that Sr-Q is isotopic in framework structure with the natural zeolite yugawaralite [10]. As seen in Table 4.2, for the formation of CIT-4 from P1 the Si/Al ratio of the starting P1 can range from 2.7 to 3.0. At Si/Al ratios lower than 2.7 (e.g. Si/Al = 2.5), no conversion of P1 takes place, and at higher Si/Al ratios the strontium aluminosilicate hydrate results as the only product. The Si/Al ratio of the CIT-4 product is typically in the range of 2.9 - 3.0 with samples synthesized from more aluminous P1's exhibiting the lower Si/Al ratios. For the majority of experiments conducted here seeds of natural brewsterite were used; crystals of CIT-4 were also used as seeds in few experiments with similar results.

Na-P1, Ca-P1, and Sr-P1 can be converted to CIT-4 as shown by the data given in Table 4.3. As seen from the entries in Table 4.3, for a given concentration of the solution phase, the conversion of P1 to CIT-4 occurs with increasing rates for the series: Sr-P1 > Na-P1 > Ca-P1.

Furthermore, the rate of conversion increases with increasing concentration of the solution phase for Na-P1 and Ca-P1, but remains the same for Sr-P1. These observations suggest that the conversion of P1 to CIT-4 appears to be preceded by the ion-exchange of the P1 to the strontium form. A similar observation was made in our earlier study on the conversion of P1 to synthetic heulandite where ion-exchange of Na-P1 to Ca-P1 preceded crystallization of CIT-3 [6]. The product of the reaction at longer times is typically the strontium aluminosilicate referred to above.

Conversion of P1 to CIT-4 is limited to a strontium-dominant reaction mixture as shown by the results listed in Table 4.4. The natural occurrence of Ba-dominant brewsterite (Sr/Ba = 0.01[3]) seems to indicate that it may be possible to form brewsterite in the presence of Ba instead of Sr. Also, given the narrow channel size and the location of the cation in the center of the channel, ion-exchange of brewsterite is unlikely (as has been noted by Robinson et al.[4]). Therefore, in natural samples that are Ba-dominant, barium is likely to have been incorporated in the structure of the zeolite during the nucleation and crystal growth rather than by subsequent ion-exchange mechanisms. Thus, one might expect that P1 could be converted to CIT-4 using $BaCl_2/Ba(OH)_2$ solutions. However, as shown by the results in Table 4.4, harmotome (Ba-analogue of zeolite phillipsite) is the product in this case. Thus far, we have not been able to synthesize a brewsterite-like structure in a barium-dominant system.

4.4 Summary

The synthetic analogue of brewsterite has been synthesized and named CIT-4. This zeolite possesses the BRE topology and has a composition of $SrO : Al_2O_3 : 5.8 - 6\ SiO_2 : 4.5\ H_2O$. CIT-4 is formed via hydrothermal conversion of zeolite P1 by strontium-containing solutions in the presence of seeds of brewsterite. For the successful conversion of P1 to brewsterite, the Si/Al ratio of P1 should be in the range

of 2.7 to 3.0. In the absence of seeds or at Si/Al ratios higher than 3.0, a hydrated strontium aluminosilicate phase that appears similar to Barrer's Sr-Q crystallizes. Previously, we have discussed conversion of specifically-prepared zeolites of P1 topology to the zeolites heulandite and epistilbite via treatment with calcium-containing solutions [6]. Syntheses of brewsterite and harmotome via conversion of zeolite P1 represent generalizations of our previous procedures for the synthesis of natural zeolites that have either proven difficult to synthesize in the laboratory or have defied laboratory synthesis altogether.

Acknowledgments

The authors thank AKZO Nobel for financial support.

4.5 References

[1] G. Gottardi and E. Galli, *Natural Zeolites*, Springer-Verlag, Heidelberg, 1985.

[2] R. W. Tschernich, *Zeolites of the World*, Geoscience Press Inc., Tuscon, AZ, 1992.

[3] R. Cabella, G. Luddhetti, A. Palenzona, S. Quartieri and G. Vezzalini, *Eur. J. Miner.*, 5 (1993) 353.

[4] G. W. Robinson and J. D. Grice, *Can. Miner.*, 31 (1993) 687.

[5] J. L. Schlenker, J. J. Pluth and J. V. Smith, *Acta Cryst.*, B33 (1977) 2907.

[6] S. Khodabandeh and M. E. Davis, *Micropor. Mater.*, 9 (1997) 149.

[7] M. Akizuki, *Amer. Miner.*, 27 (1987) 645.

[8] R. M. Barrer and D. J. Marshal, *J. Chem. Soc.*, (1964) 485.

[9] R. M. Barrer and D. J. Marshall, *Amer. Miner.*, 50 (1965) 484.

[10] S. M. Meier, D. H. Olson and C. Baerlocher, *Atlas of Zeolite Structure Types*; 4th. ed., Elsevier, London, 1996.

Table 4.1 Powder X-ray Data for CIT-4.

d (A)	Rel. Int. (%)	h	k	l
8.730	15	0	2	0
7.718	3	0	0	1
7.049	10	0	1	1
6.753	43	1	0	0
6.298	93	1	1	0
5.283	12	-1	0	1
5.055	54	-1	1	1
4.900	19	1	0	1
4.722	32	1	1	1
4.647	100	0	3	1
4.512	81	-1	2	1
4.371	2	0	4	0
4.274	11	1	2	1
3.911	57	-1	3	1
3.856	20	0	0	2
3.800	15	0	4	1
3.761	28	0	1	2
3.459	3	-1	0	2
3.394	19	-1	1	2
3.370	4	-1	4	1
3.259	98	1	4	1
3.191	32	1	1	2
3.180	24	1	1	2
3.042	45	1	2	2
3.016	15	2	0	1
2.965	14	2	1	1
2.921	71	2	3	0
2.912	90	0	6	0
2.847	23	1	5	1
2.792	31	-2	3	1
2.610	15	-2	1	2
2.570	26	0	0	3
2.547	5	-1	6	1
2.504	11	1	6	1
2.501	14	1	6	1
2.478	10	2	4	1
2.440	3	-1	1	3
2.425	5	2	1	2
2.404	11	-2	3	2
2.371	6	-1	2	3
2.323	8	0	6	2
2.258	25	2	3	2
2.137	18	2	4	2
2.121	7	3	0	1
2.100	14	0	8	1
2.063	14	-2	2	3
2.012	29	-3	0	2

Table 4.2 Representative syntheses of CIT-4 from Ca-P1[a].

Si/Al[b]	Sr^{2+}] (N)	T (°C)	pH	Seed	Result[c]
2.7	0.1	240	11	3%	CIT-4 (14 d)
2.9	0.1	240	11	3%	CIT-4 (14 d)
3.0	0.1	240	11	3-5%	CIT-4 (14 d)
3.0	0.1	240	12	5%	CIT-4 (14d)
3.0	1.0	240	11	5%	CIT-4 (14d)
3.0	1.0	240	12	5%	CIT-4 (7d)
3.0	1.0	240	12	5%	CIT-4 (7d)
3.0	1.0	200	12	5%	CIT-4 (14 d)
3.0	1.0	270	12	5%	CIT-4 (7 d)
3.0	0.1	240	12	---	Sr-aluminosilicate (7 - 14 d)[d]
3.2	0.1	240	11	10%	Sr-aluminosilicate (7 - 14 d)[d]
3.2	0.1	240	11	---	Sr-aluminosilicate (7 - 14 d)[d]
3.2	1.0	240	11	10%	Sr-aluminosilicate (7 - 14 d)[d]

[a] 0.20 gram of Ca-P1 was reacted with 10 ml of solution at 240°C. The pH was adjusted by the addition of a few drops of saturated $Sr(OH)_2$ solution.

[b] Si/Al ratio of the starting P1 zeolite.

[c] The synthesis time is given in parentheses.

[d] This material has an XRD pattern similar to Barrer's Sr-Q [8,9].

Table 4.3 Effect of the extraframework cation of the starting P1 on the rate of conversion to synthetic CIT-4.[a]

P1-type	$[Sr^{2+}]$, N	4 days	7 days	14 days
Ca-P1	0.1	P1	P1 + (CIT-4)	CIT-4
Ca-P1	1.0	P1	CIT-4	CIT-4
Na-P1	0.1	P1 + (CIT-4)	CIT-4	CIT-4 + Sr-aluminosilicate[b]
Na-P1	1.0	CIT-4 + P1	CIT-4	CIT-4 + Sr-aluminosilicate[b]
Sr-P1	0.1	CIT-4 + P1	CIT-4	CIT-4 + Sr-aluminosilicate[b]
Sr-P1	1.0	CIT-4	CIT-4	CIT-4 + Sr-aluminosilicate[b]

[a] 0.2 g of P1 and 10 ml of solution where used with 5% seeds. pH = 11 adjusted by the corresponding hydroxide of the cation. Temperature = 240°C. Reaction time = 14 days.

[b] This material has an XRD pattern similar to Barrer's Sr-Q [8,9].

Table 4.4 Effect of the solution phase on the alteration products of Ca-P1 (Si/Al = 3).[a]

Solution	Concentration (N)	Result
$SrCl_2$	0.01	P1
$SrCl_2$	0.1	CIT-4
$SrCl_2$	1.0	CIT-4
$BaCl_2$	0.1	Harmotome
$BaCl_2$	1.0	Harmotome
$CaCl_2$	0.1	EPI
$CaCl_2$	1.0	EPI

[a] 0.2 g of P1 and 10 ml of solution where used with 5% seeds. pH = 11 adjusted by the corresponding hydroxide of the cation. Temperature = 240°C. Reaction time = 14 days.

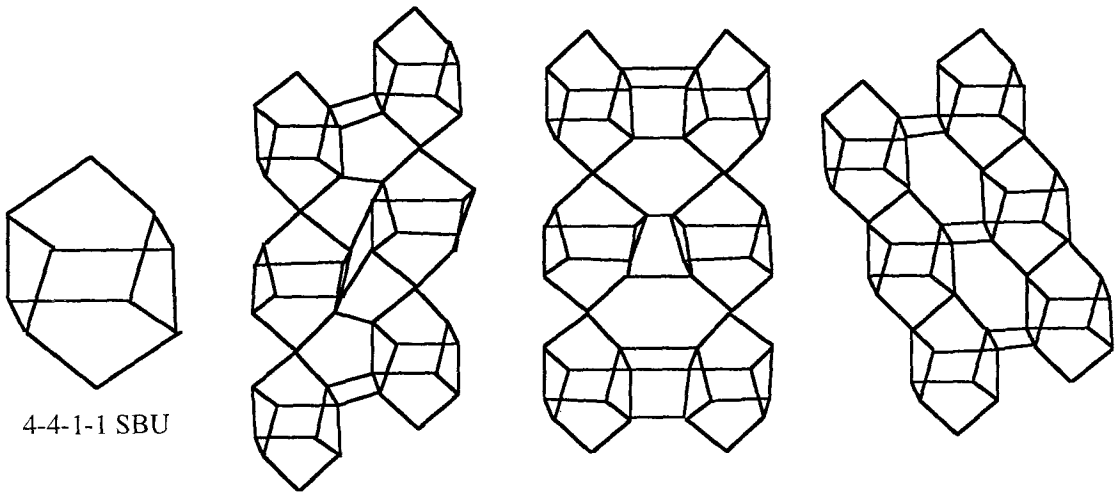

Figure 4.1 Schematic of the frameworks of brewsterite (CIT-4), heulandite (HEU) and stilbite (STI) as represented by different linkings of the 4-4-1-1 secondary building unit.

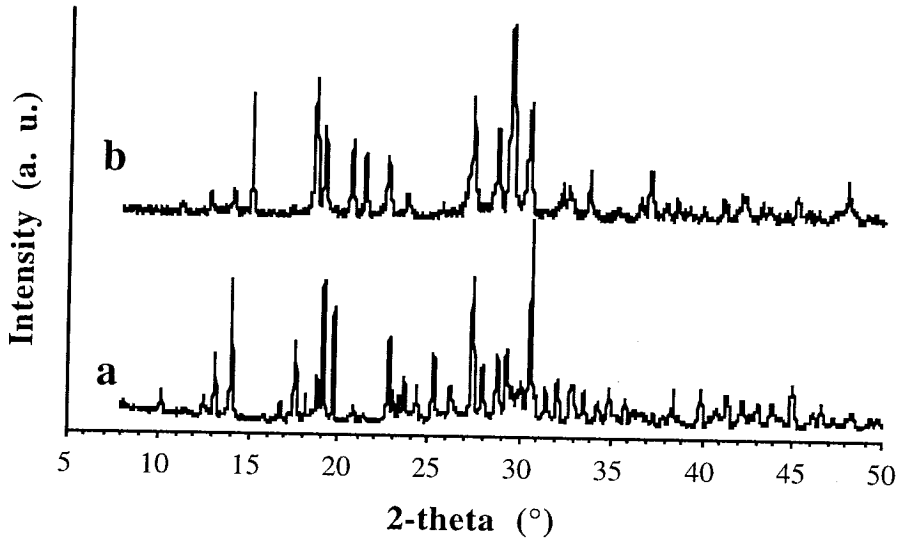

Figure 4.2 Powder X-ray diffraction pattern of CIT-4 (a) and the strontium aluminosilicate hydrate similar to Sr-Q (b).

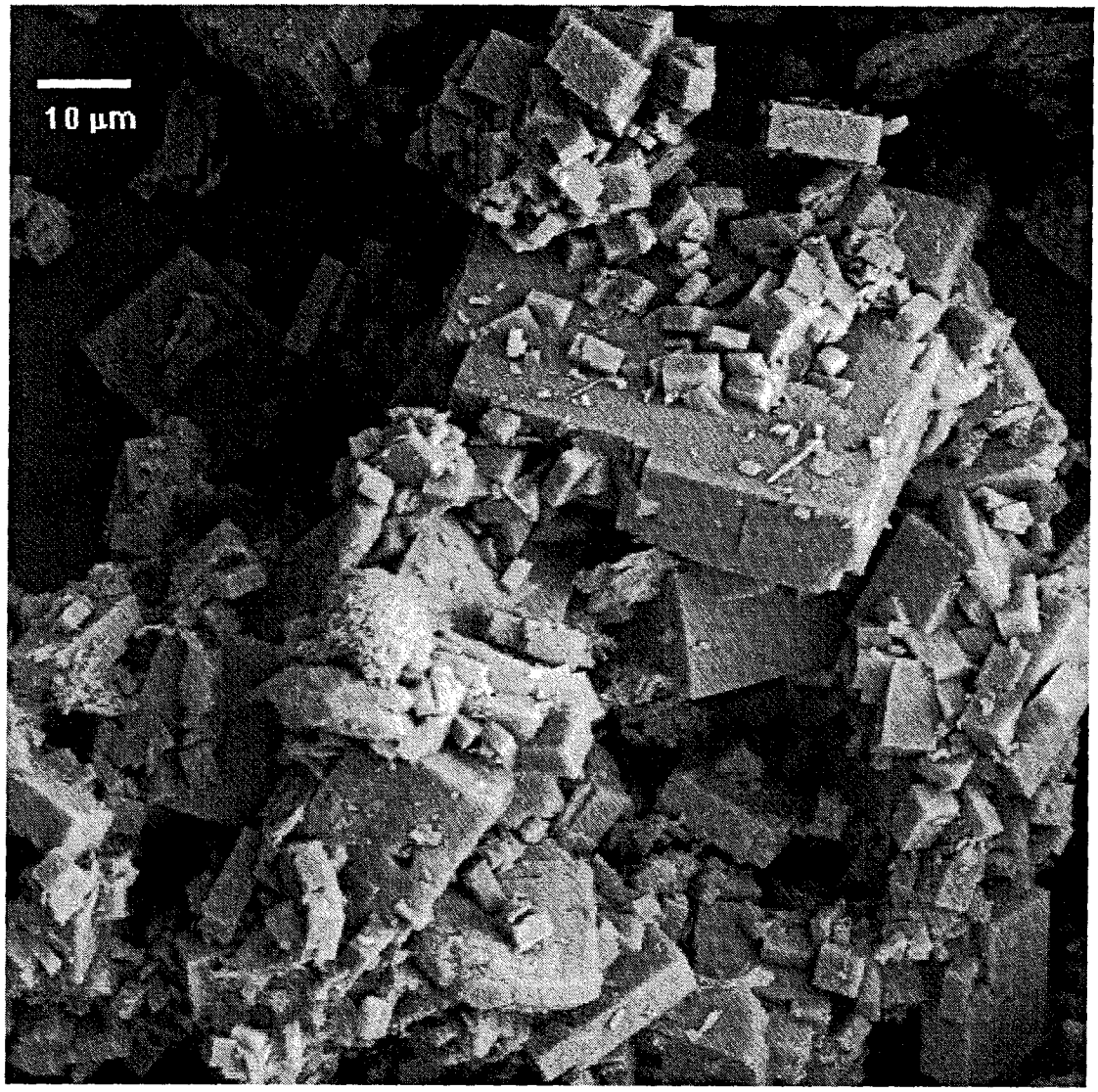

Figure 4.3 Scanning electron micrograph of CIT-4.

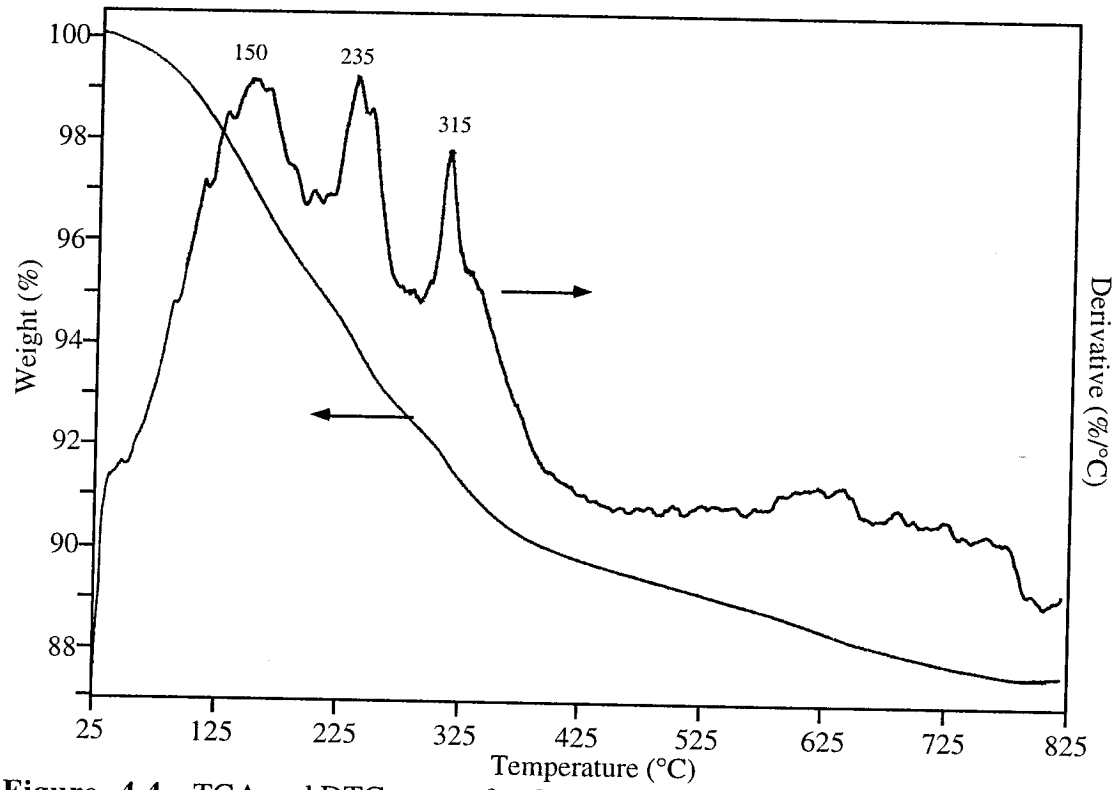

Figure 4.4 TGA and DTG curves for CIT-4

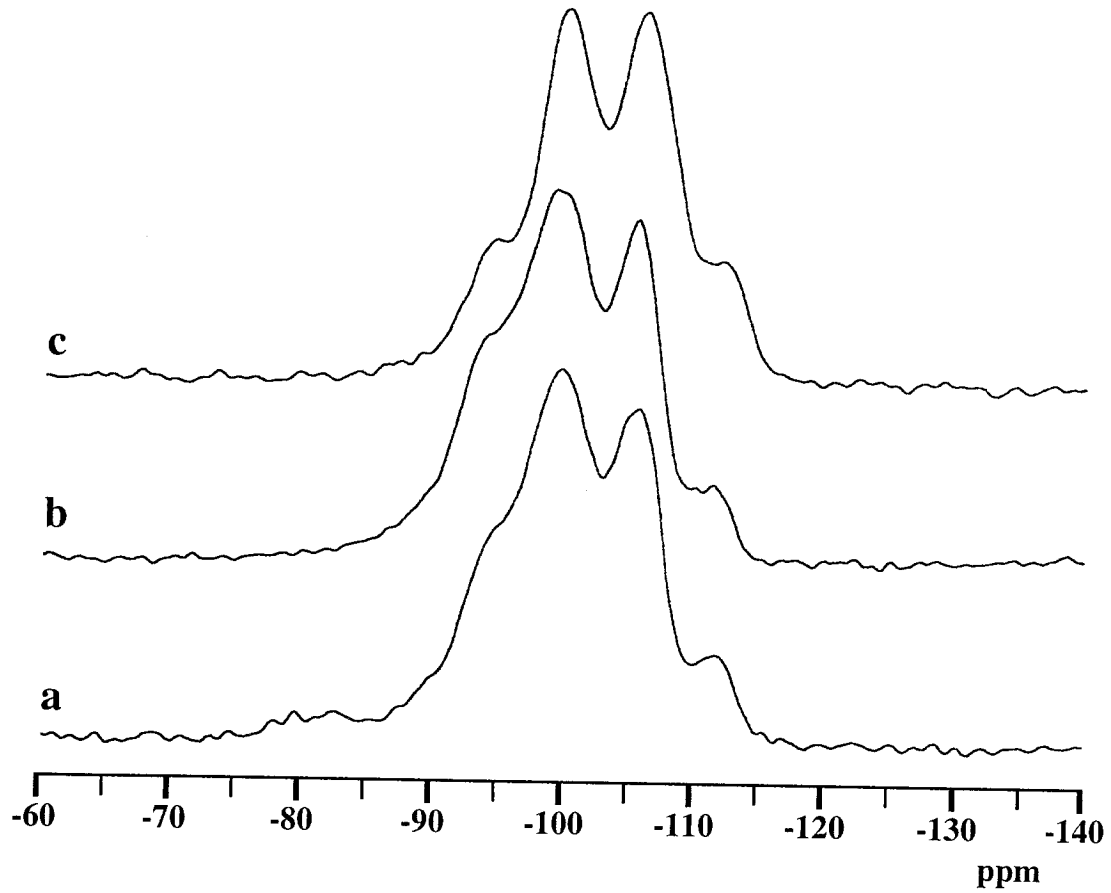

Figure 4.5 ^{29}Si NMR (a) and ^{1}H-^{29}Si CPMAS NMR (b) spectra of CIT-4 and ^{29}Si NMR spectrum of synthetic heulandite (c).

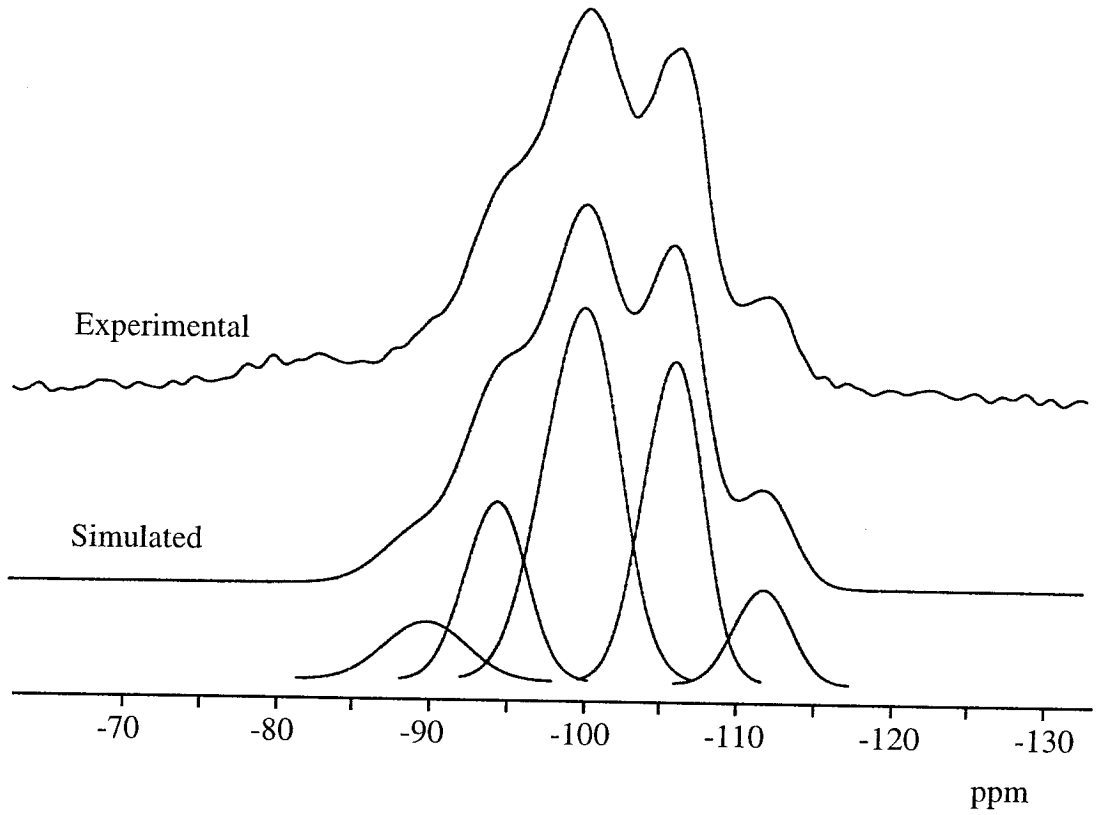

Figure 4.6 Experimental and simulated ^{29}Si NMR spectra of CIT-4.

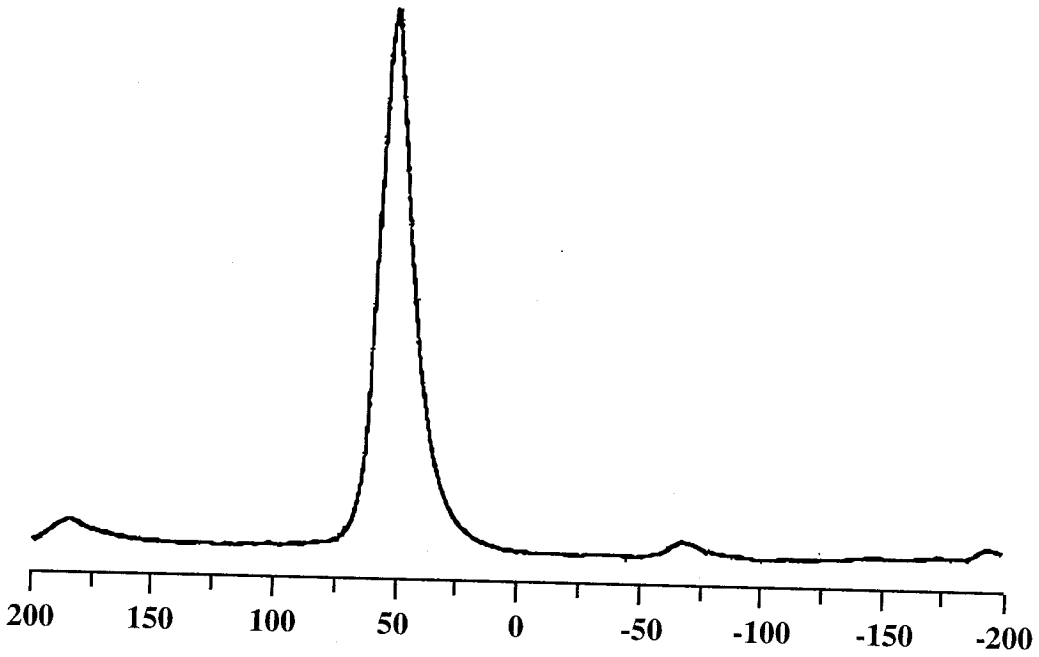

Figure 4.7 ^{27}Al NMR spectrum of CIT-4.

CHAPTER FIVE

Zeolite P1 as a Precursor for the Preparation of Alkaline-earth zeolites

5.1 Introduction

Early work in the field of zeolite synthesis focused on preparations from aluminosilicate gels in the presence of alkali metal cations. A large portion of the phase space in terms of composition of the aluminosilicate gel and crystallization times was explored relatively quickly and methods for the preparation of synthetic analogues of some natural zeolites as well as novel zeolites with no natural counterparts were developed. Following Barrer's pioneering work [1] involving the use of tertiary alkylammonium cations instead of inorganic cations, research efforts were quickly focused on incorporating organic structure-directing agents (SDA's) in the synthesis mixture to affect the crystallization of zeolites. Since then, many synthesis procedures have been developed for the preparation of synthetic zeolites and phosphate-based molecular sieves that now comprise over 90 distinct topologies. In contrast, about 25% of all natural zeolites known to date remain unsynthesized. The majority of the yet unsynthesized natural zeolites that are found in nature have calcium or other alkaline-earth cations as the dominant cation in their composition. Natural crystallization of these zeolites in the absence of organic structure directing agents that are commonly used for zeolite synthesis in the laboratory is an indication that the phase space for the "organic-free" synthesis of zeolites is far from completely investigated.

Recently, we demonstrated that a number of alkaline-earth zeolites are obtainable via hydrothermal conversion of zeolite P1. Preparation methods for the synthetic analogues of the zeolites heulandite (CIT-3) [2] and brewsterite (CIT-4) [3] were reported. It was noticed that zeolite P1 was especially suited as a precursor zeolite and that depending on its initial composition (in terms of Si/Al ratio and dominant cation), the solution composition, and the presence of seeds, zeolite P1 could be converted to various alkaline-earth zeolites.

The idea to use zeolite P1 as the starting material was conceived during our initial investigation on the hydrothermal transformation of natural glasses to zeolites [4]. It was observed that in the presence of aqueous calcium, very often the first alteration product of a volcanic glass was a gismondine-like phase, most similar to zeolite P1. As the alteration progressed, the gismondine-like phase was converted to the calcium zeolite heulandite. In this work, we present more details of the conversions of P1 to other zeolites, particularly alkaline-earth zeolites. Conversions of zeolite P1 to synthetic analogues of zeolites heulandite, epistilbite, harmotome, brewsterite, and yugawaralite are presented. The factors that determine the alteration products are the Si/Al ratio and the dominant cation in the starting zeolite P1, the composition of the solution phase, the presence or absence of seeds and the reaction time. The reaction temperature appears to only affect the kinetics of the reaction and not the product distributions. The Si/Al ratio of the starting zeolite P1 appears to be one of the most important factors affecting the final product. This influence is discussed in light of simple dissolution experiments carried out on different P1 zeolites with varying Si/Al ratios. In addition, conversion reactions of zeolite L (LTL) have been carried out and results are compared to reactions of zeolite P1.

5.2 Zeolite topologies and compositions

5.2.1 CIT-3 (HEU)

CIT-3 is a synthetic analogue of the natural, calcium-zeolite heulandite. This material typically crystallizes with a composition of CaO : Al_2O_3 : 7 - 7.2 SiO_2 : 6 H_2O and has a two dimensional pore system defined by intersecting 8- and 10-member ring pores.

5.2.2 Epistilbite (EPI)

Synthetic epistilbite has a typical composition of CaO : Al_2O_3 : 6 SiO_2 : 5 - 5.5 H_2O and is characterized by the epistilbite topology that consists of intersecting two-dimensional channels bounded by 8- and 10-ring pores [5].

5.2.3 CIT-4 (BRE)

CIT-4 is the first synthetic analogue of the rare, natural zeolite brewsterite. It has a composition of SrO : Al_2O_3 : 5.8 - 6 SiO_2 : 4.5 H_2O and possesses the brewsterite topology, which consists of intersecting 8-ring pores in two dimensions.

5.2.4 Yugawaralite or Sr-Q (YUG)

Yugawaralite is a rare calcium-zeolite with typical composition of CaO : Al_2O_3 : 6 SiO_2 : 4 H_2O and is characterized by a two-dimensional channel system composed of intersecting 8-member ring pores [6]. Previously, Barrer and Marshal have synthesized a strontium-aluminosilicate which they named Sr-Q that has an X-ray powder diffraction pattern similar to yugawaralite [7,8].

5.2.5 Harmotome (PHI)

Harmotome is the Ba-dominant analogue of the zeolite phillipsite [5]. It has a typical composition of BaO : Al_2O_3 : 6 SiO_2 : 6 H_2O and the PHI topology which consists of 8-ring channels in three crystallographic directions.

5.2.6 Zeolite P1 (GIS)

Zeolite P1 is the sodium aluminosilicate analogue of the natural calcium zeolite gismondine. It typically crystallizes with a Si/Al ratio of 1.5 - 2.7 [9], although we have been able to obtain this zeolite at Si/Al ratios as high as about 3.2.

5.3 Experimental Section

5.3.1 Preparation of Starting Zeolites

Zeolite P1 was prepared by heating at 150 to 175°C for a period of 3.5 days a gel of composition 4.5-5.5 Na_2O : Al_2O_3 : 11-18 SiO_2 : 370-400 H_2O. The aluminum source was aluminum trihydroxide (Reheis, F2000) and the silicon source was colloidal silica (Ludox, AS-40). The gel was prepared according to our previous procedures [2,3].

Two different samples of zeolite L (LTL) were used. K-L with micron-sized particles was a sample obtained from Union Carbide. Nano-crystalline zeolite L (~ 80 nm) was prepared according to procedures outlined previously [10].

Zeolites P1 or L were ion-exchanged into their Ca- or Sr- forms by contact with 1.0 N chloride solutions of the desired cation at 70 - 80°C overnight (performed 2x).

5.3.2 Conversions of Zeolites P1 and L

Conversions of zeolite P1 were carried out in Teflon-lined Parr autoclave reactors at temperatures of 200 to 270°C. Typically, 0.20 grams of P1 were used with 10 ml of the solution. 0.01 to 1.0 N chloride solutions of various cations (Na^+, Ca^{2+}, Sr^{2+}, Ba^{2+}) were used. The pH of the solution was varied from 8 to 12 and was adjusted by either adding a small amount of NaOH (0.9 to 2.0 mN) or by the addition of few drops of a concentrated solution of the corresponding hydroxide.

5.3.3 Characterization

X-ray diffraction patterns were recorded on a Scintag XDS 2000 diffractometer using Cu-K$<\alpha>$ radiation. The diffracted beam was detected by a liquid nitrogen-cooled germanium solid-state detector. For the calculation of the unit cell parameters, a

long step-scan was taken with a step size of 0.02° and radiation time of 10 seconds per step. The XRD profile was deconvoluted using split-Pearson lineshapes and the cell parameters were refined using the Scintag cell refinement program.

Solid-state NMR spectroscopy was performed on a Bruker AM 300 spectrometer equipped with solids accessories. Samples were packed into 7-mm ZrO_2 rotors and spun in air. ^{29}Si (59.63 MHz) NMR spectra were obtained using magic-angle spinning (MAS) at spinning rates of 3 - 4 kHz, pulse widths of 4 μs (40° pulse), and recycle delay times of 30-60 seconds. Tetrakis(trimethylsilyl) silane was used as the external reference material for ^{29}Si NMR chemical shift determination, and all chemical shifts are reported in ppm relative to TMS. No linebroadening was applied to the NMR data. Spectral deconvolution and simulation was performed using both the Bruker Linesim and the MacFID software packages.

5.3.4 Dissolution Experiments

In order to investigate the dissolution behavior of zeolite P1 as a function of the framework Si/Al ratio, three different samples were prepared with Si/Al ratios of 2.5, 2.7, 3.0, and 3.2 according to procedures outlined above. The samples were washed with copious amounts of distilled H_2O until the pH of the aqueous mixture containing the solids was neutral. After the samples were dried, they were sieved to ensure that all particles fall in the size range of 47 to 53 microns. One hundred mg of each sample was contacted with 20 ml of 0.01 N NaOH solution in polyethylene bottles at 70°C for periods of 8 and 16 hours. After partial dissolution, the liquid phase was extracted and filtered through a 0.2 μ filter. The Si and Al contents of this solution were analyzed using ICP.

5.4 Results and Discussions

5.4.1 Conversions of Zeolite P1

Zeolite P1 synthesized with framework Si/Al ratio in the range of 2.7 to 3.3 was used as the starting material. The conversion of this material to other zeolites in solutions containing mainly Ca^{2+}, Sr^{2+}, Ba^{2+}, and Na^{+} was investigated. The reactions were carried out as described in the experimental section.

5.4.1.1 Zeolite P1 in a calcium-dominant reaction medium

The products of conversion of P1 in a calcium-dominant aqueous reaction medium are CIT-3 (HEU) and epistilbite as shown in Table 5.1. Na-P1 or Ca-P1 are converted to either CIT-3 or to epistilbite upon reaction with solutions containing 0.01 to 1.0 N Ca^{2+}. This conversion occurs typically in about 16 days at a temperature of 240°C. At 270°C, the conversion occurs in 7 days and at 200°C, it typically takes 24 days. The Si/Al ratio of P1 can range from 3.0 to 3.2 for successful conversion to either CIT-3 or to epistilbite. The only factor that determines the conversion product appears to be whether or not seeds of heulandite are present. For the transformation of P1 to CIT-3, seeds of HEU are necessary and in the absence of seeds, the synthetic epistilbite phase results. The amount of HEU seeds can be as low as 3 - 5%. The XRD pattern of CIT-3 is given in Figure 5.1a and that of epistilbite appears in Figure 5.1b.

5.4.1.2 Zeolite P1 in a sodium-dominant reaction medium

In a sodium-dominant aqueous reaction medium, the products of conversion of P1 are either analcime, or a mixture of analcime and mordenite. When the Si/Al ratio of P1 is less than about 2.6 analcime forms, while for the cases where the Si/Al ratio is higher than 2.7, a mixture of analcime and mordenite results. The extent of the

conversion at 240°C depends on the pH of the solution: for pH $\leq$ 11, the conversion takes about 16 to 24 days. When pH $\geq$ 12, the conversion is complete within 7 - 10 days. In a sodium-dominant reaction medium it has not been possible to transform P1 to CIT-3 or CIT-4 even in the presence of 20% seeds of the appropriate crystals. These observations suggest that the presence of seeds of a particular crystal does not simply determine the final products obtained. Rather, the composition of the reaction mixture is crucial in determining the final zeolites that form. A summary of some of these results is given in Table 5.2.

5.4.1.3 Zeolite P1 in a barium-dominant reaction medium

In a barium-dominant aqueous reaction medium, P1 is converted readily to harmotome. Typical reaction have been carried out using either Ca-P1, Na-P1 or Ba-P1 as the starting material. The solution phase used is $BaCl_2$ at a concentration ranging from 0.1 to 1.0 N and pH = 11 - 12 (adjusted by the addition of $Ba(OH)_2$). In the presence of seeds of heulandite or brewsterite, the product of the reaction is still harmotome. The XRD pattern of this zeolite is shown in Figure 5.1c, and is characterized by both sharp and broad peaks indicative of possible stacking faults that are also commonly observed in natural harmotomes [5].

5.4.1.4 Zeolite P1 in a strontium-dominant reaction medium

In a strontium-dominant aqueous reaction medium, three strontium zeolites are obtained. We have been able to transform zeolite P1 to brewsterite (CIT-4), Sr-heulandite, and a strontium aluminosilicate zeolite most similar to zeolite Sr-Q first synthesized by Barrer and Marshal [7,8]. The XRD patterns for these phases appear in Figure 5.2 a-c. The factors that determine the final products of conversion of P1 in a strontium-dominant reaction medium are Si/Al ratio of the P1, the cation type, and the

presence or absence of seeds. Table 5.3 summarizes these results. As seen by the entries in Table 5.3, for the transformation of P1 to CIT-4, seeds of brewsterite are necessary. The conversion of P1 to CIT-4 is limited to P1 with Si/Al in the range of 2.7 to 3.0 and occurs only in the presence of seeds of brewsterite. In the absence of seeds, a strontium aluminosilicate hydrate is obtained that resembles Barrer's Sr-Q as described above. It is interesting to note that Sr-P1 (Si/Al = 3.2) can be transformed into Sr-heulandite in the absence of heulandite seeds. Even in the presence of seeds of brewsterite, Sr-P1 (Si/Al = 3.2) is converted to Sr-heulandite. This is in contrast to our previous work on the conversion of Ca-P1 to CIT-3 where we noticed that the transformation required the addition of crystal seeds of heulandite [2]. Furthermore, only the strontium form of P1 is converted to Sr-heulandite; the calcium form results in the crystallization of Sr-Q. Transformation of Sr-P1 with Si/Al = 3.2 to Sr-heulandite has been difficult to reproduce. We carried out over 80 experiments in order to identify the exact synthesis conditions for the conversion of Sr-P1 to Sr-heulandite. In about 20 experiments, Sr-heulandite was obtained, while in the rest of the experiments, Sr-heulandite was obtained along with impurities of Sr-Q. In order to determine the factors responsible for the lack of reproducibility of this transformation, great care was taken to standardize factors such as P1 crystal and particle size, temperature, composition of the starting P1, pH, and the solution concentration. All other factors being the same, the only measurable difference between the experiments where pure Sr-HEU was formed and those where Sr-Q appeared with Sr-HEU is the ^{29}Si NMR lineshapes of the starting P1. Figure 5.3 shows the ^{29}Si NMR spectra for two different P1 materials with Si/Al = 3.2. These two different P1 zeolites are referred to as $P1_a$ and $P1_b$. $P1_a$ is the type of P1 zeolite that is converted to a mixture of Sr-Q and Sr-heulandite, whereas $P1_b$ is converted to Sr-heulandite with near 100% reproducibility. These two materials are similar in all aspects investigated (chemical composition, XRD,

TGA, SEM, ^{27}Al NMR spectra, adsorption) but differ in their ^{29}Si NMR spectra. As seen in the Figure, $P1_b$ is characterized by NMR lineshapes with larger linewidths and much higher Lorentzian character while the NMR lineshape for $P1_a$ is narrower and more Gaussian. This indicates local disorder in the Si-O-T (T = Si, Al) bond angles, not measurable by XRD, for $P1_b$. Thus, the two different P1's are characterized by different extents of local disorder, and it is the more disordered species that is fully converted to Sr-heulandite. We were only able to synthesize $P1_b$ (with the larger linewidths) a few times and to the best of our ability, we could not determine the factors during the synthesis that determine the extent of local disorder in the final product, i.e., factors that determine whether $P1_a$ or $P1_b$ would form.

From the results presented above, it is clear that zeolite P1 (Si/Al = 2.7 - 3.2) is a particularly useful starting phase for the preparation of a number of alkaline-earth zeolites. Figure 5.4 summarizes results of all the conversions of zeolite P1 to other zeolites obtained in our research so far.

5.4.2. Effect of Si/Al ratio of zeolite P1

As shown in the data presented above, among other things, the Si/Al ratio of the starting zeolite P1 strongly affects the final product obtained. For example, in a calcium-dominant reaction medium, it is not possible to convert zeolite P1 to CIT-3 if the Si/Al ratio is other than 3.0 - 3.2. As another example, P1 will transform into CIT-4 (BRE) if it has an initial Si/Al ratio in the range of 2.7 - 3.0, but will transform to Sr-Q if the Si/Al ratio is increased to 3.2. Thus, a minor variation in the Si/Al ratio of zeolite P1 can dramatically affect the course of reaction.

Zeolite P1 can be obtained with Si/Al ratios varying from 2.5 to 3.2 by simple modifications of the synthesis conditions outlined in the experimental section. The XRD pattern of zeolite P1 (Si/Al = 3.0) is given in Figure 5.5. Similar patterns are

observed for P1 zeolites with other Si/Al ratios. As expected, there is a systematic decrease in unit cell size with increasing Si/Al ratio as shown in Table 5.4.

A scanning electron micrograph of zeolite P1 (Si/Al = 2.9) ratios is shown in Figure 5.6. Typical crystals have a cubic morphology, are 0.5 to 1 micron in size, and are aggregated to form polycrystalline spheres.

Figure 5.7 shows the ^{29}Si NMR spectra for four zeolite P1 samples with Si/Al varying from 2.5 to 3.2. The four NMR peaks observed correspond to the following environments in the direction of decreasing chemical shift: Si(3Al), Si(2Al), Si(1Al) and Si(0Al). Assuming complete randomness in the distribution of aluminum in the framework, it is possible to calculate the framework Si/Al ratio according to the equation :

$$Si/Al = \frac{\sum_{n=0}^{4} I_{Si(nAl)}}{\sum_{n=0}^{4} \frac{n}{4} I_{Si(nAl)}}$$

where the intensities of the peaks corresponding to Si(0Al) through Si(4Al) are determined by simulating the NMR spectrum. ^{29}Si NMR spectroscopy was used to determine the true framework Si/Al ratio of all P1 zeolites used in our experiments, and the values reported in Figure 5.7 and thus far in the text and tables are obtained via this method. None of the P1 zeolites (either in Na- or Ca-forms) used as starting material could adsorb N_2 at 77K, and all P1 samples exhibited very similar TGA profiles. Thus, it appears that the Si/Al ratio of the starting P1 is the only significant factor that affects the final products obtained.

The conversion of P1 to other zeolites is likely to take place via gradual dissolution of zeolite P1 with the release of silicate, aluminate, and aluminosilicate species into the solution phase. Subsequent condensation of these species results in the

formation of new zeolite crystals. This is consistent with the observation that during the transformation of zeolite P1 to other zeolites, no amorphous phase is observed by XRD. This seems to suggest that the conversion of P1 to other zeolites proceeds via a dissolution reprecipitation cycle as is the case for the alteration of glasses [11,12] and also previously suggested in our earlier work on the synthesis of CIT-3 [2].

One possible explanation for the observed difference in the reaction products of P1's with different Si/Al ratios could be that P1 zeolites with different Si/Al ratios release different aluminosilicate species into the solution phase. In other words, it is possible that P1 with Si/Al = 2.7 releases a different distribution of aluminosilicate species into the reaction mixture than P1 with Si/Al = 3.0. To test this hypothesis, four samples of zeolite P1 with Si/Al ratios of 2.5, 2.7, 3.0 and 3.2 were prepared and contacted with NaOH solutions for 16 hours. The details of these experiments are outlined in the experimental section. In particular, to minimize particle size effects on the rate of dissolution, all samples were sieved to a particle size of 40 - 70 microns.

Dissolution of a zeolite is a very complex process involving many simultaneous equilibria between various aluminate, silicate and aluminosilicate species. These equilibri are extremely sensitive to pH, temperature, the type and concentration of cations present in the solution. Thus, obtaining quantitative information regarding the actual oligomeric aluminosilicate species in the solution phase is not trivial. Even though no information on the actual aluminosilicate species released into the solution phase was obtained, differences were observed in the relative amounts of dissolved Si and Al between P1 zeolites with different Si/Al ratios. These results are summarized in Table 5.5 and Figure 5.8.

In Table 5.5, dissolution data as a function of the initial framework Si/Al ratio are given. Figure 5.8 shows the Si/Al ratio in the solution as a function of the initial framework Si/Al ratio. It is observed that the framework Si/Al ratio of the zeolite

affects the Si/Al ratio in the solution phase. Furthermore, it is seen that the solution Si/Al ratio is always higher than that of the initial framework. This suggests preferential solubilization of silicon relative to aluminum, which is expected since the activity of Si in alkaline environment is higher than that of Al. The lack of a linear relation between the solution Si/Al ratio and the framework Si/Al ratio as shown in Figure 5.8 is particularly interesting and unexpected. In other words, one would expect that the Si/Al ratio in the solution phase would be directly related to the framework Si/Al ratio. Rather, a maximum is observed in the Si/Al range of 2.7 to 3.0. These results suggest that the dissolution behavior of P1 with Si/Al ratio ca. 3 is anomalous.

Even though the data in Figure 5.8 are only semi-quantitative and do not track actual species present in the solution phase, they clearly demonstrate that the dissolution behaviors for P1 zeolites with varying framework Si/Al ratios are somewhat different. The trends observed in this simple experiment are not expected by any means to apply to the reaction conditions during which zeolite P1 is transformed to alkaline-earth zeolites. These data are presented merely to suggest that the framework Si/Al ratio of the zeolite P1 affects the solution composition. Considering that the conversion of P1 is likely to proceed via multiple dissolution-reprecipitation cycles, it is quite conceivable that even minor differences in the dissolution behavior of P1 could greatly affect the distribution of aluminosilicate species in the solution phase and thus the final zeolite obtained.

The observation that the Si/Al ratio of the solution phase does not vary with direct relation to the initial Si/Al ratio of the zeolite is somewhat puzzling. One possible explanation for the results presented in Figure 5.8 could be compositional zoning. It is possible that the P1 zeolites with the higher framework Si/Al ratio have crystallized with a silicon-rich core and a thin aluminum-rich shell, although due to small crystallite

size, this cannot be ascertained experimentally. Interestingly, the anomalous behavior is observed for Si/Al = 3 - 3.2, which happens to be the value necessary to accomplish the majority of zeolite transformations discussed so far. What is so special about zeolite P1 with Si/Al ratio ca. 3? One possible response is that the ideal Si/Al ratio of the alkaline-earth zeolites synthesized in this work is commonly around 3 which means that zeolite P1, exchanged for the appropriate cation, is compositionally very similar to the final alkaline-earth zeolite to which it will be transformed. It is also worthwhile to look at the field of formation of this zeolite. Whereas zeolite P1 readily crystallizes with a framework Si/Al ratio in the range of 2.0 to 2.7, it is difficult to obtain this zeolite at higher Si/Al ratios. All P1 zeolites in this work have been synthesized using the same procedures with the only difference being the amount of SiO_2 added to make the gel while keeping the amount of NaOH constant. Table 5.6 summarizes the effect of the silica content of the gel on the framework Si/Al ratio of the P1 zeolite obtained. In order to increase the Si/Al ratio of P1 from 2.5 to 3.2 (an increase of 30%), the silica content of the gel needs to increase from 13 to 17 (also an increase of 30%). However, an increase in the silica content of the gel beyond this value hinders crystallization of P1 all together. Considering the data presented in this table, it appears that a value of 3 - 3.2 for the framework Si/Al ratio of zeolite P1 marks a compositional border for the field of formation of this zeolite. In fact, no reports of synthesis of P1 with Si/Al > 3.0 in the absence of organics appears in the literature. Thus, it is reasonable to state that the "ideal" Si/Al ratio of zeolite P1 is not ca. 3, and this may account for the anomalous dissolution behavior observed.

5.4.3. Conversions of zeolite L (LTL)

All conversion products of zeolite P1 are zeolites that have Si/Al ratios very similar to the initial Si/Al ratio of zeolite P1. Thus, one could simply argue that any

zeolite with the same initial Si/Al ratio would be suitable as a starting material. To gain further insight into why zeolite P1, particularly with Si/Al = 3, is such a versatile precursor for the formation of other zeolites, a few experiments using zeolite L were carried out. Zeolite L (LTL) is a particularly good candidate for comparison purposes since it can crystallize only with a framework Si/Al ratio of 3.0. Thus, it is likely that any difference in terms of reactivity and products obtained between zeolite P1 (Si/Al = 3) and zeolite L (Si/Al = 3) is due to the differences in the framework structure. In order to rule out any particle size effects, we carried out parallel reactions involving zeolite L with micron-sized crystals and also nano-crystalline zeolite L with submicron particle size. No difference was observed in the final products obtained indicating that particle size in this case does not appear to be an important factor.

Table 5.7 lists several reactions where zeolite L is used as the starting phase. As seen by the entries in Table 5.7, it is possible to synthesized epistilbite, CIT-4 and Sr-Q from zeolite L. Also, it is possible to transform zeolite L to Sr-heulandite. However, a few differences are observed between zeolite L and zeolite P1 as starting materials. For example Ca-L is not converted to a heulandite-like phase even in the presence of 20% seeds; instead, epistilbite is the final product of this transformation. Also, it is not possible to obtain pure CIT-4 from either Sr-L or Ca-L. Instead, the product is always a mixture of CIT-4 and Sr-Q.

Figure 5.9 shows a series of XRD patterns taken at intermediate stages and depicting the conversion of zeolite L to epistilbite. Similar XRD patterns are observed in the presence of heulandite seeds. It is clear that during the transformation of zeolite L to epistilbite, the solid phase goes through an amorphous phase and then is converted to epistilbite. This is observed also for the case where heulandite seeds were used as well. In this regard, transformation of zeolite L to epistilbite is different from that of zeolite P1. Conversion of P1 to epistilbite or any other zeolite is likely to proceed via

gradual dissolution of zeolite P1 and the subsequent condensation of aluminosilicate species released into the solution phase (vide supra). This does not seem to be the case for the conversion of zeolite L to epistilbite. In this case, zeolite L is slowly dissolved and precipitates as an amorphous aluminosilicate. This amorphous phase is subsequently converted to epistilbite. Therefore, crystallization of epistilbite in this system is probably not due to a gradual dissolution of LTL and subsequent nucleation of epistilbite, as is the case with zeolite P1. Interestingly, this amorphous transient phase is not present during conversion of zeolite L to CIT-4 and Sr-Q. XRD patterns obtained at intermediate stages of these reactions reveal simultaneous presence of both Sr-Q, CIT-4, and P1 until of course all of P1 is converted to Sr-Q and CIT-4.

Zeolite L has Si/Al = 3.0. Furthermore, the same final products are obtained from zeolite L regardless of the particle size (vide supra). On the other hand, the results of conversion of zeolite L (Si/Al = 3.0) are somewhat different from those of zeolite P1 (Si/Al = 3.0), particularly in the calcium-rich environment. These observations seem to suggest that differences in the framework structure of the starting zeolite affect the reaction path and the final products obtained even though the composition of the reaction mixtures could be essentially identical.

5.5 Conclusions

We have shown that hydrothermal treatment of zeolite P1 (Si/Al = 2.7 - 3.2) with solutions containing alkaline-earth cations is a suitable method for the synthesis of a number of alkaline-earth zeolites. Among these zeolites are synthetic analogues of zeolites heulandite, epistilbite, brewsterite, harmotome and yugawaralite. The conversion of zeolite P1 to these zeolites is likely to occur via the continuous and gradual dissolution of P1 and the subsequent nucleation of the aluminosilicate species released into the solution phase. Among the factors that affect the final products of

conversion are the Si/Al ratio of the starting zeolite P1, the composition of the solution phase and the presence or absence of seeds. In some instances, the addition of seeds is necessary for the crystallization of a particular zeolite. However, the presence of seeds of a particular zeolite does not necessarily result in the formation of a product with the same topology as that of the seed crystals. Rather, other factors such as the solution composition and the Si/Al ratio of the starting zeolite P1 must also favor the formation of that particular zeolite. The initial framework Si/Al ratio of zeolite P1 has a significant influence on the final zeolites obtained.

Zeolite L (LTL) has also been used as a precursor to alkaline-earth zeolites, however the alteration behavior of zeolite L is somewhat different from zeolite P1, particularly in the calcium-dominant reaction media. These differences seem to suggest that during alteration of a zeolite to another, it is not only the overall composition of the reaction mixture that is important. Rather, the atomic structure of the starting zeolite is likely to affect the concentration and distribution of the aluminosilicate species released into the solution phase that ultimately affect the final zeolites obtained.

Acknowledgment

We thank Akzo Nobel for financial support and Mr. Mark Lovallo for providing us with a sample of nanocrystalline zeolite L.

5.6 References

[1] R. M. Barrer and P. J. Denny, *J. Chem. Soc.*, (1961) 971.

[2] S. Khodabandeh and M. E. Davis, *Microporous Mater.*, 9 (1997) 149.

[3] S. Khodabandeh and M. E. Davis, *Micropor. Mater.*, (submitted).

[4] S. Khodabandeh and M. E. Davis, *Microporous Materials*, 9 (1997) 161.

[5] G. Gottardi and E. Galli,*Natural Zeolites*, Springer-Verlag, Heidelberg, 1985.

[6] S. M. Meier, D. H. Olson and C. Baerlocher, *Atlas of Zeolite Structure Types*; 4th. ed., Elsevier, London, 1996.

[7] R. M. Barrer and D. J. Marshal, *J. Chem. Soc.*, 485 (1964)

[8] R. M. Barrer and D. J. Marshall, *Amer. Miner.*, 50 (1965) 484-489.

[9] See a) R. Szostak, *Handbook of Molecular Sieves*, Van Nostrand Reinhold, New York, 1992, pp. 351-352. b) D. W. Breck, *Zeolite Molecular Sieves*, John Wiley & Sons, New York, 1973, p. 276.

[10] M. Tsapatsis, M. Lovallo, T. Okubo, Davis.M.E.; and M. Sadakata, *Chem. Mater.*, 7 (1995) 1734-1741.

[11] G. N. Kirov and N. Petrova, *Stud.Surf. Sci. Catal.*, 84 (1994) 291.

[12] N. Petrova and G. N. Kirov, *Thermochim. Acta.*, 269 (1995) 443-452.

Table 5.1 Reactions of P1 with calcium-containing solutions.[a]

Starting phase[b]	$[Ca^{2+}]$, N	pH[c]	Seeds	Result
Ca-P1	0.1 - 1.0	11.0	HEU (3 - 10 %)	CIT-3
Ca-P1	0.1 - 1.0	11.0	---	EPI
Na-P1	0.01	11.0	HEU (20%)	P1 + ANA
Na-P1	0.1	11.0	HEU (5 %)	P1 + CIT-3
Na-P1	1.0	11.0	HEU (5 %)	CIT-3

[a] 0.20 g of P1 was reacted with 10 ml of solution at 240°C.
[b] Si/Al = 3.0.
[c] pH was adjusted by the addition of a few drop of dilute NaOH solution.

Table 5.2 Reactions of P1 with sodium-dominant solutions.[a]

Starting Phase	Si/Al	$[Na^{+}]$, N	pH[b]	Seeds	Result
Na-P1	2.5	0.01	11	---	ANA + P1
Ca-P1	2.6	0.1	11	---	ANA + P1
Na-P1	3.0	0.1	11	---	ANA
Na-P1	3.0 - 3.2	0.01 - 0.1	11	HEU (20%)	ANA + P1
Na-P1	3.0	0.01 - 0.1	11	BRE (20%)	ANA + P1

[a] 0.20 g of P1 was reacted with 10 ml of solution at 240°C.
[b] pH was adjusted by the addition of a few drops of dilute NaOH solution.

Table 5.3 Reactions of P1 with strontium-dominant solutions.[a]

P1 type	Si/Al	seed[b]	Result
Ca-P1	2.5	BRE	P1
Ca-P1	2.7	BRE	CIT-4
Ca-P1	2.7	---	Sr-Q
Ca-P1	2.9	BRE	CIT-4
Ca-P1	3.0	BRE	CIT-4
Ca-P1	3.0	---	Sr-Q
Sr-P1	3.0	BRE	CIT-4
Na-P1	3.0	BRE	CIT-4
Ca-P1	3.2	BRE	Sr-Q
Ca-P1	3.2	---	Sr-Q
Sr-P1	3.2[c]	BRE	HEU
Sr-P1	3.2[c]	---	HEU
Ca-P1	3.2[c]	---	Sr-Q
Ca-P1	3.2[c]	BRE	Sr-Q
Sr-P1	3.2	---	HEU + Sr-Q
Sr-P1	3.0	---	Sr-Q

[a] 0.20 g of P1 was reacted with 10 ml of solution at 240°C. pH = 11, adjusted by the addition of few drops of saturated $Sr(OH)_2$ solution.
[b] 5 to 10 % seeds were used.
[c] $P1_b$ was used for these reactions (see section 5.4.1.4 for a description of $P1_b$).

Table 5.4 Variations in the unit cell parameters of zeolite P1 with the framework aluminum content.

Si/Al	a (Å)	V (Å^3)
2.5	10.039 ± 0.005	1011.72
2.7	10.020 ± 0.005	1006.01
3.0	10.006 ± 0.004	1001.73
3.2	9.989 ± 0.006	996.62

Table 5.5 Concentration of Al and Si species in the solution phase after 16 hours of dissolution.

Initial Framework Si/Al	[Si] (ppm[a])	[Al] (ppm[a])	$(Si/Al)_{solution}$
2.5	1.5	0.45	3.31
2.7	1.6	0.41	3.96
3.0	0.98	0.26	3.86
3.2	1.36	0.38	3.54

[a] ppm = mg/L

Table 5.6 The effect of the silica content of the gel on the framework Si/Al ratio of the P1 zeolite obtained.

Na_2O	Al_2O_3	SiO_2	Product
5.5	1	10.0	P1 + ANA
5.5	1	13.0	P1 (Si/Al = 2.5)
5.5	1	14.0	P1 (Si/Al = 2.6)
5.5	1	15.0	P1 (Si/Al = 2.7)
5.5	1	15.5	P1 (Si/Al = 2.9)
5.5	1	15.9	P1 (Si/Al = 3.0)
5.5	1	16.2	P1 (Si/Al = 3.0)
5.5	1	17.0	P1 (Si/Al = 3.2)
5.5	1	17.5	P1 (Si/Al = 3.2)
5.5	1	18.0	P1 (Si/Al = 3.2)
5.5	1	19.0	amorphous
5.5	1	20.5	amoprphous
5.5	1	23.4	amorphous

Table 5.7 Products of conversion of zeolite L

Zeolite type	Solution	pH	seed[b]	Product
Ca-L	$CaCl_2$	10 - 11	HEU	EPI
Ca-L	$CaCl_2$	10 - 11	___	EPI
Ca-L	$SrCl_2$	11 - 12	BRE	CIT-4+ Sr-Q
Sr-L	$SrCl_2$	11 - 12	BRE	CIT-4 + Sr-Q
Ca-L	$SrCl_2$	11 - 12	BRE	CIT-4 + Sr-Q
Sr-L	$SrCl_2$	11 - 12	___	Sr-Q
Sr-L	$SrCl_2$	12	HEU	Sr-heu

[a] 0.20 g of zeolite L was reacted with 10 ml of solution at 240°C. pH = was adjusted by the addition of few drops of the corresponding hydroxide solution.
[b] 5 to 10 % seeds were used.

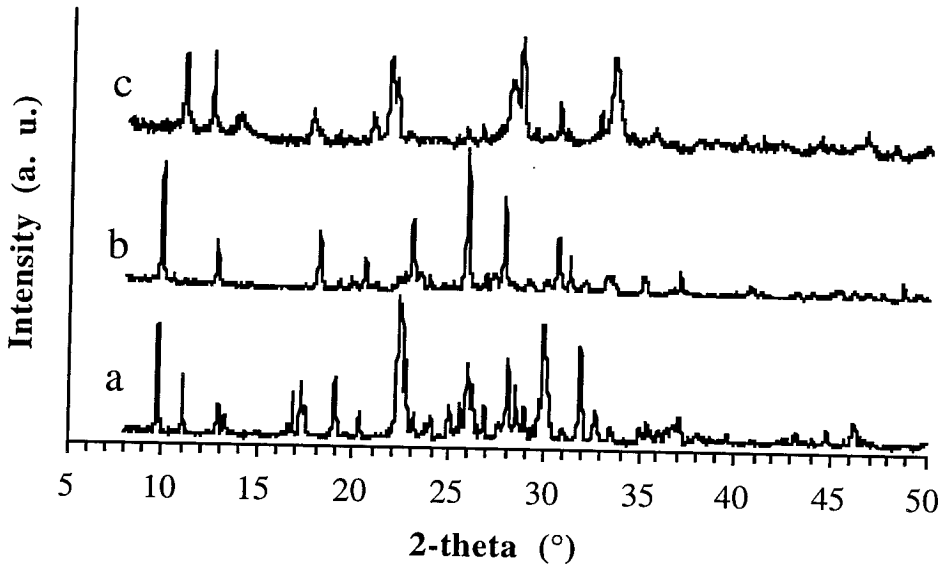

Figure 5.1 XRD patterns of a) CIT-3, b) synthetic epistilbite and c) synthetic harmotome.

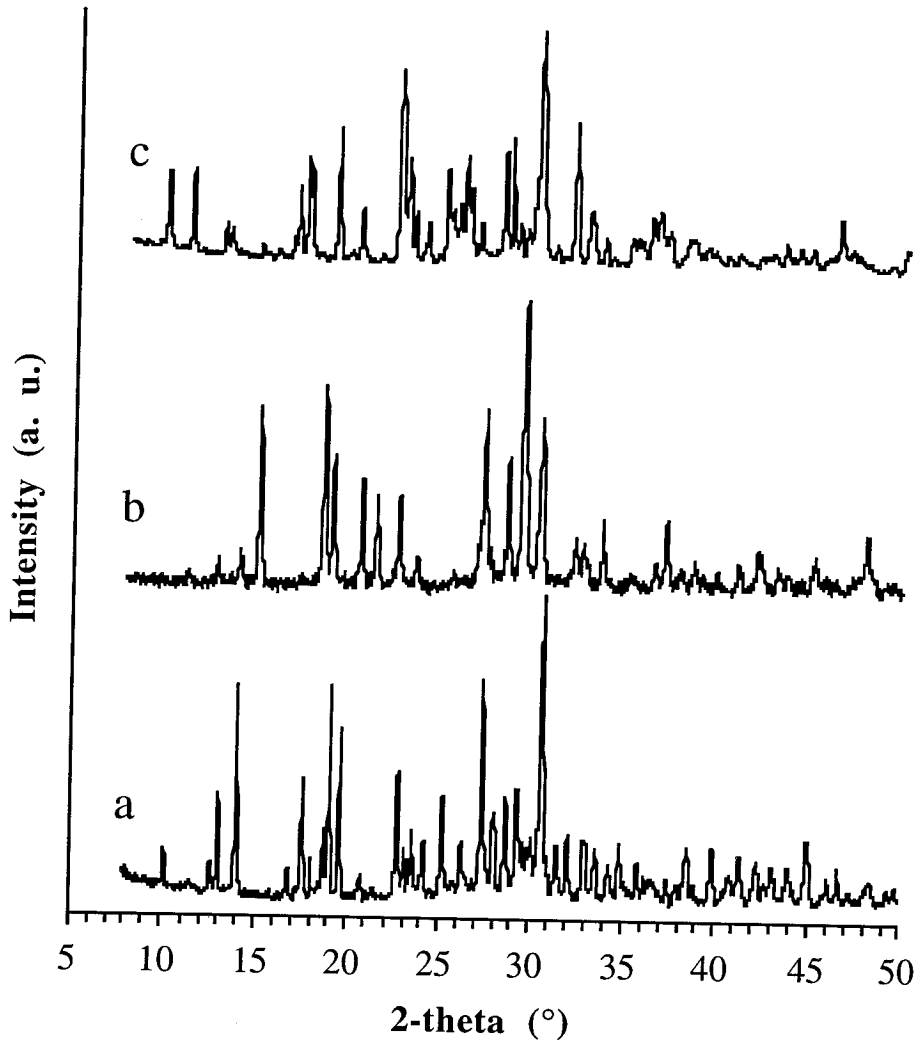

Figure 5.2 XRD patterns of a) CIT-4, b) Sr-Q and c) Sr-heulandite

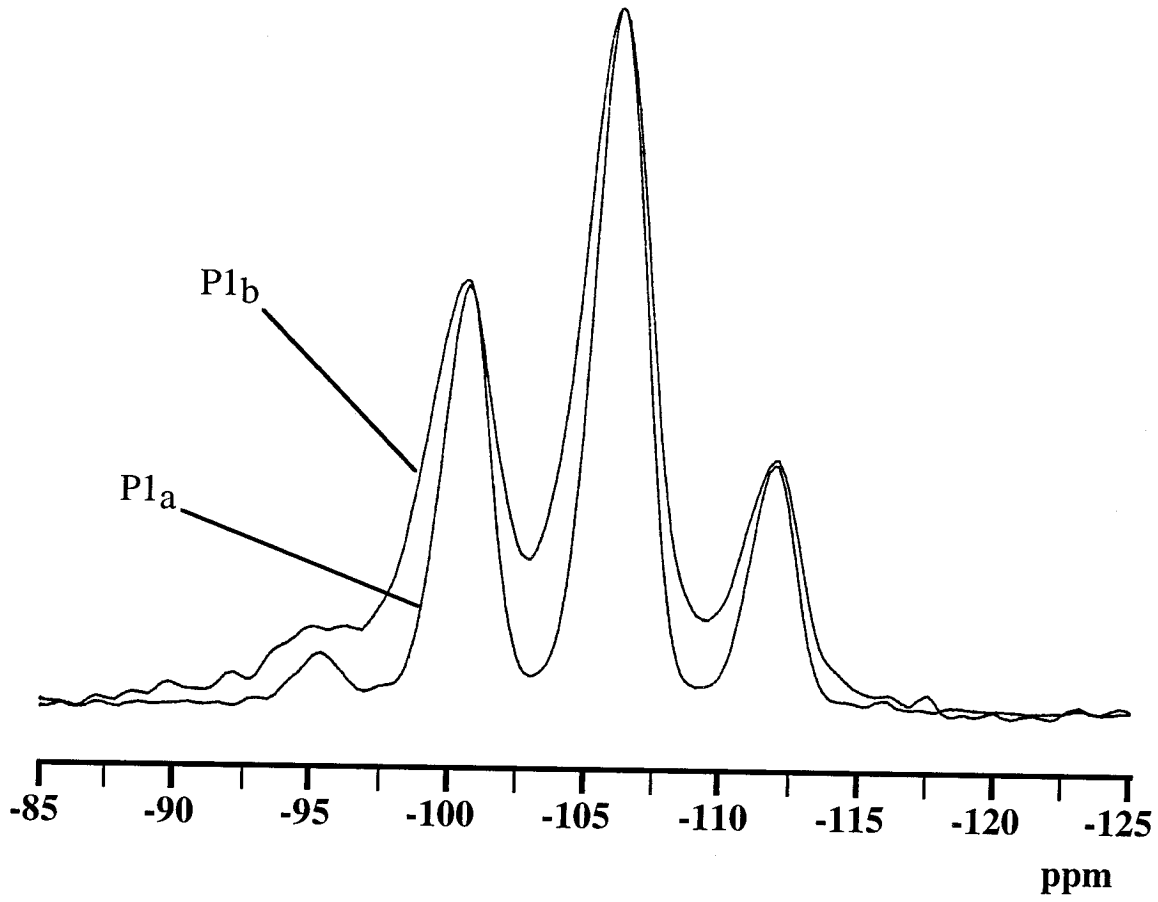

Figure 5.3 ^{29}Si NMR spectra of $P1_a$ and $P1_b$.

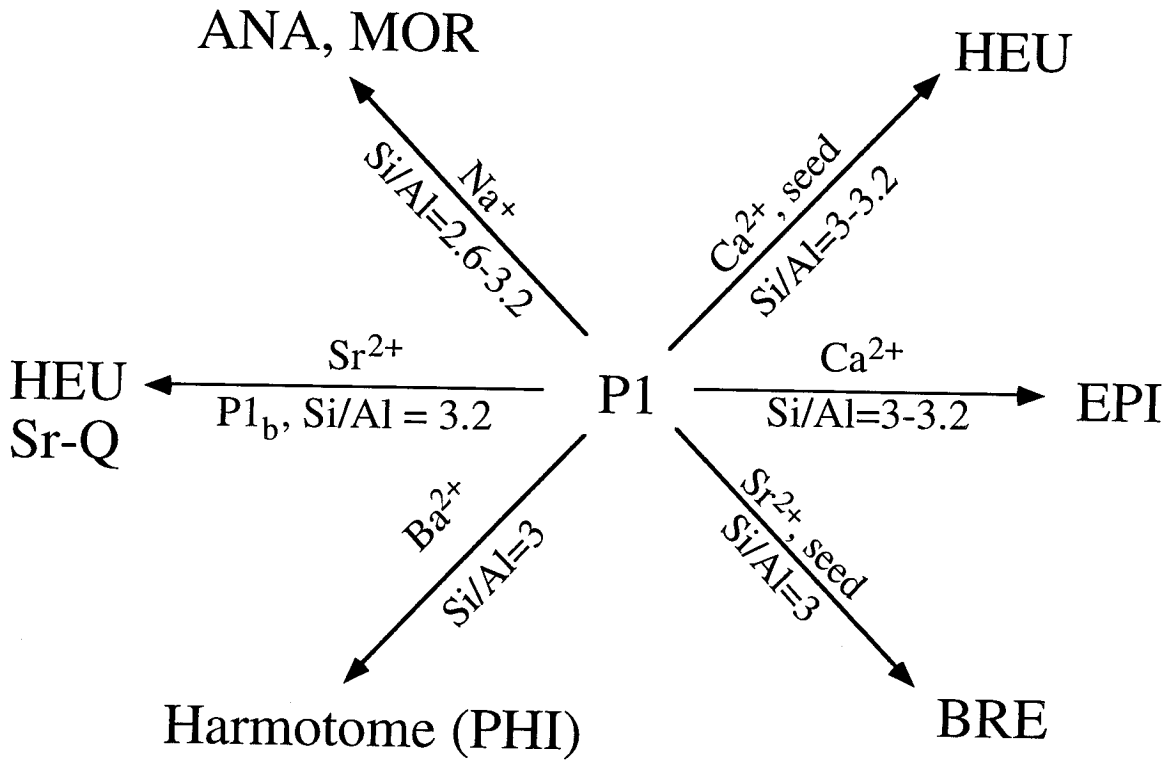

Figure 5.4 Summary of alteration products of zeolite P1.

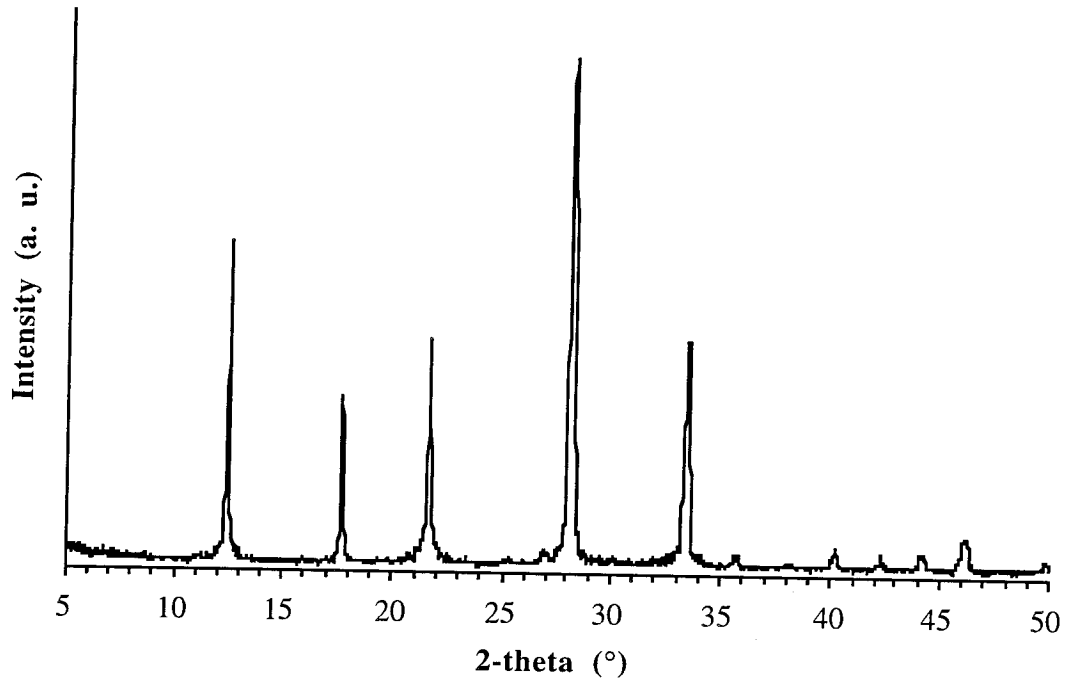

Figure 5.5 XRD pattern of zeolite P1 (Si/Al = 3).

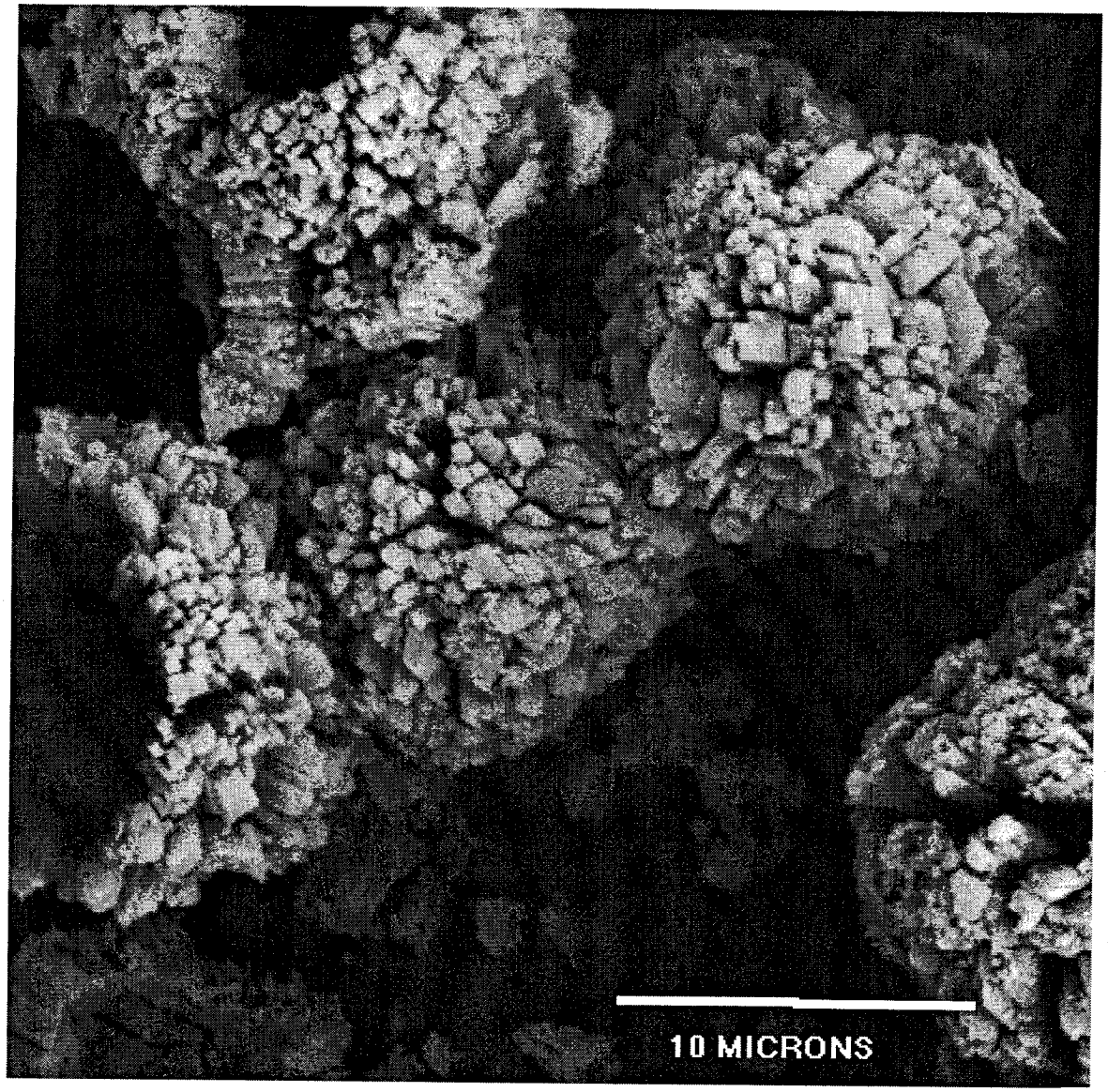

Figure 5.6 Scanning electron micrograph of P1 (Si/Al = 2.9)

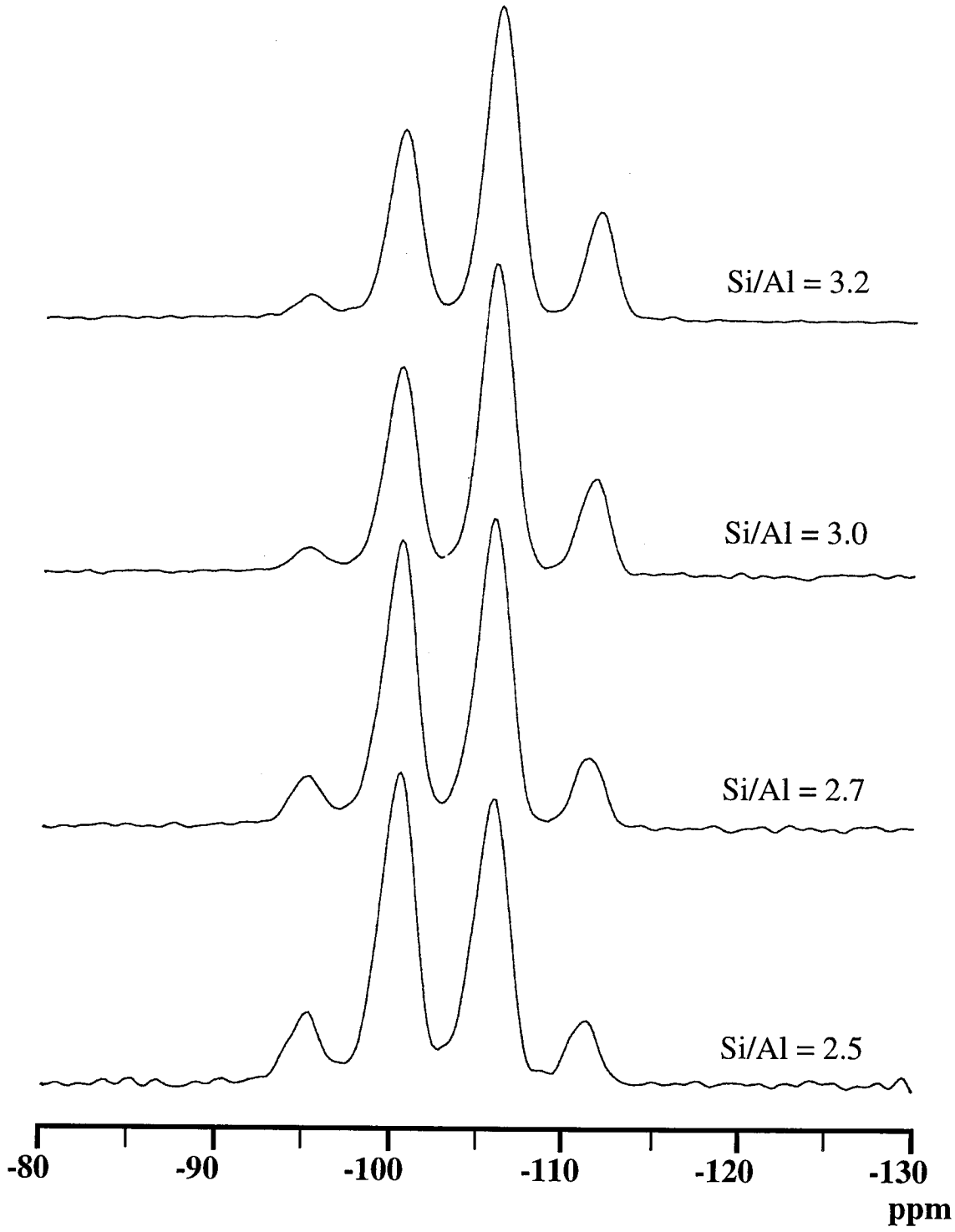

Figure 5.7 ^{29}Si NMR spectra of zeolite P1 with various framework Si/Al ratios.

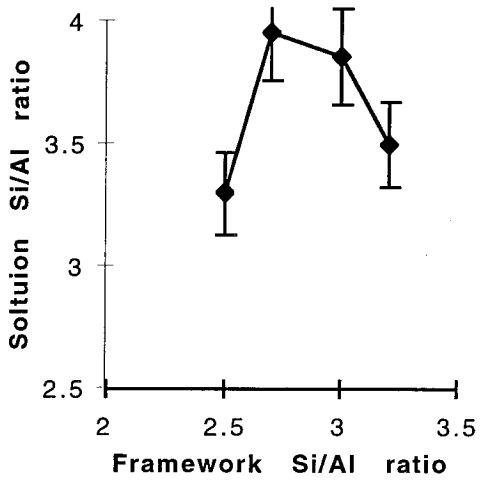

Figure 5.8 Si/Al ratio of the solution phase as a function of the initial framework Si/Al ratio.

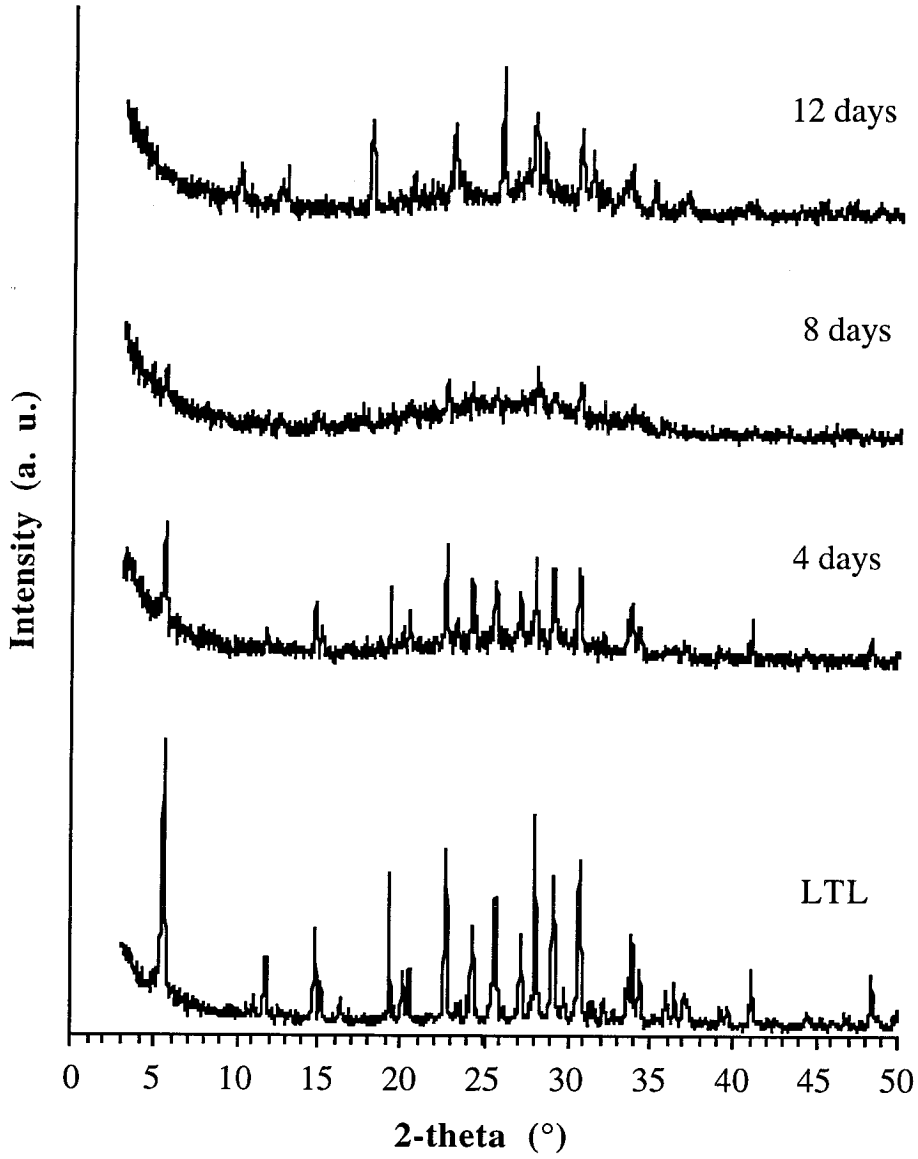

Figure 5.9 Conversion of zeolite L to epistilbite.

CHAPTER SIX

An Investigation of the IR Spectra of Zeolites Containing the 4-4-1-1 Secondary Building Unit

Abstract:

The infrared spectra of zeolites containing the 4-4-1-1 secondary building unit (SBU) are recorded in order to determine whether this SBU results in any characteristic vibrations observed by IR spectroscopy. The IR spectra of zeolites CIT-1 (CON), CIT-3 (HEU), CIT-4 (BRE), stellerite (STI), and SSZ-33 are compared . The HEU, BRE and STI topologies can be constructed using exclusively the 4-4-1-1 SBU while the CON topology contains double 5-rings as well as the 4-4-1-1 SBU. Two vibrations at 600 ± 3 cm^{-1} and 784 ± 4 cm^{-1} are observed for all these zeolites. The data suggest that the simultaneous presence of both absorptions in the IR spectrum of a zeolite with unknown structure may be regarded as an indication of the presence of the 4-4-1-1 SBU in the framework. This information may prove useful in the process of structure determination of a zeolite with unknown topology.

6.1 Introduction

The primary building units in zeolite frameworks are oxygen-coordinated tetrahedral atoms of silicon or aluminum. Various zeolite framework structures can be visualized as consisting of secondary building units (SBU's), which are formed by simple combinations of the primary tetrahedra. Figure 6.1 shows some secondary building units commonly found in zeolite frameworks. Each apex denotes a tetrahedral atom (Si or Al) and the solid line between them represents a bridging oxygen atom that connects the two tetrahedral atoms. SBU's should be solely regarded as hypothetical entities with the mere purpose of classifying and visualizing zeolite structures. Thus, one should not infer that the SBU's seen in Figure 6.1 actually exist as chemical moieties during crystallization of zeolites. Structural similarities between various zeolites are better understood in terms of the type of the SBU's present and the various ways of linking the SBU's to form fully condensed 3-dimensional structures. For example the framework structures of the zeolites epistilbite (EPI), mordentie (MOR), ferrierite (FER), and ZSM-5 (MFI) can be differentiated based upon various linkings of the same secondary building unit, namely the 5-1 unit.

The 4-4-1-1 unit is a rather rare SBU that is observed in the structure of relatively few zeolites. The 4-4-1-1 SBU exists in the framework structures of natural zeolites with the heulandite (HEU), brewsterite (BRE), stilbite (STI) and boggsite (BOG) topologies. This SBU exists also in the frameworks of the synthetic molecular sieves CIT-1, SSZ-33 and SSZ-26. SSZ-26 and SSZ-33 are intergrowth structures consisting of two polymorphs (A and B) and are differentiated based on the degree of faulting [1]. CIT-1 (CON) is the pure, fault-free polymorph B [2]. The framework structure of heulandite, brewsterite and stilbite can be visualized as being composed entirely of 4-4-1-1 SBU, while the frameworks of boggsite, CIT-1 and SSZ-33 cannot be constructed using solely the 4-4-1-1 SBU. These latter structures also contain

double 5 rings (D5R). A schematic of the 4-4-1-1 secondary building unit is given in Figure 6.2. This figure also illustrates the framework topologies for HEU, STI, and BRE. Notice the 4-4-1-1 SBU's in these structures.

A familiarity with the secondary building units as well as more complicated and extended building units (tertiary building units, TBU) is extremely useful in the process of structure solution of novel zeolite materials. Typical zeolite crystals are much too small for single crystal X-ray analysis to be applicable with any success. Consequently, the process of structure solution is commonly an iteration on the tedious steps of model-building and simulation of the powder X-ray pattern of the resulting structure and subsequent modification of the model to minimize the differences between the experimental and the simulated powder patterns. Thus, one makes a physical model of the zeolite structure, optimizes the bond lengths and simulates the powder X-ray diffraction pattern. After a comparison of the experimental and the simulated X-ray patterns, the starting model is either modified or discarded altogether. This process continues until a reasonable fit between the experimental and the simulated X-ray patterns is obtained.

Although powder X-ray diffraction is the corner stone of any attempt to solve an unknown zeolite structure, other physical characterization techniques such as solid-state Nuclear Magnetic Resonance (NMR) spectroscopy, Tunneling Electron Microscopy (TEM) and adsorption studies offer clues towards the model used as the initial guess. If in addition to the information obtained from such techniques, one knows a priori about the types of secondary building units (SBU's) present in the structure, the number of possible guesses for the initial model will be dramatically reduced.

Infrared (IR) spectroscopy is one potential tool that can be complementary to diffraction analysis. The structural vibrations of zeolites can generally be classified into

two categories: 1) Those arising from the internal tetrahedra (TO_4 units), and 2) those resulting from more extended units formed by combination of the primary tetrahedra [3]. The first group of vibrations are independent of the structure of the zeolite and result in a strong absorption around 1000 cm^{-1}, which is due to the asymmetric stretch of the T-O (T = Si, Al) bond. Also, a band appearing between 400-500 cm^{-1} is assigned to the T-O bending mode of the internal tetrahedra. These vibration have components due to the Si-O and Al-O bonds and thus have frequencies that are sensitive to the Si/Al ratio of the zeolite. Linear correlations between the frequency of these vibrations and the mole fraction of aluminum in the zeolite samples have been found for zeolites A, X, Y, and Omega [4].

The second category of vibrations are structure-sensitive as opposed to those mentioned previously, which are structure-insensitive. These vibrations are typically grouped into four regions as shown in Table 6.1. Those in the range of 300 - 400 cm^{-1} are thought to have components arising from pore opening vibrations in the zeolite. Those around 500 - 600 are believed to signify the presence of double rings. And two sets of stretching vibrations at 750 - 820 cm^{-1} and 1050 - 1150 cm^{-1} are symmetric and asymmetric stretches, respectively, arising from more complicated linkages of the primary tetrahedra. It is not difficult to appreciate why Infrared spectroscopy applied to the characterization of the framework structure of zeolites has been controversial. Although valuable information can be gained regarding specific characteristics of a zeolitic material (such as presence of silanol defect sites, acid site strength, state and amount of adsorbed water or other adsorbate), drawing conclusions concerning the actual framework structure is not trivial. Despite this, investigation of a number of molecular sieves containing similar structural features has been somewhat successful in providing some general conclusions regarding the presence or absence of certain structural units. For example, an absorption band near 550 cm^{-1} has been assigned to

the presence of 5 member-ring blocks [5,6]. Three types of 5 MR blocks are shown in Figure 6.3. Table 6.2 lists some of the structure-sensitive vibrations of zeolites containing 5MR units. As seen in this table, zeolites that contain the 2-connected 5-5 block (see Figure 6.1) exhibit IR absorptions at 550, 780-790, and 1225 cm^{-1}. Zeolite epistilbite which does not possess the 2-connected 5-5 block and instead has the 5-3 block exhibits a vibration at 563 and one at 795 but no bands at 1225 cm^{-1}.

Thus, it appears that the existence of three bands at 550, 780-790, and 1225 cm^{-1} in the IR spectrum of an unknown molecular sieve might signal the presence of double 5-rings in the zeolite structure. This information may be extremely helpful in building the first few topological models of the structure.

As mentioned previously, the 4-4-1-1 SBU is a rather uncommon secondary building unit existing in the framework structure of only a few rare zeolites. An examination of the IR spectra of these zeolites may prove useful in determining whether the 4-4-1-1 SBU has any characteristic absorptions observable by infrared spectroscopy. To this end, the IR spectra of CIT-3 (HEU), CIT-4 (BRE), stellerite (STI), CIT-1 (CON) and SSZ-33 are recorded and compared.

6.2 Experimental Section

6.2.1 Zeolites.

Zeolites CIT-3 (HEU) and CIT-4 (BRE) were synthesized according to procedures outlined in Chapters 3 and 4, respectively. Zeolite CIT-1 was prepared according to procedures outlined by Lobo and Davis [2]. SSZ-33 was supplied by Dr. Stacey Zones of Chevron Research and Technology Co. Stellerite was used as a zeolite with the STI topology; stellerite crystals were purchased from Excalibur-Cureton Company and originated near Ritter Hot Springs, Grant County, Oregon. Boggsite crystals (Goble, Oregon) were purchased from Cureton Mineral Company. For all

zeolites other than boggsite, ample amounts of sample were available. However, only about 0.1 mg of boggsite sample was available due to the extreme rarity of this zeolite.

6.2.2 IR and Raman spectroscopy

Infrared spectroscopy was performed on a Nicolet System 800 FTIR instrument. The samples were prepared as KBr pellets using 3 weight % of zeolite. For the boggsite sample the KBr pellet contained only about 0.2% zeolite due to the small amount of sample available. For all sample other than boggsite 128 or 256 scans were obtained. For boggsite 4096 scans were obtained since sufficient sample was not available. In order to enhance the spectral resolution, the fourier self-deconvolution method was used for cases were overlapping absorptions were suspected. Raman spectra were obtained on a Nicolet FT-Raman 950 spectrometer for all samples other than boggsite, for which no Raman spectra were recorded due to the insufficiency of the sample.

6.3 Results and Discussions

The IR spectra in the range of 400 - 4000 cm^{-1} is given in Figure 6.4. Figure 6.5 shows the IR spectra in the range 550-820 cm^{-1}; the spectrum of zeolite Y with the faujasite (FAU) topology is also included for comparison. The FAU framework contains double 6 rings and 6-2 subunits and does not contain the 4-4-1-1 SBU. Figure 6.5 shows that there are two IR absorptions at ca. 600 cm^{-1} and ca. 780 cm^{-1} that are observed in the spectra of all of the molecular sieves except zeolite Y. These two bands are also absent in the spectrum of other common zeolites such as A, X, P1, and ZSM-5, none of which possesses the 4-4-1-1 SBU.

Table 6.3 lists IR and Raman data obtained here for zeolites and molecular sieves that contain the 4-4-1-1 SBU. As mentioned previously, two absorptions at 600

and 780 cm^{-1} are apparent for these zeolites. The band at 780 cm^{-1} is also observed for zeolites ZSM-5 and other molecular sieves with the MFI structure as shown by the data in Table 6.2. This band has also been attributed to structures containing the double 5 ring (D5R) as mentioned above. Furthermore, as shown in Table 6.2, zeolites containing the D5R in their framework structure also exhibit an IR absorption ca. 1225 cm^{-1}. Figure 6.6 shows IR spectra in the range of 800 - 2000 cm^{-1} for the zeolites containing the 4-4-1-1 SBU as well as ZSM-5. The band at 1225 cm^{-1} is observed for ZSM-5, CIT-1 and SSZ-33. Double 5 ring units exist in the framework structures of these zeolites. In contrast, the 1225 cm^{-1} band is not observed for the zeolites CIT-3 (HEU), CIT-4 (BRE), stellerite (STI). These zeolites are composed entirely of the 4-4-1-1 SBU.

So far, one can draw the following conclusions considering the few structures investigated thus far: 1) All zeolites investigated thus far that contain the 4-4-1-1 SBU show the two IR absorptions ca. 600 and 784 cm^{-1}. 2) HEU, BRE, and STI, which are composed entirely of the 4-4-1-1 SBU, do not show the asymmetric stretch at 1225 cm^{-1}. 3) CIT-1 and SSZ-33, which contain the 4-4-1-1 SBU and double 5 ring blocks, also exhibit the absorption at 1225 cm-1 in addition to the two bands at 600 and 784 cm^{-1}.

Thus, it appears that the presence of two absorption bands ca. 600 and 780 cm^{-1} might signal the possibility that the framework structure may contain 4-4-1-1 SBU's. One way to gain more confidence in this hypothesis would be to look at the IR spectrum of boggsite. However, due to extreme rarity of this zeolite, it was not feasible to obtain sufficient sample. As a result, the IR spectrum of boggsite was not satisfactory. Nonetheless, this spectrum is shown in Figure 6.7 and is characterized by very low absorbance due to small amount of sample. An absorption ca. 800 cm^{-1} is

observed however, it is not clear whether or not a significant absorption around 600 cm^{-1} is also present.

6.4 Summary

The infrared spectra of zeolites CIT-3 (HEU), CIT-4 (BRE), stellerite (STI), CIT-1 (CON) and SSZ-33 are compared. These zeolites all possess the 4-4-1-1 secondary building unit. The HEU, BRE and STI topologies contain exclusively the 4-4-1-1 SBU, whereas the CON topology contains both the 4-4-1-1 SBU and double 5-rings. All these zeolites exhibit two IR absorptions at ca. 600 and 784 cm^{-1}. In addition, CIT-1 and SSZ-33, which also contain double 5-rings, exhibit a band at 1225 cm^{-1}. No satisfactory spectrum of boggsite was obtained due to the difficulty in obtaining sufficient amounts of high quality sample for this zeolite. The two bands at 600 and 784 cm-1 are not observed for zeolites that do not contain the 4-4-1-1 SBU such as zeolites X, Y, A, P1, and ZSM-5. These observations suggest that the presence of the two bands at 600 and 784 cm^{-1} in the IR spectrum of a new zeolite with unknown structure may indicate the existence of the 4-4-1-1 SBU in the framework of that zeolite. This information may prove extremely valuable in the process of structure solution of zeolites with unknown topologies.

6.5 References

[1] R. L. Lobo, M. Pan, I. Chan, H. X. Li, R. C. Medrud, S. I. Zones, P. A. Crozier and M. E. Davis, *Science*, 262 (1993) 1543.

[2] R. L. Lobo and M. E. Davis, *J. Am. Chem. Soc.* 117 (1994) 3764.

[3] D. W. Breck, *Zeolite Molecular Sieves*, John Wiley & Sons, New York, 1974, p. 418.

[4] E. M. Flanigen, H. Khatami and H. A. Szymanski,*Molecular Sieve Zeolites*, American Chemical Society, Washington, D. C., 1971, p. 201.

[5] P. A. Jacobs, H. K. Beyer and J. Valyon, *Zeolites*, 1 (1981) 161.

[6] G. Coudurier, C. Naccache and J. C. Vedrine, *J. Chem. Soc., Chem Commun.* (1982) 1413.

Table 6.1 Two types of IR vibrations observed in zeolites.[a]

Type of Vibration	Wavenumber (cm^{-1})	Assignment
1. Structure-insensitive	950 - 1250	Asym. stretch
	650 - 720	Sym. stretch
	420 - 500	T-O bend
2. Structure-sensitive	500 - 650	Double ring
	300 - 420	Pore opening
	750 - 820	Sym. stretch
	1050 sh - 1150	Asym. stretch

[a] Adapted from reference 3..

Table 6.2 Infrared structure-sensitive vibrations of zeolites containing 5 member rings.[a]

Zeolite	Asym. Stretch (cm^{-1})	Sym. Stretch (cm^{-1})	Double Ring (cm^{-1})
Silicalite	1225	790	550
ZSM-5	1225	790	550
Boralite	1228	790	550
ZSM-11	1225	790	550
Mordenite	1223	800	560, 580
Ferrierite	1218	780	563
Epistilbite	1175	795	463

[a] Adapted from R. Szostak, *Molecular Sieves: Principles of synthesis and identification*, Van Nostrand Reinhold, New York, 1989.

Table 6.3 Summary of IR and Raman data for zeolites containing the 4-4-1-1 SBU.

Structure	IR (cm^{-1})		Raman (cm^{-1})
STI	784	600	790
HEU	788	598	788
BRE	785	601	---
SSZ-33	783	601	---
CIT-1	780	592-605 (broad)	~800 (broad)
BOG	795	not clear	not obtained

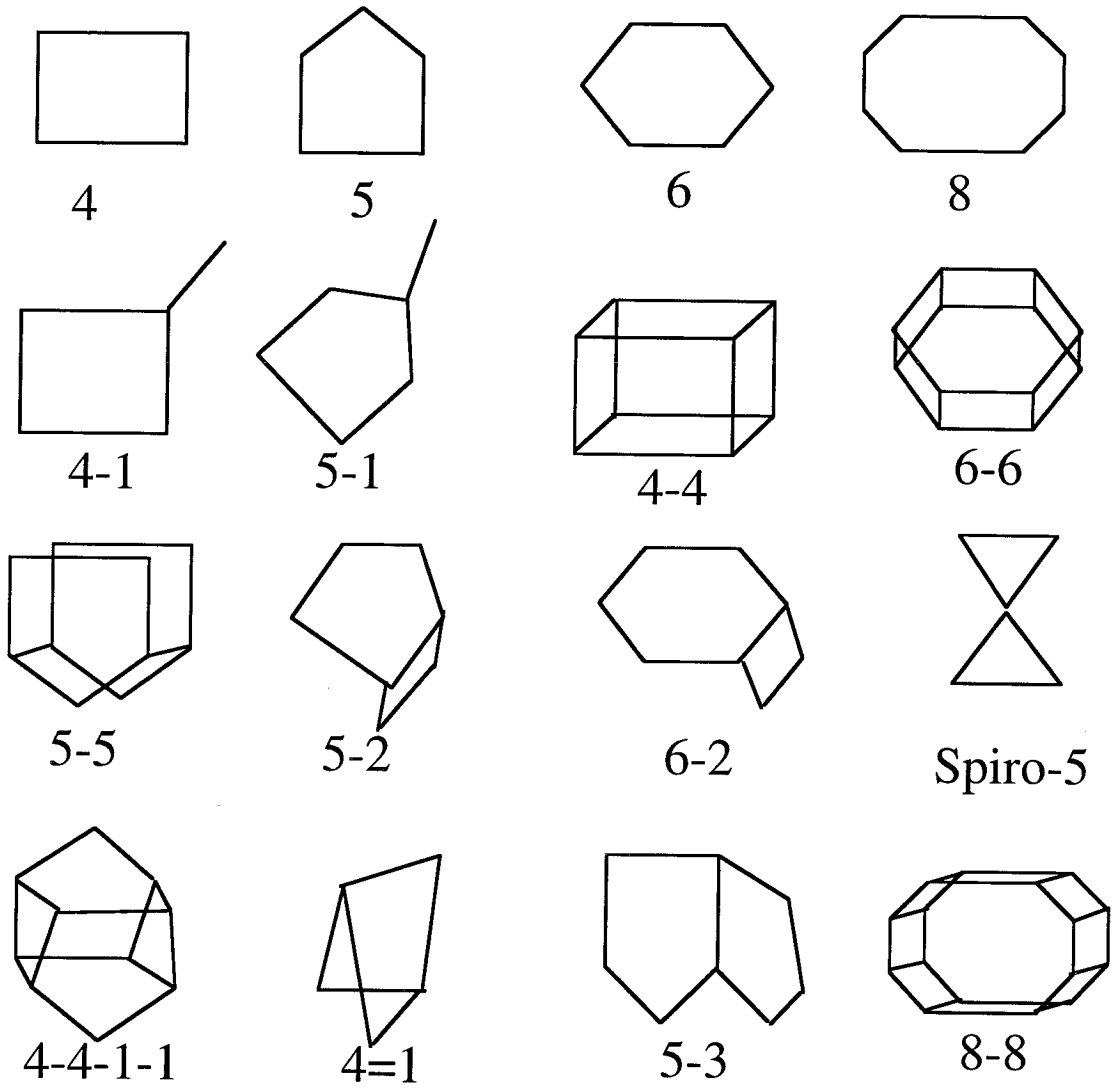

Figure 6.1 Secondary building units (SBU's).

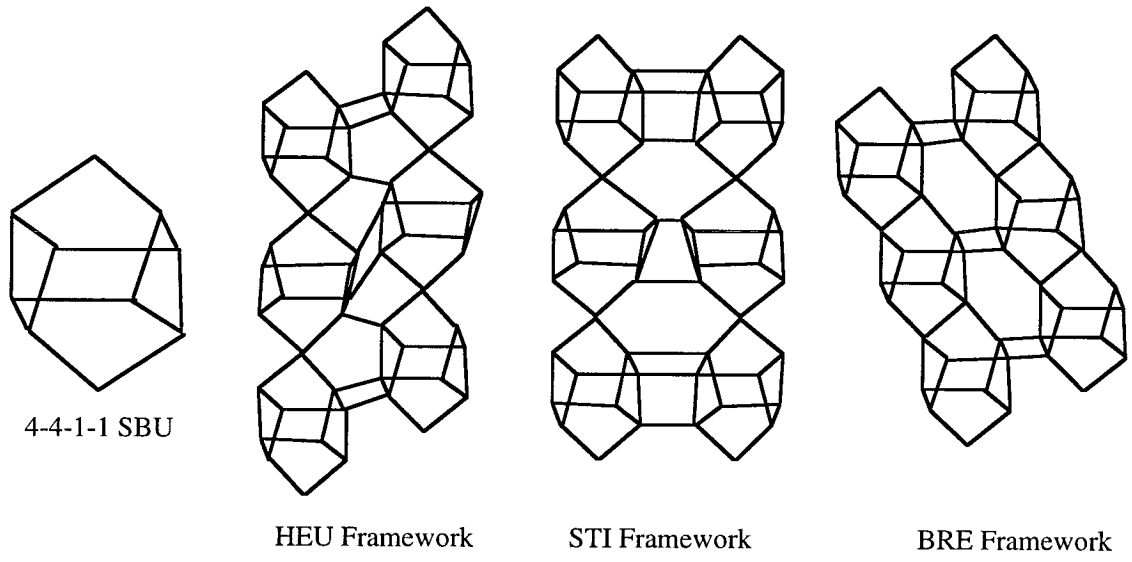

Figure 6.2 Framework structures of HEU, STI and BRE as represented by different linkings of the 4-4-1-1 SBU.

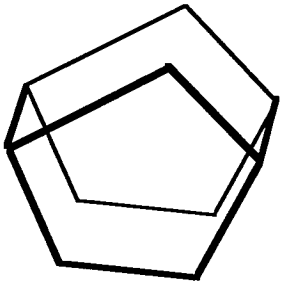

5-5 block
2-connected

ZSM-5, ZSM-11,
MOR

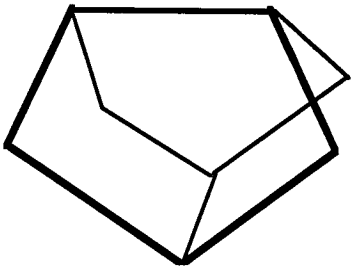

5-3 Block

ZSM-5, ZSM-11, MOR
FER, EPI

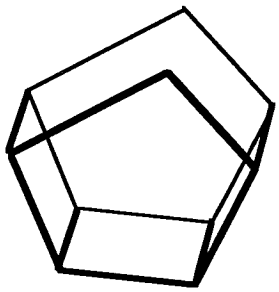

5-5 block
4-connected

CIT-1, SSZ-33

Figure 6.3 Various 5-member ring blocks.

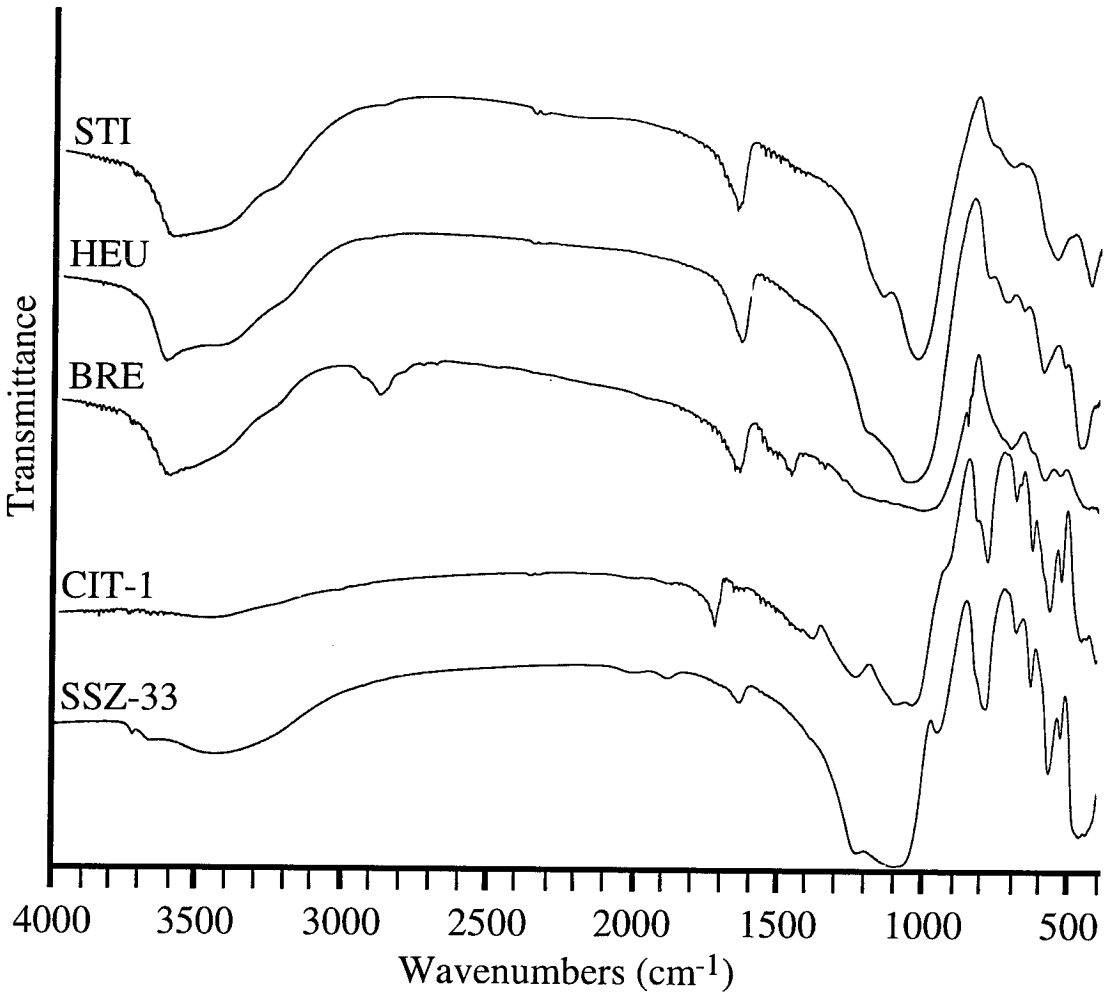

Figure 6.4 IR spectra of zeolites containing the 4-4-1-1 SBU.

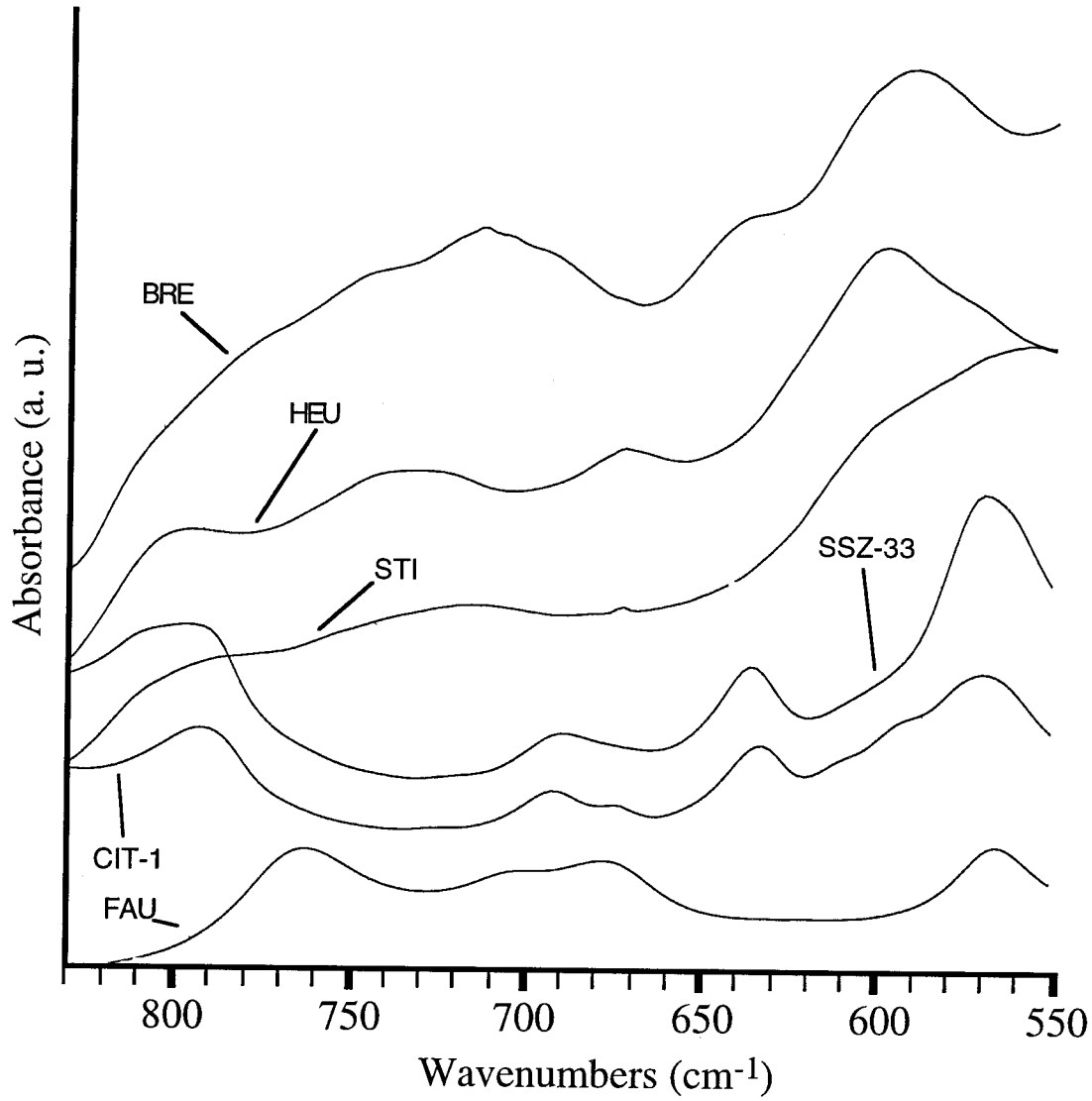

Figure 6.5 IR spectra of zeolites containing the 4-4-1-1 SBU and zeolite Y (FAU).

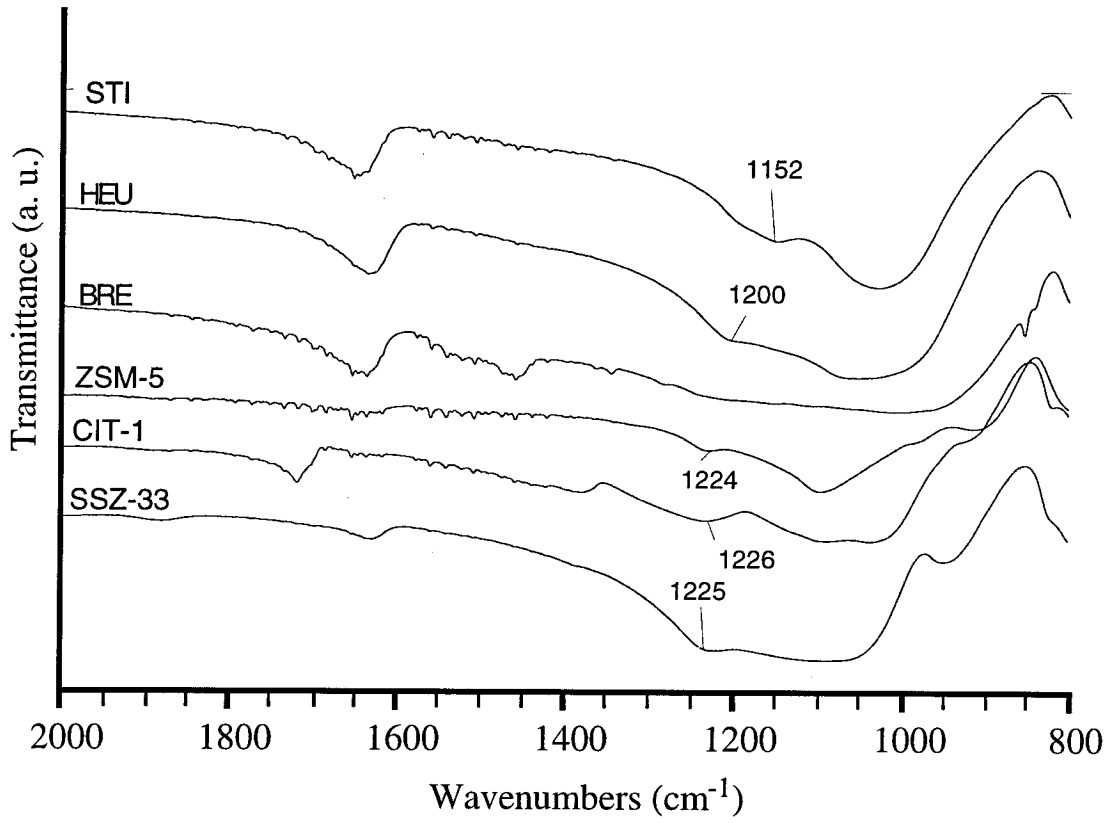

Figure 6.6 IR spectra exhibiting the band at 1225 cm^{-1} characteristic of zeolites containing the double 5-ring subunit.

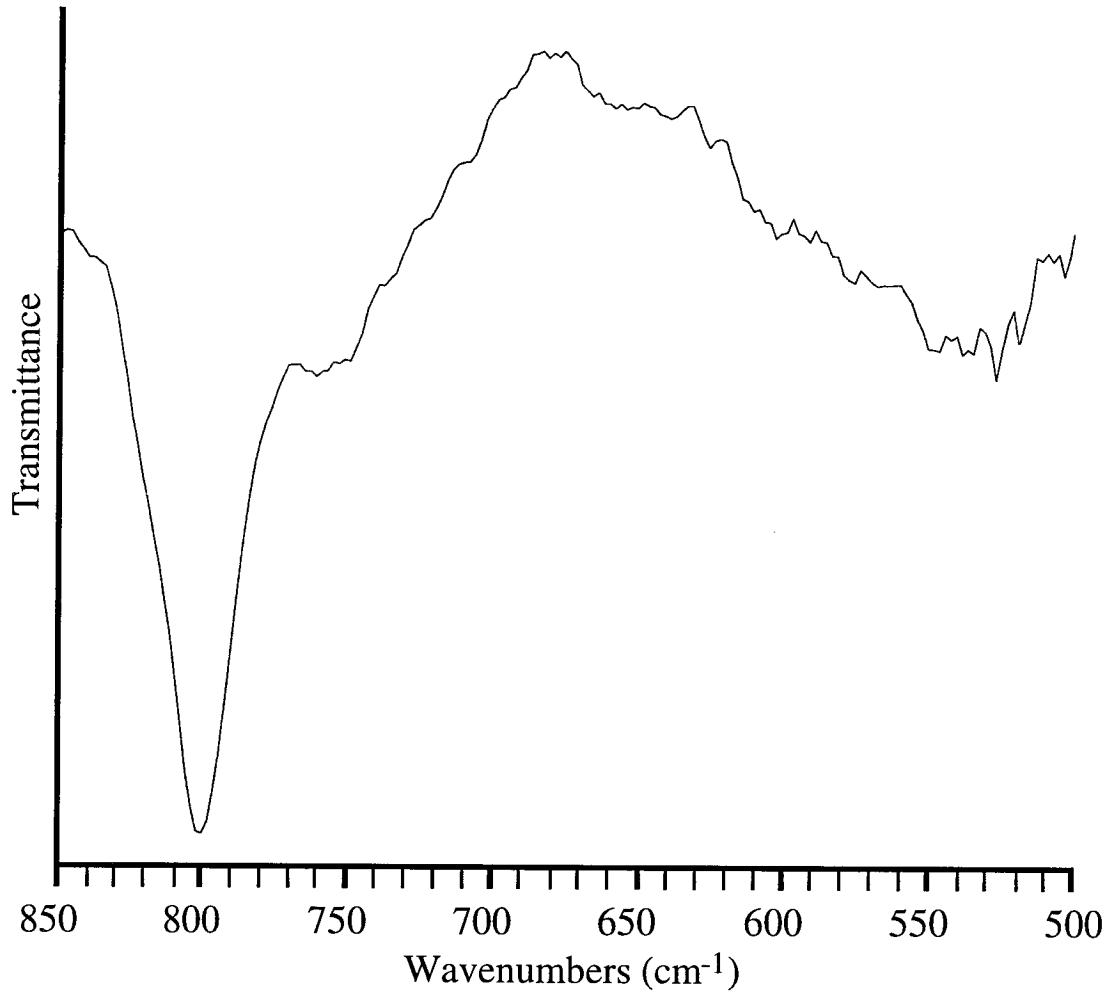

Figure 6.7 IR spectrum of boggsite.

CHAPTER SEVEN

Conclusions

The study of the alteration of volcanic glasses to zeolites proved to be a viable first step towards developing alternate synthesis procedures for obtaining alkaline-earth zeolites. The natural formation of calcium zeolites was simulated by using perlite glass as the starting material and treating it with calcium-containing solutions under conditions similar to those observed in nature. Investigation of the alteration of perlite to calcium zeolites afforded a better understanding of the factors involved in the formation of such zeolites in nature. Results obtained during this investigation were used to develop a novel methodology for the preparation of alkaline-earth zeolites from pure starting reagents.

Conversions of perlite glass to calcium zeolites gismondine, epistilbite, heulandite and the pillared compound tobermorite were investigated. In particular, it was observed that during the transformation of perlite to heulandite, a gismondine-type zeolite appeared as an intermediate phase and was later converted to heulandite. This gismondine-type phase was most similar to the synthetic zeolite P1 with a Si/Al ratio ca. 3. Next, methodology was developed for the preparation of a P1 zeolite with Si/Al ratio varying in the range of 2.5 to 3.2. The P1 zeolites having the appropriate Si/Al ratios and cation compositions were used as precursor materials and were transformed to alkaline-earth zeolite upon treatment with solutions containing the proper alkaline-earth cations.

The zeolites obtained using this methodology include CIT-3 (HEU), CIT-4 (BRE), epistilbite (EPI), harmotome (PHI) and yugawarlite (YUG). CIT-3 is the first calcium aluminosilicate with the heulandite topology that has been synthesized under typical hydrothermal conditions. CIT-4 is the first synthetic analogue of the rare natural zeolite brewsterite.

It was established that the products of conversion of zeolite P1 were determined by factors such as the initial composition of zeolite P1, the composition of the solution

phase and the presence or absence of seeds. Additionally, it was observed that the inclusion of seed crystals of a particular zeolite in the reaction mixture did not necessarily result in the formation of a zeolite with the same topology as that of the seed crystals. Rather, the crystallization of an alkaline-earth zeolite very often required the presence in relatively high concentration of a particular alkaline-earth cation. For example, synthesis of epistilbite, harmotome and CIT-4 were accomplished only in the presence of Ca^{2+}, Sr^{2+} and Ba^{2+}, respectively. These latter results are particularly relevant to one of the most controversial questions regarding the natural formation of zeolites: Is it possible that the extraframework cations found in the composition of a natural zeolite have not been instrumental during its crystallization, but instead have been incorporated in the void structure of the zeolite via natural ion-exchange mechanisms? Although this hypothesis cannot be definitively ruled out, the results obtained in this work suggest that the presence of a particular alkaline-earth cation during crystallization favors the formation of the types of zeolites that are found in nature dominant in that same cation.

Synthesis methodology developed in this work is not necessarily limited to zeolite P1 as preliminary investigations on the conversion reactions of zeolite L has demonstrated that it is possible to synthesize alkaline-earth zeolites from zeolite L as well. Results obtained on the conversion reactions of zeolite L and zeolite P1 are not identical in all cases. This observation suggests that the composition of the reaction mixture is not the only factor determining the final product, and that the atomic structure of the precursor zeolite also has an affect on the reaction pathway. Although the results obtained on the conversion reactions of zeolite L and zeolite P1 are not identical, the similarity in the composition of the two zeolites suggests that a particularly suitable composition for the precursor zeolite is one with a Si/Al ratio ca. 3. This is consistent

with the observation that the majority of alkaline-earth zeolites that have defied synthesis or proven difficult to synthesize occur in nature with Si/Al ratios ca. 3.

The work presented here has demonstrated that synthesis of calcium zeolites under typical hydrothermal conditions is not necessarily limited by the low solubility of calcium in alkaline environments. Rather, synthesis in relatively low alkalinity environments (pH < 12) via alteration of other zeolites is a viable alternative.